

الجمهورية الجزائرية الديمقراطية الشعبية
People's Democratic Republic of Algeria
وزارة التعليم العالي والبحث العلمي
Ministry of Higher Education and Scientific Research



Ziane Achour University of Djelfa
Faculty of Exact Sciences and Computer Science
Physics department

Order n°:.....



THESIS
presented to obtain

3rd Cycle doctoral degree

Option: Physics

Specialty: Materials Physics

Presented by:

HAFIFA Loumafak

**Study of the electro-optical properties of nanostructured
inorganic solar cells with an ultra-thin absorber layer**

Defended on: 04 / 07 / 2024

Jury members:

DEROUICHE Yazid	Prof.	University of Djelfa – Ziane Achour	President
MAACHE Mostefa	Prof.	University of Djelfa – Ziane Achour	Supervisor
OUAHAB Abdelouahab	Prof.	University of Biskra – Mohamed Khider	Examiner
MANSOUR Omar	Prof.	University of Djelfa – Ziane Achour	Examiner
CHALA Slimane	MCA	University of Boumerdes – M'Hamed Bougara	Examiner
BENBOUZID Yazid	MCA	University of Djelfa – Ziane Achour	Examiner

University year: 2023/2024

Dedication

To my beloved parents

To my brothers and sisters

To my friends and all those who are dear to me

Loumafak

Acknowledgements

I would like to thank first of all our God, **ALLAH** the Almighty, who is always with me in the easy and difficult moments of life.

The research work developed in this thesis was carried out within the Physico-Chemistry of Materials and Environment Laboratory (**LPCME**) at Ziane Achour University, Djelfa.

I would like to express my deep gratitude and warm thanks to **Prof. MAACHE Mostefa**, professor at Ziane Achour university of Djelfa, for agreeing to direct my work. I thank him for his advice and his human qualities, his scientific and fruitful discussions, he never deprives me of his support, whether technical or material.

I would also like to offer my thanks, my respect and my gratitude to Prof. **DEROUICHE Yazid**, professor at Ziane Achour university of, Djelfa for the honor he gave me, for agreeing to chair the jury.

I also wish to offer my thanks and sincere appreciation to Prof. **OUAHAB Abdelouahab** professor at Mohamed Khider university of Biskra, Dr. **BENBOUZID Yazid**, ‘‘MCA’’ at Ziane Achour university of Djelfa, Prof. **MANSOUR Omar**, professor at Ziane Achour university of Djelfa and Dr. **CHALA Slimane**, ‘‘MCA’’ at M’Hamed Bougara University of Boumerdes who agreed to examine and judge this modest work.

Finally, I truly want to thank my parents, relatives, friends and all those who have contributed directly or indirectly to the accomplishment of this work.

ملخص

أظهرت الخلايا الشمسية ذات الشرائح الرقيقة من تيلوريد الكاديوم (CdTe) كفاءة عالية وفعالية في الأداء من حيث التكلفة في توليد الكهرباء النظيفة. ومع ذلك، فإن الطبقة العازلة CdS الشائعة الاستخدام في هذه الخلايا تثير مخاوف بيئية وصحية بسبب محتواها من الكاديوم. تبحث هذه الأطروحة في أداء الخلايا الشمسية CdTe مع طبقات عازلة مختلفة خالية من الكاديوم تعتمد على الكوجينيد الزنك (ZnS، ZnSe، ZnO) باستخدام برنامج المحاكاة العددية Silvaco-Atlas. تمت أولاً دراسة ومحاكاة هيكل مرجعي للخلية للتحقق من صحة المحاكاة ومدى توافق النتائج المتحصل عليها مع النتائج التجريبية والنظرية السابقة لهيكل الخلية الشمسية الأساسي CdS/CdTe، كفاءة التحويل التي تم الحصول عليها هي 22.14٪، بما يتوافق مع النتائج التجريبية والنظرية السابقة. في الخطوة الثانية، من أجل تحسين أداء الخلايا الشمسية CdTe، تم اقتراح استبدال طبقة العازل CdS بـ ZnO و ZnSe و ZnS مما أدى إلى تحسين الكفاءة بنسب 23.04٪ و 23.13٪ و 24.48٪ على التوالي. تم الحصول على أداء عالٍ من خلال المزيد من التحسينات في سماكة الطبقتين الماصة والعازلة وكثافات التطعيم بتحقيق أفضل كفاءة بنسبة 25.23٪ و 25.04٪ للهياكل بالطبقات العازلة على الترتيب ZnS و ZnSe. يُعزى الأداء المتفوق للطبقات العازلة القائمة على الزنك إلى فجوات النطاق الأكبر مقارنة بـ CdS، مما يسمح لمزيد من الفوتونات بالوصول إلى الطبقة الماصة CdTe، وانخفاض قابليتها للتفاعلات الضارة مع الكلور أثناء تصنيع الخلية. توضح هذه النتائج إمكانات الطبقات العازلة لكالكوجينيدات الزنك الخالية من الكاديوم، كبديل عالية الكفاءة وصديقة للبيئة لـ CdS في الخلايا الشمسية ذات الشرائح الرقيقة CdTe. تحفز النتائج إجراء المزيد من الدراسات التجريبية للتحقق من نتائج المحاكاة وتسريع تطوير أجهزة CdTe الكهروضوئية الخالية من الكاديوم لتوليد طاقة نظيفة مستدامة.

الكلمات المفتاحية: النمذجة والمحاكاة، الخلايا الشمسية ذات الشرائح الرقيقة CdTe، كالكوجينيد الزنك، SILVACO، طبقة عازلة؛ كفاءة.

Résumé

Les cellules solaires en couches minces de tellurure de cadmium (CdTe) ont démontré une efficacité élevée et une rentabilité dans la production d'électricité propre. Cependant, la couche tampon de CdS couramment utilisée dans ces cellules pose des problèmes environnementaux et sanitaires en raison de sa teneur en cadmium. Cette étude examine les performances des cellules solaires CdTe avec diverses couches tampons à base de chalcogénures de zinc sans Cd (ZnO, ZnSe, ZnS) en utilisant des simulations numériques avec le logiciel Silvaco-Atlas. La structure de base de la cellule solaire CdS/CdTe a d'abord été validée, donnant un rendement de conversion de 22,14%, en accord avec les résultats expérimentaux et théoriques précédents. Le remplacement de la couche tampon CdS par ZnO, ZnSe et ZnS a permis d'améliorer le rendement de 23,04%, 23,13% et 24,48% respectivement. Une optimisation supplémentaire des épaisseurs et des densités de dopage de la couche absorbante et de la couche tampon a permis d'atteindre les meilleurs rendements de 25,23% et 25,04% pour les couches tampons ZnS et ZnSe. Les performances supérieures des couches tampons à base de Zn sont attribuées à leurs plus grands gaps par rapport à CdS, permettant à plus de photons d'atteindre la couche absorbante CdTe, et à leur susceptibilité réduite aux interactions néfastes avec le chlore pendant la fabrication des cellules. Ces résultats démontrent le potentiel des couches tampons de chalcogénure de zinc sans Cd, en tant qu'alternatives à haut rendement et respectueuses de l'environnement au CdS dans les cellules solaires en couches minces de CdTe. Les résultats motivent d'autres études expérimentales pour valider les résultats de simulation et accélérer le développement de dispositifs photovoltaïques CdTe sans Cd pour une production d'énergie propre et durable.

Mots clés: Modélisation et Simulation, Cellule Solaire en Couches Minces, CdTe, Chalcogénure de Zinc, SILVACO, Couche tampon, Efficacité.

Abstract

Cadmium Telluride (CdTe) thin film solar cells have demonstrated high efficiency and cost-effectiveness in generating clean electricity. However, the commonly used CdS buffer layer in these cells poses environmental and health concerns due to its cadmium content. This study investigates the performance of CdTe solar cells with various Cd-free zinc chalcogenide-based buffer layers (ZnO, ZnSe, ZnS) using numerical simulations with the Silvaco-Atlas software. The baseline CdS/CdTe solar cell structure was first validated, yielding a conversion efficiency of 22.14%, in good agreement with previous experimental and theoretical results. Replacing the CdS buffer layer with ZnO, ZnSe, and ZnS, resulted in improved efficiencies of 23.04%, 23.13%, and 24.48%, respectively. Further optimization of the absorber and buffer layer thicknesses and doping densities enabled achieving best efficiencies of 25.23% and 25.04% for the ZnS and ZnSe buffer layers. The superior performance of the Zn-based buffers is attributed to their larger bandgaps compared to CdS, allowing more photons to reach the CdTe absorber layer, and their reduced susceptibility to detrimental interactions with chlorine during cell fabrication. These findings demonstrate the potential of Cd-free zinc chalcogenide buffer layers, as high-efficiency and environmentally friendly alternatives to CdS in CdTe thin film solar cells. The results motivate further experimental studies to validate the simulation outcomes and accelerate the development of Cd-free CdTe photovoltaic devices for sustainable clean energy generation.

Key words: Modeling and Simulation, Thin film Solar Cell, CdTe, Zinc Chalcogenide, SILVACO, Buffer layer, Efficiency.

Table of contents

Dedication.....	I
Acknowledgements.....	II
Abstract.....	V
Table of contents.....	VI
List of figures.....	IX
List of tables.....	XI
General Introduction.....	1
References.....	6
Chapter I Generalities on photovoltaic cells.....	8
I.1 Introduction.....	9
I.2 Introduction to Material Environments.....	9
I.2.1 Conductors.....	9
I.2.2 Insulators.....	10
I.2.3 Semiconductors.....	10
I.3 Intrinsic Semiconductors.....	10
I.4. Extrinsic Semiconductors.....	11
I.5 PN junction.....	13
I.5.1 Heterojunction.....	14
I.6 Solar Energy.....	15
I.7 Solar Radiation.....	15
I.8 History of Photovoltaics.....	17
I.9 Principle of Photovoltaic Conversion.....	18
I.10 Photovoltaic Cell Technologies.....	19
I.10.1 First Generation.....	20
I.10.2 Second Generation.....	21
I.10.3 Third Generation.....	24
I.10.4. Fourth Generation.....	25
I.11 Physical Parameters of a Solar Cell.....	27
I.12 Conclusion.....	30
References.....	31

Chapter II Properties of thin-film solar cell materials based on CdTe	32
II.1 Introduction.....	33
II.2 CdTe-based thin film solar cells	33
II.3 Different components of a CdTe-based thin film solar cells	36
II.3.1 The substrate	38
II.2.2 The front contacts	40
II. 3.3 Buffer Layer.....	41
II.3.4 The Absorber Layer	44
II.3.5 The Back Contact.....	45
II.4 Conclusion	46
References	47
Chapter III Description of the Silvaco-Atlas simulation software	50
III.1 Introduction	51
III.2 Silvaco Overview	51
III.3 Presentation of Silvaco-Atlas Software	52
III.4 The main groups and categories of commands and instructions of Silvaco-Atlas	54
III.5 Structure Determination	55
III.5.1 Mesh Determination	57
III.5.2 Determination of regions (layers) and names of materials	58
III.5.3 Determination of electrodes.....	58
III.5.4 Determination of doping.....	59
III.6 Determination of materials and models.....	60
III.6.1 Determination of materials	60
III.6.2 Determination of models	60
III.6.3 Determination of Defects (traps) and interfaces	61
III.6.4 Determination of the solar spectrum	61
III.7 Determination of the numerical calculation method	61
III.7.1 Determination of the solution	61
III.7.2 Analysis of results	61
III.8 Conclusion	62
References	63
Chapter IV Results and discussion	64
IV.1 Introduction	65

IV.2 Conceptual and Numerical Model.....	66
IV.3 Design and Material Parameters of CdTe Thin Film Solar Cells.....	68
IV.4 Discussion and Analysis of Results.....	69
IV.4.1 Numerical Simulation of the CdTe Solar Cell	69
IV.4.2 Influence of Different Buffer Layers.....	70
IV.4.3 Correlation Between Buffer Layer Characteristics and CdTe Cell Efficiency	72
IV.4.4 Impact of Absorber Layer Thickness Variation	75
IV.4.5 Comparative Performance Analysis of Optimized CdTe Cell with Various Buffer Layers	76
IV.4.6 Effect of Operating Temperature on the Performance of Optimized CdTe Cell	78
IV.5 Conclusion.....	81
References	82
General Conclusion	85

List of figures

Figure I.1: Energy band structure of materials: Insulators, Semiconductors, and Metals.....	9
Figure I.2: Populations of carriers in the intrinsic semiconductor and Fermi level.	11
Figure I.3: Release of an electron by the phosphorus atom and band diagram.....	12
Figure I.4: Hole release by the boron atom and band diagram.....	13
Figure I.5: Structure of a PN junction (on the left), its band diagram (on the right).....	14
Figure I.6: Solar irradiance spectrum above atmosphere and at Earth surface	16
Figure I.7: Schematic of the Principle of Photovoltaic Conversion.	19
Figure I.8: Different generations of Photovoltaic cells	20
Figure I.9: Crystalline silicon cell	21
Figure I.10: Absorption of a photon in a semiconductor material; (a): direct band gap structure and (b): indirect band gap structure.....	22
Figure I.11: Amorphous silicon solar cell.	23
Figure I.12: Schematic representation of a typical thin-film-based solar cell.....	24
Figure I.13: NREL Best Research-Cell Efficiencies chart	26
Figure I.14. I-V characteristics of a solar cell	28
Figure II.1 Crystal structure (zinc blend cubic) of CdTe	34
Figure II.2: The CdTe/CdS solar cell	37
Figure II.3: Transmittance spectra of commonly used substrates such as soda-lime glass (SLG) and polyimide in CdTe-based solar cells.....	39
Figure II.4: Illustrates the transmittance spectra of SLG, coated solely with FTO or ITO, and SLG coated with FTO or ITO coupled with ZnO serving as a HRT layer	40
Figure II.5: The two types of CdS lattice structure (a) cubic zinc blende structure of sphalerite (b) hexagonal wurtzite structure	42
Figure II.6: Transmittance spectra of sputtered CdS film : (a) prepared by CSS in Ar + O ₂ atmosphere: (1) as-deposited, (2) after annealing for 30 min at 420 °C in 400 mbar of Ar containing 20% of H ₂ ; (b) 80 nm thick sputtered CdS film: (1) deposited in pure Ar and (2) deposited in Ar + CHF ₃	43
Figure III.1: Types of input and output information of Atlas	53
Figure III.2: The groups or categories of command logic of Silvaco-Atlas programming	54

Figure III.3: The DeckBuild simulation window of Silvaco-Atlas software displaying some constructive commands of our simulated CdTe solar cell before the start of command executions.55

Figure III.4: The DeckBuild simulation window of Silvaco-Atlas software displaying some constructive commands of our simulated CdTe solar cell after the execution of the commands has started.56

Figure III.5: The mesh of our CdTe solar cell structure displayed by the Tonyplot window of the Silvaco-Atlas software.....57

Figure III.6: The regions and materials for each region of our CdTe solar cell displayed by Silvaco-Atlas software.....58

Figure III.7: The doping density distribution for each region of our CIGS solar cell structure displayed by Silvaco-Atlas.59

Figure III.8: The current-voltage curve of our basic CdTe solar cell displayed by the TonyPlot window of the Silvaco-Atlas software.....62

Figure VI.1: Schematic representation of the proposed CdTe/CdS thin film solar cell structure..67

Figure VI.2: Current density-voltage (J-V) characteristics of the CdTe solar cell.....69

Figure VI.3: Comparative analysis of J-V characteristics of CdTe solar cells incorporating various buffer layers, including CdS, ZnSe, ZnO, and ZnS.....70

Figure VI.4: Investigation of the influence of buffer layer thickness on CdTe solar cell performance parameters: (a) J_{SC} (b) V_{oc} (c) Fill factor FF (d) Efficiency η72

Figure VI.5: Evaluation of CdTe solar cell performance parameters as a function of donor defect density (N_D): (a) J_{SC} (b) V_{oc} (c) Fill factor FF (d) Efficiency η73

Figure VI.6: Examination of the impact of absorber layer thickness on CdTe solar cell performance parameters: (a) J_{SC} (b) V_{oc} (c) Fill factor FF (d) Efficiency η74

Figure VI.7: Current-voltage characteristics of the optimized CdTe solar cells.76

Figure VI.8: Assessment of the effect of operating temperature on CdTe solar cell performance parameters: (a) J_{SC} (b) V_{oc} (c) Fill factor FF (d) Efficiency η78

List of tables

Table II.1 Material properties of CdTe	33
Table VI.1 Material properties and parameters employed in the numerical simulation of CdTe thin-film solar cells.....	68
Table VI.2 Comparative of CdTe/CdS solar cells photovoltaic performance parameters between different results.....	69
Table VI.3 Numerically simulated photovoltaic performance parameters of CdTe cells incorporating various buffer layers.....	71
Table VI.4 Comparison between suggested structure and previous works.....	77

General Introduction

Amidst escalating global energy demands driven by population expansion and the economic ascension of developing nations, the prevailing reliance on non-renewable energy sources, including oil, natural gas, coal, and uranium, poses substantial environmental and geopolitical challenges. These traditional energy vectors are substantial contributors to anthropogenic greenhouse gas emissions, exacerbating global climate change. Furthermore, the finite nature of fossil fuel reserves fails to align with the surging global energy requirements, while the heterogeneous distribution of these resources fosters geopolitical instability and conflicts. Such dynamics underscore the imperative for a transition to cleaner, more sustainable energy alternatives to fossil and nuclear sources. In this context, photovoltaic solar energy emerges as a paramount solution amidst the spectrum of renewable energy technologies. Photovoltaic technology, characterized by its non-polluting and silent operational nature, enables the direct conversion of solar radiation into electrical energy through a mechanism known as the "Photovoltaic Effect", facilitated by devices termed "Solar Cells". This approach not only offers a viable pathway to mitigate the environmental footprint of energy production but also holds the potential to address the energy security concerns presented by the dwindling and unevenly distributed reserves of conventional energy sources. One of the main obstacles for photovoltaic panels to become more popular is the cost per watt of electricity produced by them, which in most cases is non-competitive with that produced by conventional methods. Solar cells are currently the subject of multiple research efforts aimed at achieving the best balance between energy efficiency and cost. Despite crystalline silicon forming the basis of over 80% of commercial photovoltaic (PV) modules, they exhibit limitations such as substantial material consumption and reduced cost-effectiveness [1]. Thin-film PV technologies have significantly mitigated active material consumption in solar cells, consequently enhancing cost-effectiveness. Additionally, these technologies have achieved higher efficiencies compared to conventional silicon cells [2]. Consequently, thin-film cells have become the preferred alternative in contemporary solar cell development initiatives, given their notable advantages over their bulky and more expensive silicon counterparts. The primary thin-film technologies deployed in photovoltaic systems encompass CIGS, a-Si, and CdTe as absorber layers, all of which have currently reached the commercialization stage [1]. Among these technologies, CdTe photovoltaic stands out as the most cost-effective option [1,3]. CdTe technology not only offers superior cost-efficiency but also commands a

significant market share in comparison to a-Si and CIGS technologies. The efficiency of CdTe surpasses that of a-Si and closely approaches that of CIGS [2]. Furthermore, CdTe cells present an array of advantages, including reliability [3], flexibility [4], long-term stability [5,6], simplicity, and cost-effectiveness [6,7]. As an absorber material, CdTe emerges as a highly promising choice, characterized by its straightforward binary compound structure featuring wurtzite and zinc blende structures [5]. Notably, CdTe exhibits a high absorption coefficient (exceeding 10^5 cm^{-1}), boasts a direct band gap (E_g) of 1.5 eV which is very close to the ideal band gap for solar cells, and p-type conductivity [5,8–12]. Recent advancements in CdTe solar cells have garnered considerable attention. Over the last few years, significant efficiency enhancements have been achieved. A notable redesign led to a CdS/CdTe solar cell achieving a 22.1% conversion efficiency [13]. Similarly, Mrinmoy et al. (2017) reached a 22.51% efficiency by integrating a BSF (back surface field: Copper Telluride (Cu_2Te)) beneath the absorber layer, effectively mitigating recombination losses [14]. Furthermore, numerical studies by Shah et al. reported a conversion efficiency of 19.18% [15]. Another study by Tinedert et al. reported a theoretical efficiency of 23.01% for a CdS/CdTe solar cell design [16].

CdS is commonly used as a buffer layer in CdTe thin-film solar cells. However, its band gap, approximately 2.4–2.5 eV, does not ideally suit solar cell performance, especially within the 400 nm to 500 nm short wavelength range, due to optical absorption losses. Moreover, the toxicity of Cd and the classification of CdS as a carcinogen pose significant health and environmental concerns [17,18]. Consequently, ongoing intensive research focuses on alternative buffer layers, concentrating on wide band gap materials such as ZnO, ZnS, and ZnSe. These materials, being n-type semiconductors, are capable of forming a p–n junction with the CdTe absorber layer [19]. Their larger band gaps compared to CdS potentially allow for enhanced photon transmission to the absorber layer.

Chlorine-based treatments used during the fabrication process can improve the electronic and doping properties of CdTe cells. However, their interaction with CdS may result in the formation of insulating CdCl_2 precipitates [20]. Zinc chalcogenides, being less reactive with chlorine, can effectively prevent the formation of cadmium chloride and may

also mitigate interface diffusion issues into the CdTe/CdS layer, hence potentially reducing long-term solar cell degradation.

The exploration of alternative buffer materials for CdTe solar cells has yielded varying efficiencies. Jannatun et al. reported a conversion efficiency of 17.29% utilizing 3C–SiC as a non-toxic buffer layer [21]. Other studies have documented efficiency improvements to 18.7% with the replacement of CdS by $Mg_xZn_{1-x}O$ (MZO) [22]. An optimized CdZnS layer enhanced simulated efficiency from 15.42% to 17.71%, in comparison to the sole use of CdS [23].

This thesis investigates the performance of CdTe solar cells with various Cd-free zinc chalcogenide-based buffer layers (ZnO, ZnSe, ZnS) using numerical simulations with the Silvaco-Atlas software.

This manuscript consists of four chapters. It begins with a *general introduction* in which the problem and its origin are presented.

Chapter I discusses the concept of semiconductors, the characteristics of solar radiation, the description of photovoltaic conversion, solar cells, and their four generations, as well as their photovoltaic parameters.

In the *second chapter*, we present the CdTe thin-film solar cell and its many advantages that led us to choose this cell. Understanding the materials composing the CdTe thin-film solar cell is necessary to improve this cell. That is why the layers and material components of this solar cell are detailed.

In the *third chapter*, we will present the physical models of the CdTe solar cell and the TCAD-Silvaco used for simulation.

In the *fourth chapter*, we will present in detail the simulation and discussion of the results of our simulated CdTe solar cell. First, a basic CdTe solar cell is simulated at a room temperature of 300 K using the Atlas-Silvaco simulation software. We validate the model and the parameters used for our CdTe solar cell by comparing the main photovoltaic performance parameters, such as short-circuit current density (J_{SC}), open-circuit voltage (V_{OC}), fill factor (FF), and conversion efficiency (η), of our basic CdTe solar cell with those of recent experimental and theoretical studies. Our study is a contribution where we examined the effect of the alternative Cd-free zinc chalcogenide-based (Zn(O,S,Se)) buffer layers, not or less

studied, on the performance of the CdTe-based thin-film solar cells. Finally, we optimize the temperature of our CdTe solar cell by varying the temperature between 260 K and 340 K to see its effects on the photovoltaic performance of the cell. The key findings obtained are summarized in *the general conclusion*.

References

- [1] T.D. Lee, A.U. Ebong, A review of thin film solar cell technologies and challenges, *Renew. Sustain. Energy Rev.* 70 (2017) 1286–1297. <https://doi.org/10.1016/j.rser.2016.12.028>.
- [2] M.A. Green, E.D. Dunlop, J. Hohl-Ebinger, M. Yoshita, N. Kopidakis, X. Hao, Solar cell efficiency tables (version 63), *Prog. Photovoltaics Res. Appl.* 30 (2022) 3–12. <https://doi.org/10.1002/pip.3506>.
- [3] O. Rashwan, G. Sutton, L. Ji, Optical modeling of periodic nanostructures in ultra-thin CdTe solar cells with an electron reflector layer, *Superlattices Microstruct.* 149 (2021) 106757. <https://doi.org/10.1016/j.spmi.2020.106757>.
- [4] J. Ramanujam, D.M. Bishop, T.K. Todorov, O. Gunawan, J. Rath, R. Nekovei, E. Artegiani, A. Romeo, Flexible CIGS, CdTe and a-Si: H based thin film solar cells: A review, *Prog. Mater. Sci.* 110 (2020) 100619.
- [5] A. (Antonio) Luque, S. Hegedus, *Handbook of photovoltaic science and engineering*, Wiley, 2011.
- [6] R. Noufi, K. Zweibel, High-efficiency CdTe and CIGS thin-film solar cells: highlights and challenges, in: *2006 IEEE 4th World Conf. Photovolt. Energy Conf.*, IEEE, 2006: pp. 317–320.
- [7] H.P. Mahabaduge, W.L. Rance, J.M. Burst, M.O. Reese, D.M. Meysing, C.A. Wolden, J. Li, J.D. Beach, T.A. Gessert, W.K. Metzger, High-efficiency, flexible CdTe solar cells on ultra-thin glass substrates, *Appl. Phys. Lett.* 106 (2015).
- [8] M.A. Islam, K.S. Rahman, K. Sobayel, T. Enam, A.M. Ali, M. Zaman, M.D. Akhtaruzzaman, N. Amin, Fabrication of high efficiency sputtered CdS: O/CdTe thin film solar cells from window/absorber layer growth optimization in magnetron sputtering, *Sol. Energy Mater. Sol. Cells.* 172 (2017) 384–393.
- [9] A. Romeo, E. Artegiani, D. Menossi, Low substrate temperature CdTe solar cells: A review, *Sol. Energy.* 175 (2018) 9–15.
- [10] Y.G. Fedorenko, J.D. Major, A. Pressman, L. Phillips, K. Durose, Electronic properties of CdTe/CdS solar cells as influenced by a buffer layer, *MRS Adv.* 1 (2016) 937–942.
- [11] A.A. Al-mebir, P. Harrison, A. Kadhim, G. Zeng, J. Wu, Effect of in situ thermal annealing on structural, optical, and electrical properties of CdS/CdTe thin film solar cells fabricated by pulsed laser deposition, *Adv. Condens. Matter Phys.* 2016 (2016).
- [12] Z. Allam, C. Boudaoud, A. Soufi, B. Bouchachia, *Performance Parameters of CdTe/CdS Solar Cell with Deferent Contact Schottky*, Springer International Publishing, 2022. https://doi.org/10.1007/978-3-030-92038-8_78.
- [13] M.A. Green, E.D. Dunlop, J. Hohl-Ebinger, M. Yoshita, N. Kopidakis, K. Bothe, D. Hinken, M. Rauer, X. Hao, Solar cell efficiency tables (Version 60), *Prog. Photovoltaics Res. Appl.* 30 (2022) 687–701. <https://doi.org/10.1002/pip.3595>.
- [14] D.M. Dey, M. Dey, M.A. Matin, N. Amin, High efficient and stable ultra-thin cdte solar cell with a potential copper telluride BSF, *Proc. 9th Int. Conf. Electr. Comput. Eng. ICECE 2016.* (2017) 590–593. <https://doi.org/10.1109/ICECE.2016.7853989>.
- [15] D.K. Shah, D. KC, M. Muddassir, M.S. Akhtar, C.Y. Kim, O.B. Yang, A simulation approach for investigating the performances of cadmium telluride solar cells using doping concentrations, carrier lifetimes, thickness of layers, and band gaps, *Sol. Energy.* 216 (2021) 259–265. <https://doi.org/10.1016/j.solener.2020.12.070>.

- [16] I.E. Tinedert, F. Pezzimenti, M.L. Megherbi, A. Saadoune, Design and simulation of a high efficiency CdS/CdTe solar cell, *Optik (Stuttg)*. 208 (2020). <https://doi.org/10.1016/j.ijleo.2019.164112>.
- [17] A. Romeo, E. Arregiani, Cdte-based thin film solar cells: Past, present and future, *Energies*. 14 (2021). <https://doi.org/10.3390/EN14061684>.
- [18] S. Tobbeche, S. Kalache, M. Elbar, M.N. Kateb, M.R. Serdouk, Improvement of the CIGS solar cell performance: structure based on a ZnS buffer layer, *Opt. Quantum Electron*. 51 (2019). <https://doi.org/10.1007/s11082-019-2000-z>.
- [19] S.O. Oyedele, B. Aka, Numerical Simulation of Varied Buffer Layer of Solar Cells Based on Cigs, *Model. Numer. Simul. Mater. Sci*. 07 (2017) 33–45. <https://doi.org/10.4236/mnsms.2017.73003>.
- [20] R.K.K.G.R.G. Kumarasinghe, P.K.K. Kumarasinghe, R.P. Wijesundera, B.S. Dassanayake, Thermally evaporated CdS/CdTe thin film solar cells: Optimization of CdCl₂ evaporation treatment on absorber layer, *Curr. Appl. Phys*. 33 (2022) 33–40. <https://doi.org/10.1016/J.CAP.2021.10.011>.
- [21] J.N. Sameera, M.A. Islam, S. Islam, T. Hossain, M.K. Sobayel, M. Akhtaruzzaman, N. Amin, M.J. Rashid, Cubic Silicon Carbide (3C–SiC) as a buffer layer for high efficiency and highly stable CdTe solar cell, *Opt. Mater. (Amst)*. 123 (2022). <https://doi.org/10.1016/J.OPTMAT.2021.111911>.
- [22] A.H. Munshi, J.M. Kephart, A. Abbas, T.M. Shimpi, K.L. Barth, J.M. Walls, W.S. Sampath, Polycrystalline CdTe photovoltaics with efficiency over 18% through improved absorber passivation and current collection, *Sol. Energy Mater. Sol. Cells*. 176 (2018) 9–18. <https://doi.org/10.1016/j.solmat.2017.11.031>.
- [23] X.B. Xu, X.Y. Wang, W.P. Gu, S. Quan, Z. Zhang, Study on influences of CdZnS buffer layer on CdTe solar cells, *Superlattices Microstruct*. 109 (2017) 463–469. <https://doi.org/10.1016/j.spmi.2017.05.033>.

Chapter I Generalities on photovoltaic cells

I.1 Introduction

Photovoltaic solar energy is electric power produced from solar radiation through panels; the solar cell is the fundamental electronic component. Suitable materials for photovoltaics include semiconductors. Incident photons from solar radiation are absorbed by the semiconductor, creating electron-hole pairs that contribute to the generation of electric current.

In this chapter, we introduce the concept of semiconductors and the characteristics of solar radiation, the description of photovoltaic conversion, and the study of the physical phenomena occurring, such as the generation of photo-carriers and their recombination in a semiconductor. We also describe the operating principles and the current-voltage characteristics of solar cells, as well as their photovoltaic parameters.

I.2 Introduction to Material Environments

Based on electrical properties, materials are classified into three categories: conductors, insulators, and semiconductors, see **Figure I.1**.

I.2.1 Conductors

Metals such as iron (Fe), copper (Cu), gold (Au), silver (Ag), and aluminum (Al) are electrical conductors. The presence of free electrons in the peripheral layer (density $n \approx 10^{22}$ to 10^{23} e/cm³) is the origin of electrical conductivity. At room temperature, the resistivity ρ of conductors is very low ($\rho < 10^8 \Omega \cdot \text{cm}$).

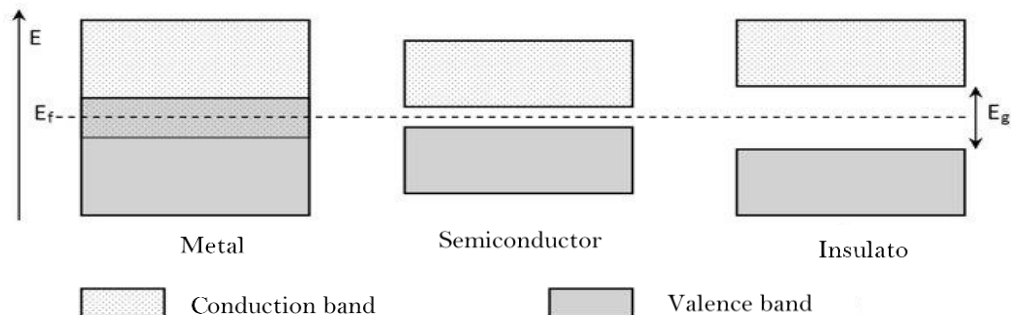


Figure I.1: Energy band structure of materials: Insulators, Semiconductors, and Metals.

I.2.2 Insulators

Materials that have a resistivity p higher than $10^8 \Omega \cdot \text{cm}$ are insulators (non-conducting materials of electric current). Among these materials: glass, mica, silica (SiO_2), and carbon (Diamond). Therefore, the conductivity of insulators is very low ($\sigma = 1/p$).

I.2.3 Semiconductors

This class of materials is between metals (conductors) and insulators (non-conductors). The resistivity p varies from 10^{-3} to 10^4 . Electrical conduction is done by electrons and holes, or preferably by one or the other type of carrier. A semiconductor can either be pure (intrinsic) or doped with impurities (extrinsic) that allow to control its resistivity. If we take, for example, pure enough Silicon and add a Boron or Phosphorus atom for every 10^5 atoms of Silicon, its resistivity goes from 10^3 to about $10^{-2} \Omega \cdot \text{cm}$. The **Figure I.1** represents the energy band structures of the insulator, the semiconductor, and the metal.

I.3 Intrinsic Semiconductors

These are very pure and well-crystallized semiconductors (displaying a periodic crystalline network) with a very low impurity rate (less than one impurity atom for 10^{13} atoms of the semiconductor element). They behave like insulators at very low temperatures and their conductivities increase with temperature. At constant temperature, a balance is established (**Figure.I.2**) between the phenomena of thermal ionization and recombination, free electrons and silicon ions appear in equal quantities. The concentration of free electrons n and free holes p are equal to n_i , the intrinsic concentration [1].

The total densities (n electrons. cm^{-3} in the conduction band and p holes. cm^{-3} in the valence band) are expressed according to the laws:

$$n = N_c \exp\left(-\frac{\Delta E_n}{KT}\right) \quad (\text{I.1})$$

$$p = N_v \exp\left(-\frac{\Delta E_p}{KT}\right) \quad (\text{I.2})$$

Where N_c and N_v are respectively the effective density of electron states in the conduction band and the effective density of hole states in the valence band. These two coefficients evolve with temperature according to a $T^{3/2}$ law.

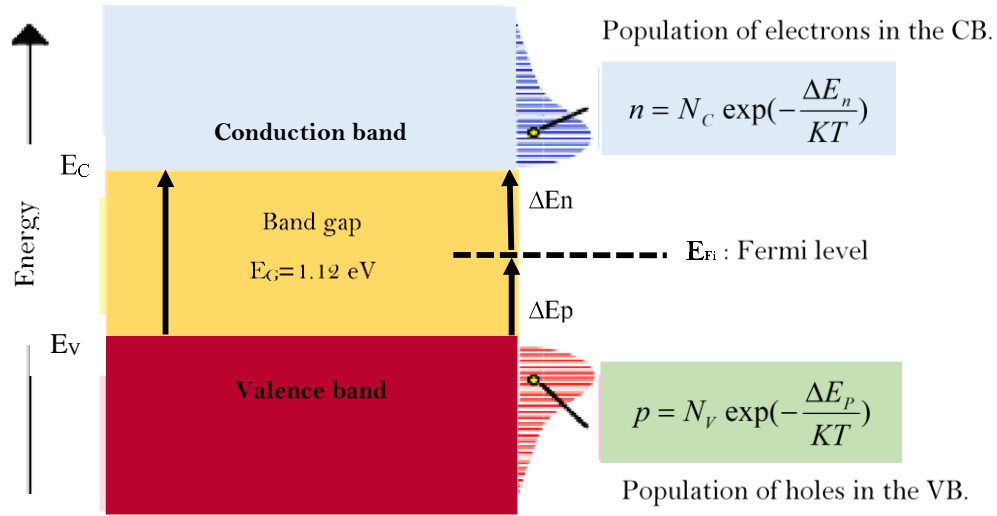


Figure I.2: Populations of carriers in the intrinsic semiconductor and Fermi level.

ΔE_n and ΔE_p represent two energy differences related to a so-called Fermi level that indicates the population differences between electrons and holes.

The intrinsic concentration of free electrons and free holes per cm^3 depends on the height of the forbidden band and the temperature T according to the law:

$$n = p = n_i = AT^{\frac{3}{2}} \cdot \exp\left(-\frac{E_g}{2KT}\right) \quad (\text{I.3})$$

A: material constant

E_g : Height of the forbidden band (eV)

K: Boltzmann constant $8.6 \times 10^{-5} \text{ eV K}^{-1}$

T: absolute temperature (K)

I.4. Extrinsic Semiconductors

To enhance the conductivity of semiconductors and make them functional, several impurities (foreign atoms) are introduced into the crystalline structure. The process of impurity introduction (through diffusion, epitaxy, or ionic implantation) is termed doping, which leads to the creation of doped or extrinsic semiconductors. The usual ratio for doping is

one impurity atom for every 10^6 to 10^9 semiconductor atoms. This represents an impurity density in the order of 10^{19} to 10^{22} cm^{-3} . Consequently, the conductivity of the doped semiconductor is determined by the nature and concentration of impurity atoms. The impurity atoms are chemical elements from either the third column (Group III: B, Boron; In, Indium), or the fifth column (Group V: P, Phosphorus; As, Arsenic; Sb, Antimony).

a. N-Type Semiconductors

An N-type semiconductor is obtained by injecting atoms that possess 5 electrons in their outer shell (phosphorus or arsenic) into the silicon crystal (**Figure I.3**).

At ordinary temperatures, almost all donor atoms are ionized. If N_D is the concentration of donor atoms, they will release $n = N_D$ free electrons. The concentrations of free electrons (n) and free holes (p) are connected by the law of mass action :

$$n \cdot p = n_i^2 \quad (\text{I.4})$$

Electrons are the majority carriers and the holes are the minority carriers. The Fermi-level indicator E_{Fn} therefore moves from the middle of the bandgap (E_{Fi}) to the conduction band in such a way that:

$$\Delta E_n = KT \cdot \ln\left(\frac{N_D}{n_i}\right) = E_{Fn} - E_{Fi} \quad (\text{I.5})$$

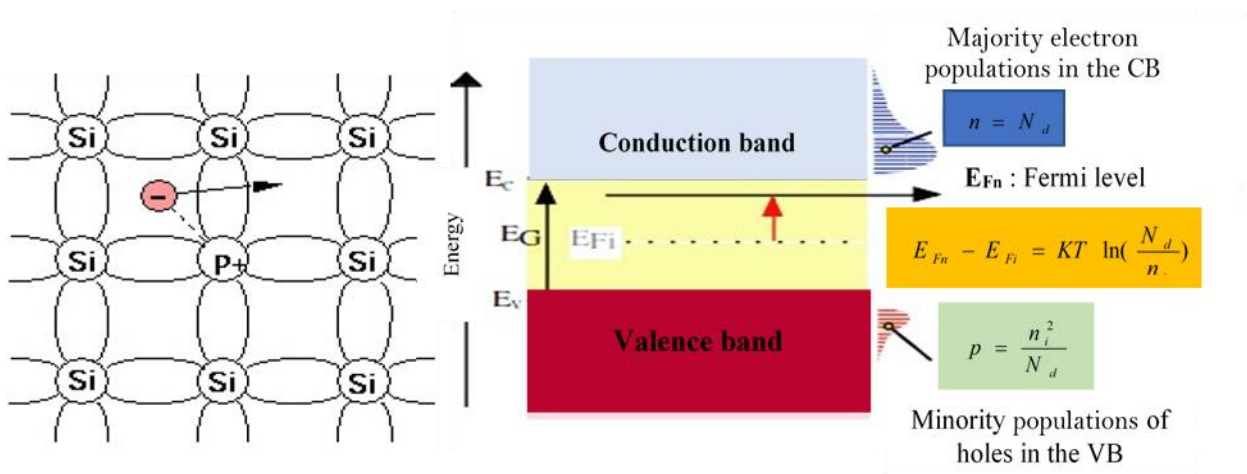


Figure I.3: Release of an electron by the phosphorus atom and band diagram.

b. P-type semiconductors

A P-doped semiconductor is obtained by injecting atoms from the 3rd column (boron, indium) which have three peripheral electrons into the silicon (**Figure I.4**).

At ordinary temperatures, almost all acceptor atoms are ionized. If N_A is the concentration per cm^3 of acceptor atoms, these will release: $p=N_A$ free holes. The concentrations of free electrons (n) and free holes (p) are linked by the law of mass action:

$$n.p = n_i^2 \quad (\text{I.6})$$

Holes are the majority carriers and the electrons are the minority carriers. The Fermi level indicator E_{Fp} moves from the intrinsic level E_{Fi} towards the valence band in such a way that:

$$\Delta E_p = KT \cdot \ln\left(\frac{N_A}{n_i}\right) = E_{Fi} - E_{Fp} \quad (\text{I.7})$$

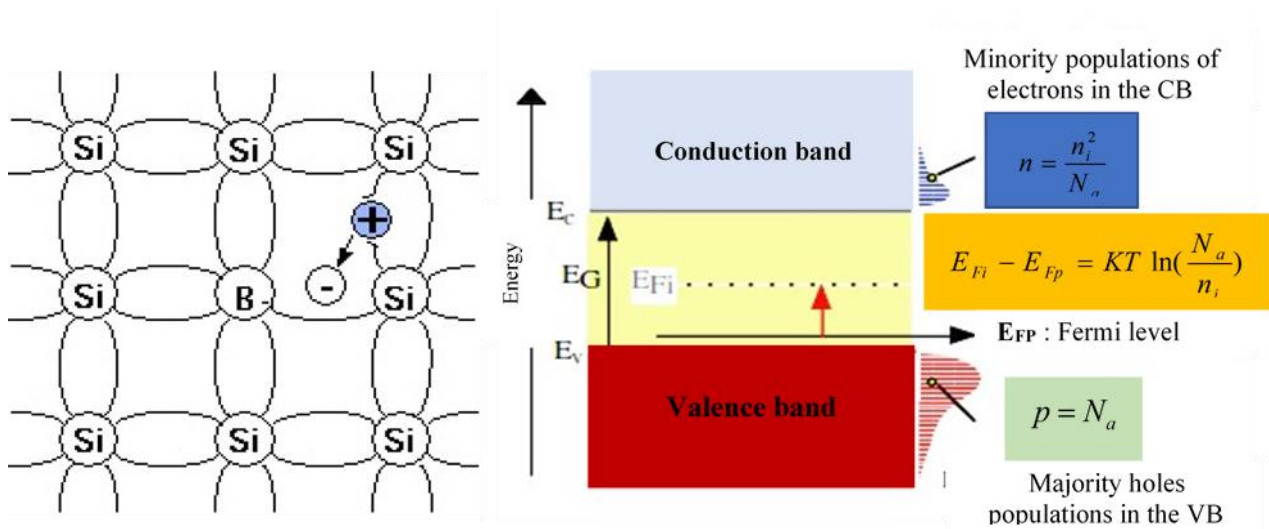


Figure I.4: Hole release by the boron atom and band diagram.

I.5 PN junction

When two P-type and N-type semiconductors are put in contact, a flow of electrons and holes diffuse respectively towards the P and N zones, to equalize the distribution of carrier concentrations in the structure. The holes from the P region will diffuse towards the N region leaving behind ionized atoms, which constitute as many fixed negative charges. The same

happens for the electrons from the N region which diffuse towards the P region leaving behind positive charges. The initially N -doped zone becomes positively charged, and the initially P -doped zone negatively charged. A depletion area also known as 'space charge zone' (**SCZ**) is formed on each side of the interface. An electric field is created in the depletion area, directed from the N -type region towards the P -type region. This field will create a potential barrier, which will prevent the electron and hole carriers from respectively diffusing towards the P and N regions [2,3]. The junctions constituted by bringing into contact two differently doped regions of the same semiconductor, are called 'homojunctions'. However, junctions realized by juxtaposing two different materials are called 'heterojunctions'.

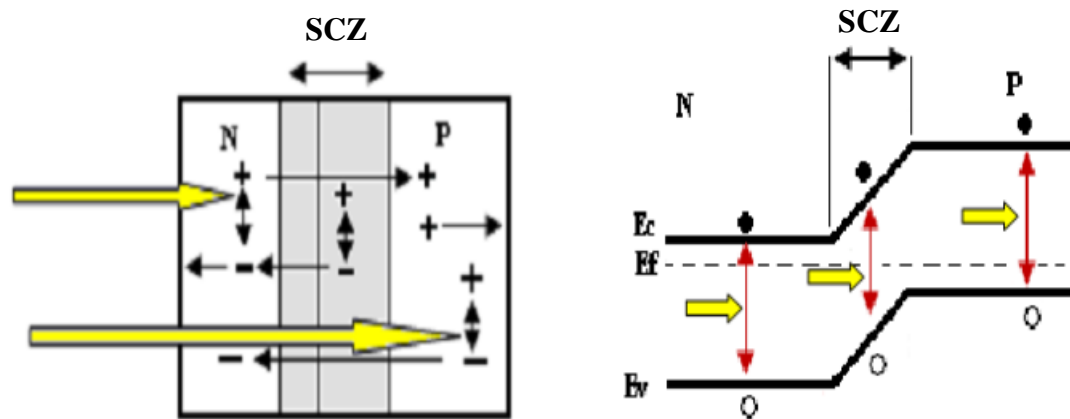


Figure I.5: Structure of a PN junction (on the left), its band diagram (on the right) [1].

I.5.1 Heterojunction

Heterojunctions are formed by adjoining two different semiconductor materials with varying bandgap energies. This results in a junction where the properties of each semiconductor influence the overall behavior of the device, such as its electronic and optoelectronic characteristics. Common materials used to form heterojunctions include combinations of III-V semiconductors (such as GaAs/AlGaAs), II-VI semiconductors (such as CdTe/CdS), and group IV semiconductors (such as Si/Ge). The choice of materials depends on the desired properties and applications.

I.6 Solar Energy

Similar to a nuclear reactor, the sun derives its energy from the fusion of the hydrogen nucleus to form a helium nucleus. This reaction produces an immeasurable amount of energy (to such an extent that the small fraction that we receive each day on Earth, from over 150 million kilometers away, would suffice to meet the energy needs of all humanity for about 30 years). But capturing this energy, as we will see, is not easy. Humans have developed two techniques to harness the sun's energy:

Solar thermal: which involves heating a liquid or gas to store the energy for later use (sanitary water, crop drying, etc.).

Photovoltaic solar: Which uses the ability of semiconductors to convert light energy into electrical energy. Although this conversion is not without losses (the efficiency of photovoltaic is about three times less than that of thermal), it allows for a wider range of applications (transport, powering small devices, etc.).

Solar energy, in particular, seems, at first glance, to be an effective solution for replacing oil. Barrel production is currently peaking and experts believe it will decrease over the next ten years. The European Union has set a target for renewable energies to make up 23% by 2022, and 45% by 2030 [2]. Solar energy production should be one of the most significant, as it has many advantages:

The sun sends to Earth more than 40,000 times the annual fossil energy needs of humanity. That means an inexhaustible energy source that is free and omnipresent. Solar energy can produce both heat (solar thermal) and electricity (photovoltaic solar).

Once the solar panel is installed, the energy costs nothing, even if investment and maintenance represent certain expenditures. Unlike other energy resources, solar energy is decentralized. This also explains why many isolated places already have access to it.

I.7 Solar Radiation

The solar energy harnessed by solar cells exhibits an emission spectrum comparable to a black body at 5800K. Outside the atmosphere, solar radiation has an average power of 1.37

kW/m^2 . However, as it passes through the atmosphere, some of this energy is absorbed by various molecules in the atmosphere, such as oxygen, ozone, and carbon dioxide. At the Earth's surface, solar radiation has a maximum power of about 1 kW/m^2 . Consequently, the solar spectrum obtained at the Earth's surface depends on the atmospheric composition, and particularly on the thickness of the atmosphere the radiation traverses.

To characterize the different incident solar spectra, the AM (Air Mass) parameter has been defined, which characterizes the atmospheric layer traversed by the radiation. Outside of the atmosphere, the AM0 spectrum is used for space applications. At the equator, the radiation crosses a layer of the atmosphere, resulting in the AM1 spectrum. When the radiation makes an angle of 60° with the equator, the AM2 spectrum is observed. The AM1.5 spectrum is defined for radiation making an angle of 41.8° with respect to the equator, which corresponds to radiation traversing 1.5 times the thickness of the atmospheric layer [3]. In these conditions, the intensity of the radiation is normally less than 1000 W/m^2 (approximately 827 W/m^2). The AM1.5 spectrum has become the standard for the standardized testing of solar cells and is thus used in this doctoral thesis. The AM0 and AM1.5G spectra are compared in **Figure I-6**.

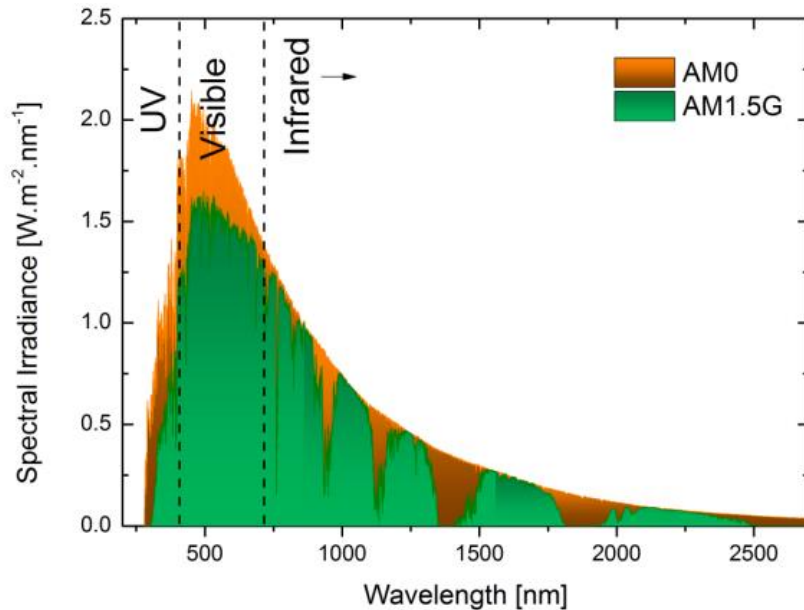


Figure I.6: Solar irradiance spectrum above atmosphere and at Earth surface [3].

I.8 History of Photovoltaics

The photovoltaic effect (or photoelectric effect) is the direct transformation of light energy into electrical energy through the process of absorption of light by matter. In 1839, physicist Antoine Becquerel discovered the photovoltaic effect by demonstrating the appearance of a voltage across two electrodes immersed in a solution electrolytic when exposed to natural light [4]. The term 'photovoltaic' comes from the Greek words 'photos' meaning light and 'volta' after Alessandro Volta, who in 1800 discovered the first battery [5].

In 1875, Werner von Siemens presented an article on the photovoltaic effect in semiconductors before the Berlin Academy of Sciences, but it remained a laboratory curiosity until the Second World War [6].

Charles Fritts developed the first solar cell in 1883 by illuminating a selenium crystal coated with a thin layer of gold with a conversion efficiency of around 1-2%. However, this discovery remained a laboratory curiosity until the Second World War [7].

The photovoltaic effect was not fully understood until 1905 when Einstein and Planck presented the principle of the photon [8]. However, a reasonably efficient solar cell generating a decent amount of power was not developed until 1954, when three American scientists at Bell Labs, Chapin, Pearson, and Prince, developed a silicon-based solar cell with an energy efficiency of 6% [4]. In 1959, the Americans launched a satellite called Vanguard, which was powered by photovoltaic batteries. All major laboratories became interested in this new technology, and in 1960, M. Rodot and H. Valdman developed the first photovoltaic cell at the French National Center for Scientific Research [9].

Following the economic crisis of the 1970s, the sharp increase in oil prices in 1973 and the nuclear accidents at Three Mile Island (USA, 1979) and Chernobyl (USSR, 1986), which reinforced the public's interest in renewable energy sources, programs for connecting solar roofs to the grid were launched in Japan and Germany, and have been rolled out in many countries since then [10]. Since 2001, there has been a rapid growth in the photovoltaic industry, with the installed capacity of the global photovoltaic park being multiplied by six times between the end of 2010 (50 GW) and the end of 2016 (305 GW) [11]. Currently, concentrated solar power, thin-film modules, organic photovoltaics, and perovskite solar cells.

I.9 Principle of Photovoltaic Conversion

The conversion of solar energy into electrical energy is based on the photoelectric effect that is, the ability of photons to create charge carriers (electrons and holes) in a material. When a semiconductor is illuminated with light of the appropriate wavelength, the energy of the photons must be at least equal to the energy gap of the material. The energy of the absorbed photons enables electronic transitions from the valence band to the conduction band of the semiconductor, thereby creating electron-hole pairs. These pairs can contribute to current transport (photoconductivity) through the material when it is biased.

If we illuminate a PN junction, the electron-hole pairs created in the junction's space-charge region are immediately separated by the electric field present in that region and driven into the neutral zones on each side of the junction. If the device is isolated, a potential difference appears across the junction, creating a photovoltage. If it is connected to an external electrical load, a current will flow, even if no voltage is applied to the device depicted in **Figure I.7**. This is the basic principle of a photovoltaic cell.

If each incident photon could inject an electron into the electrical circuit, photovoltaic devices would be extremely efficient. However, in practice, several factors limit photoconversion. The first limitation comes from the wavelength of the incident radiation; the wavelength must be short enough that the photon's energy is greater than that of the gap so it can be absorbed. With a gap of 1.14 eV, monocrystalline silicon absorbs only photons with wavelengths shorter than 1100 nm, with optimal absorption occurring around the gap energy. Given that the solar emission spectrum ranges from 250 to 2000 nm, with an emission peak in the visible range between 500 and 700 nm, only a portion of the radiation is useful for creating charge carriers.

A second limitation arises from the fact that not all photogenerated carriers are collected. After their separation in the space-charge region, electrons and holes must diffuse into the neutral areas of the semiconductor. It is not possible to prevent a certain proportion of these carriers from recombining before they reach the device's contacts, thus affecting the energy conversion efficiency. The recombination rate is higher if the material has structural defects, such as in multicrystalline or amorphous semiconductors, or impurities, like heavily doped or

chemically impure silicon. Besides these fundamental limitations, many other loss factors must also be considered, such as reflected photons, resistive losses, and metallic contacts. Shockley and Queisser have demonstrated that a PN junction solar cell cannot theoretically exceed an efficiency of 31%, corresponding to an electrical power of 190 W/m² [12]. The best laboratory prototypes of single-junction cells have not surpassed an efficiency of 26.8% to date [13].

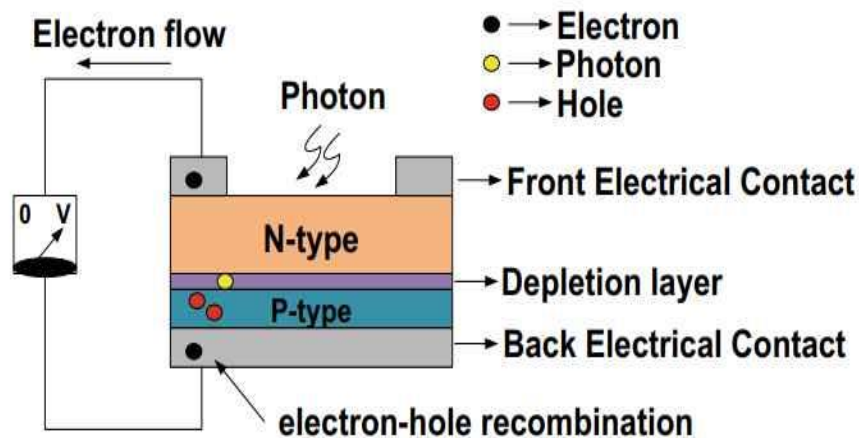


Figure I.7: Schematic of the Principle of Photovoltaic Conversion.

I.10 Photovoltaic Cell Technologies

Over the last ten years, photovoltaics has emerged as a key player in the transition towards alternative energy sources. This progress has been largely due to innovations in both materials and production techniques. Despite these advances, significant obstacles remain in achieving both cleaner and more cost-effective energy from photovoltaics. Current research efforts are concentrated on high-efficiency photovoltaic structures, including multi-junction cells, graphene or intermediate band gap cells, and materials amenable to printing technologies such as quantum dots [14]. The production of photovoltaic cells involves a range of technologies that tailor material properties to enhance the photoelectric conversion efficiency within the various components of the cell.

The development and implementation of novel, non-traditional methods for constructing operational solar cells have resulted in a categorical division of photovoltaic technologies into four principal generations, as depicted in **Figure I.8**[15].

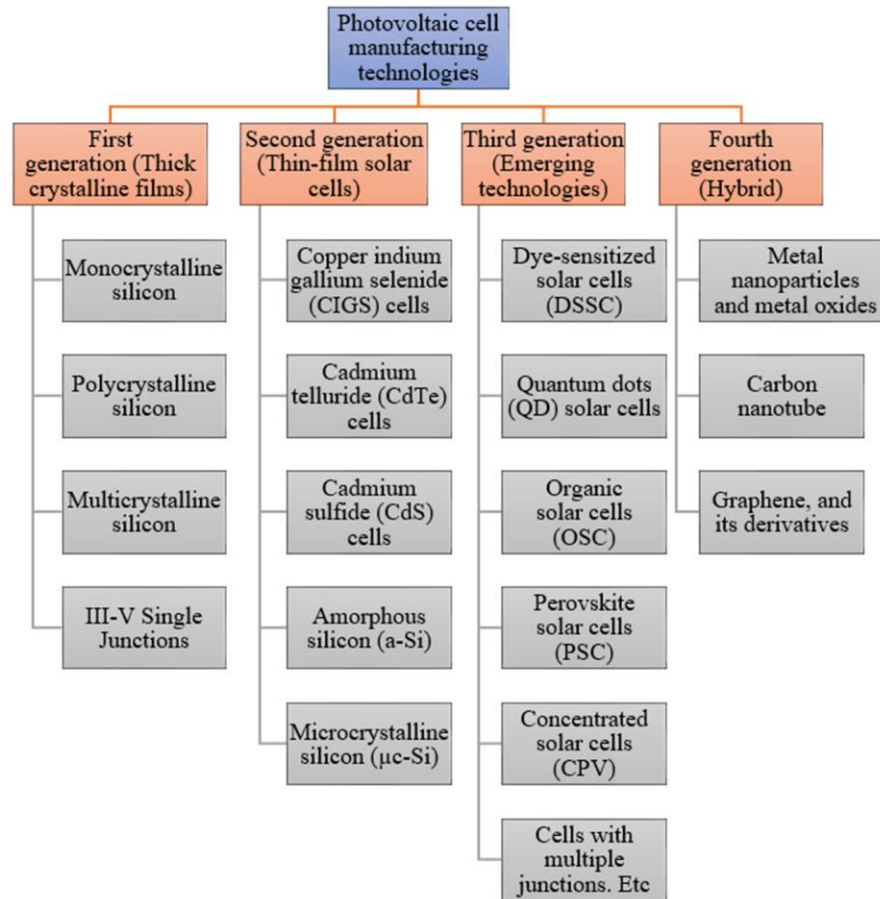


Figure I.8: Different generations of Photovoltaic cells [15]

The categorization of photovoltaic cell technologies into generations narrates the historical development of these cells since their inception. Over the past several decades, four primary generations have been identified:

I.10.1 First Generation

Encompassing technologies based on monocrystalline and polycrystalline silicon as well as gallium arsenide (GaAs). This comprises single-junction or multi-junction cells made of inorganic semiconductors. The most common cells are obtained by cooling molten silicon,

which leads to monocrystalline or polycrystalline silicon solar cells. This monocrystalline silicon cell is composed of a single crystal divided into two layers (see **Figure I.9**). The base materials for such cells are huge silicon crystals specially produced for this purpose, with a size of about 10 cm. These crystals are then cut into wafers, doped, and connected. These cells have energy conversion efficiencies of up to 27.6% in the laboratory [16].

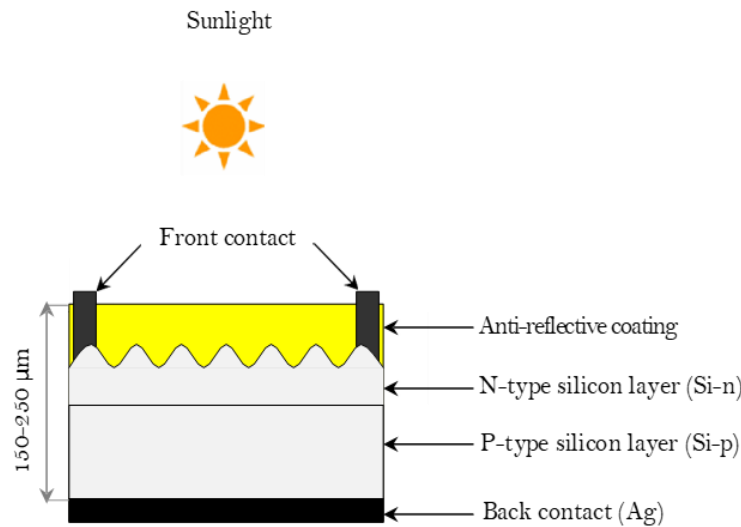


Figure I.9: Crystalline silicon cell

Their advantages include long-term stability, high mobility of charge carriers, and strong spectral absorption, which enables relatively good conversion efficiencies. They currently represent around 85% of the global photovoltaic market [17]. Their drawbacks include costly and energy-intensive production, high weight, and rigidity. Furthermore, the heating phenomena that occur during their operation cause a slight decrease in their energy conversion efficiency.

I.10.2 Second Generation

To reduce material costs and facilitate new applications, a second generation of cells based on thin-film materials was developed. Thin-film cells operate on the principle of using an absorber material with a higher optical absorption coefficient than that of crystalline Si. For this reason, materials with a direct bandgap are typically used (see **Figure I.10**), as opposed to Si, which has an indirect bandgap.

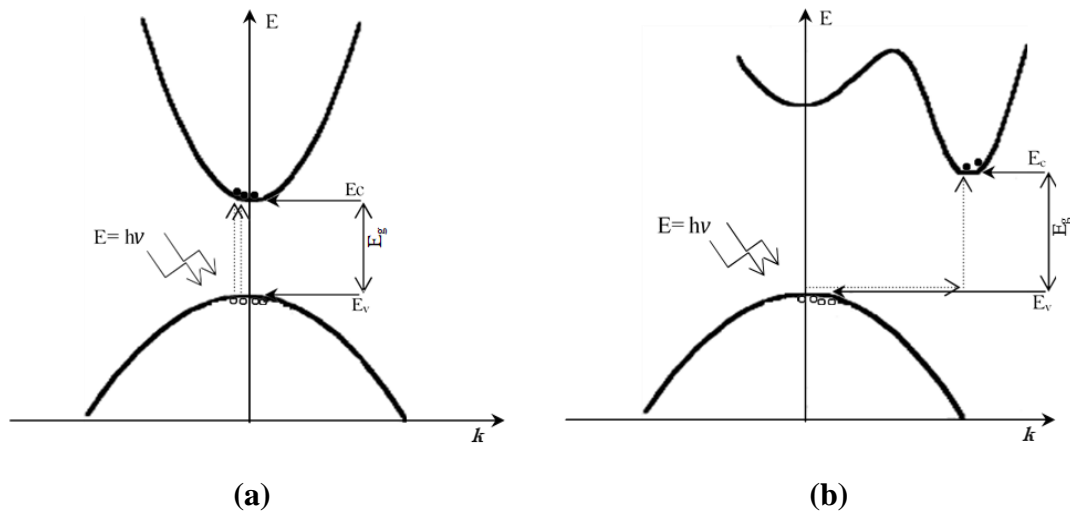


Figure I.10: Absorption of a photon in a semiconductor material; (a): direct band gap structure and (b): indirect band gap structure.

This allows the use of much thinner absorber materials, approximately $2\ \mu\text{m}$ in thickness (100 times thinner than crystalline Si), thereby reducing the amount of raw material required. The main materials used as thin-film absorbers are amorphous Si (a-Si), CdTe, and $\text{Cu}(\text{In}_{1-x}\text{Ga}_x)\text{Se}_2$ (CIGS) and CZTS ($\text{Cu}_2\text{ZnSn}(\text{S},\text{Se})_4$). Thin films consist of a deposit of semiconductor materials on either a rigid or a flexible substrate.

a) Thin-film silicon cell

The combination of silicon and hydrogen has led to the discovery of amorphous silicon (a-Si), a material that is both a semiconductor and disordered, endowed with poor electronic properties but excellent optical ones. Indeed, despite electron mobility within it being much lower than in crystalline silicon, a thickness of less than one micron suffices to absorb the solar spectrum. Although module yields are lower than those of crystalline silicon, this sector tends to develop amid high demand and positions itself after crystalline silicon sectors. The cells based on this type of material are composed of a glass or synthetic material support onto which a thin layer of silicon is deposited (see **Figure I.11**), a process requiring very little energy. The efficiency of such cells is lower than that of crystalline cells due to the low mobility of charge carriers within these materials. Amorphous cells with efficiencies exceeding 14% have been achieved [16]. This type of cell finds its main applications in small devices, such as calculators and watches.

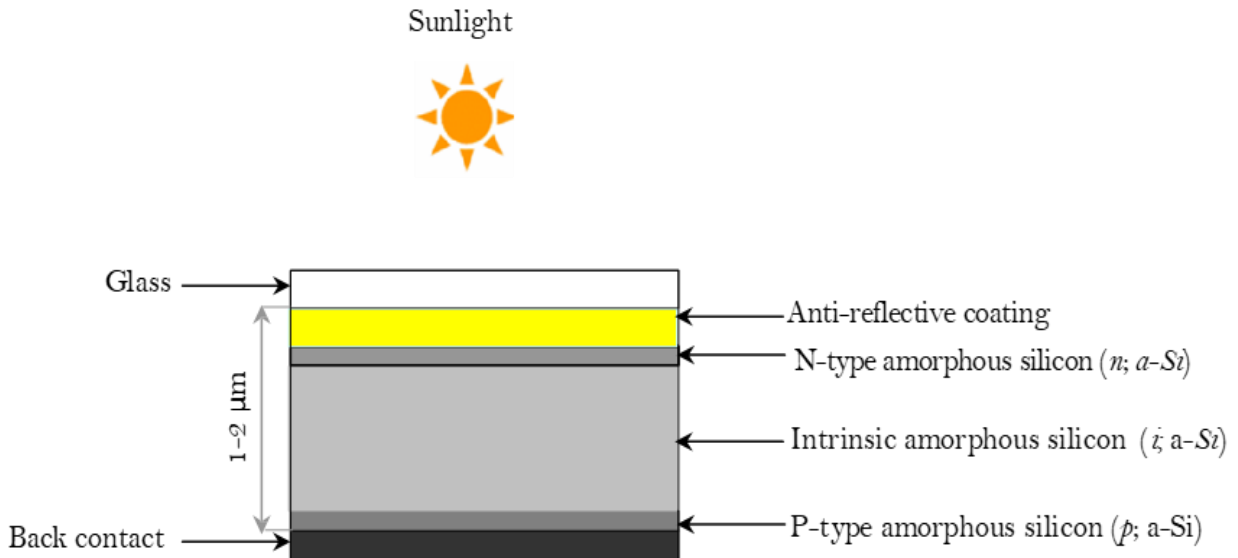


Figure I.11: Amorphous silicon solar cell.

b) Non-silicon thin-film cell

The non-silicon thin-film technology, which uses other materials such as CIGS, CdTe, and CZTS..., involves vaporizing a uniform thin layer of powdered semiconductor materials onto a substrate, such as glass or metal. Other technologies are at the research and development stage. These technological sectors are characterized by the materials used or their underlying principles. The manufacturing processes for these different technologies vary in their environmental impact.

There are generally six main layers in a thin-film solar cell (**Figure I-12**):

- The substrate: glass is common, but flexible or metallic substrates can also be used.
- The bottom contact: typically an ohmic contact, usually made of Mo or ITO.
- The absorber layer: p-type conduction and is often made of CdTe, CuInSe₂, Cu(InGa)Se₂, or Cu₂ZnSnSe₄.
- The buffer layer: n-type conduction and is often made of CdS, ZnS, etc.

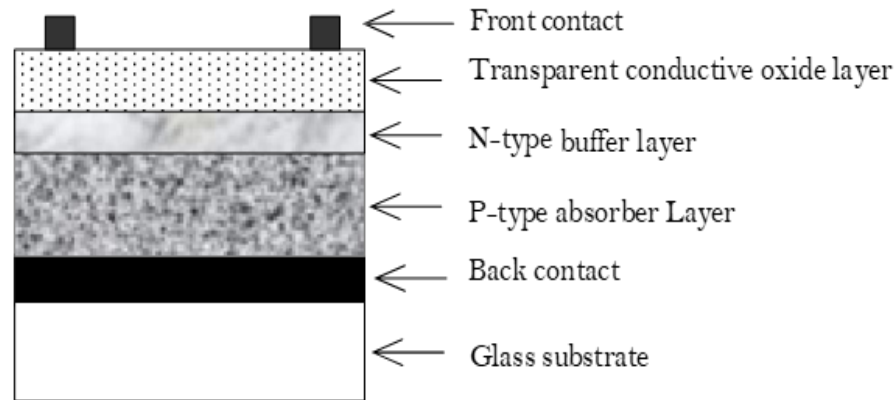


Figure I.12: Schematic representation of a typical thin-film-based solar cell.

I.10.3 Third Generation

This Current advancements in solar cell technology that aspire to surpass the Shockley-Queisser (SQ) threshold are classified as third-generation solar cells. These cells endeavor to realize the uppermost theoretical efficiency limits, estimated between 31% and 41%. The third-generation solar cells comprise:

- Quantum dot solar cells
- Dye-sensitized solar cells
- Polymer-based solar cells
- Perovskite solar cells

a. Quantum dot solar cells

In quantum dot (QD) solar cells, quantum dots, which are zero-dimensional nanomaterials, serve as the photoactive layer. These quantum dots, comprised of transition metal elements, are dispersed in a solution and then deposited onto a silicon substrate. Incident photons stimulate the creation of electron-hole pairs in the quantum dot layer, leading to electrical current flow. Notably, certain quantum dot varieties have the capability to generate multiple electron-hole pairs from a single photon.

b. Dye-sensitized solar cells

Dye-sensitized solar cells (DSSCs) operate based on the principles of synthetic photosynthesis and were initially introduced in the 1990s. DSSCs employ a dye molecule situated amongst transparent electrodes. The absorption of light by the dye molecules activates electrons, which then migrate to the opposite electrode and ultimately to an external circuit.

These cells are known for their affordability and their ability to function effectively across varied temperature ranges, reaching efficiencies up to approximately 13%.

c. Polymer-based solar cells

Polymer solar cells utilize a polymer or plastic substrate, conferring them with exceptional flexibility. These cells operate through a donor-acceptor mechanism, typically involving a polymer as the donor and fullerene as the acceptor. The diverse range of optically active polymers available allows for extensive material selection. Notable too is the potential integration of these cells into textiles, indicating a novel application for solar technology.

d. Perovskite solar cells

The development of perovskite materials marks the latest innovation within the sector. Perovskite solar cells have demonstrated peak efficiencies of up to 26.1% [18], presenting significant promise for the future evolution of solar energy systems. However, as of now, their application remains restricted primarily to laboratory settings due to their limited stability. Currently, silicon solar cell technology is the primary driver in the solar photovoltaic energy sector. Thin-film technology, however, is making inroads because it provides high-efficiency, low-cost solar cells.

I.10.4. Fourth Generation

Characterizing the latest advancements, this generation combines the adaptability and cost-effectiveness of thin film polymers with the robustness of cutting-edge inorganic nanostructures, which include metal oxides, metal nanoparticles, and organic-based nanomaterials such as graphene, carbon nanotubes, and variants of graphene.

Enhancement of photovoltaic cell performance is contingent upon the minimization of diverse loss mechanisms that impinge upon the overall cell efficiency. The National Renewable Energy Laboratory (NREL) maintains an authoritative record of peak laboratory-confirmed research cell efficiencies spanning various photovoltaic modalities, chronicled continuously from 1976 to date (**Figure I.13**). This catalog presents efficiency metrics for an array of semiconductor categories including, but not limited to, multi-junction cells, single-junction gallium arsenide cells, crystalline silicon cells, thin-film cells, and nascent photovoltaic technologies.



Best Research-Cell Efficiencies

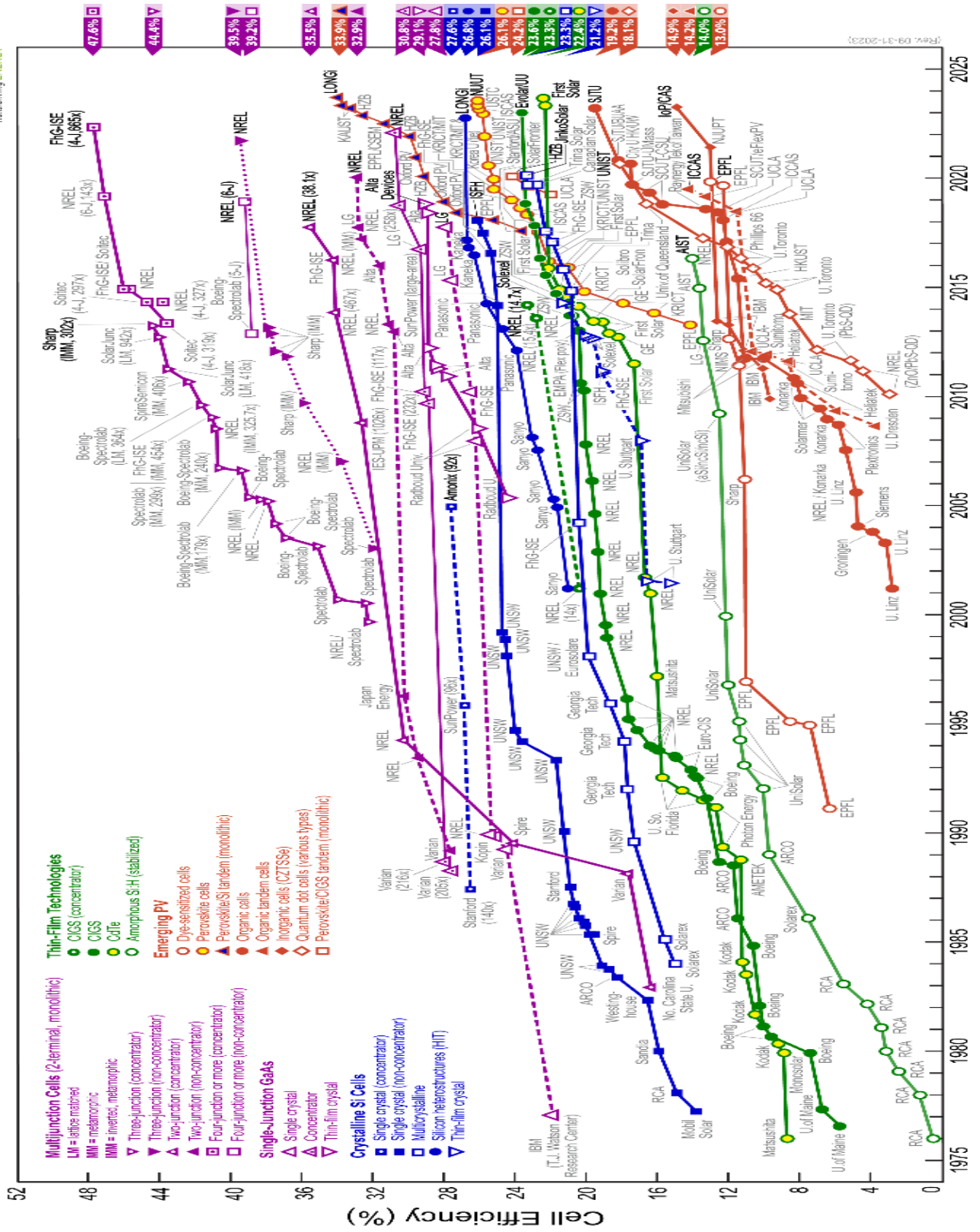


Figure I.13: NREL Best Research-Cell Efficiencies chart [18].

I.11 Physical Parameters of a Solar Cell

The I-V characteristic represents the current versus voltage behavior of a given solar cell, array, or module. This characteristic is instrumental in assessing the cell's efficiency and its capability to convert energy. Determining the maximum power output (P_{\max}) of a solar cell or panel allows for an evaluation of the device's performance and solar conversion efficiency, as cited in reference [8]. The current generated by a solar cell exhibits a direct proportionality to the incident light intensity, in accordance with the photoelectric effect, meaning that the current escalates with increasing light intensity. Conversely, the voltage of a solar cell diminishes with rising operating temperature. The I-V curve, which illustrates the relationship between the current and voltage under specific thermal and photonic conditions, furnishes vital data on the operational parameters at which a solar panel can achieve its maximum power point (P_m), the point of optimal performance.

The recording of the I(V) characteristic curve of a solar cell represents the variation of the current it produces as a function of the voltage across the cell for a given illumination (see **Figure I.14**). This measurement is carried out under a solar simulator whose illumination spectrum closely approximates the AM1.5 spectrum and under ambient operating conditions; that is, at a given ambient air temperature and speed. Each current-voltage characteristic of a cell corresponds to specific operating conditions. In the laboratory, the standard test conditions are as follows:

- The distribution of solar radiation is of the AM 1.5 type;
- The incident radiation is normal to the cell surface;
- The cell temperature is equal to (25 ± 2) °C;
- The speed of the air circulating around the cell is approximately 2 m s^{-1} .

The typical characteristic of a solar cell is shown in **Figure I.15**. An ideal photovoltaic cell would present, for given illumination, temperature, and ambient air circulation speed, a staircase-shaped curve: the current remains constant up to the open-circuit voltage, then the voltage remains constant up to zero current; the current abruptly transitions from the short-circuit current I_{SC} to 0.

From the current-voltage characteristic of the photovoltaic cell, one can determine its physical parameters namely: the open-circuit voltage, the short-circuit current, the characteristic power, the maximum power, the peak power, the fill factor, and the efficiency. Brief definitions of these parameters, as well as their determination from the characteristic, are given hereinafter.

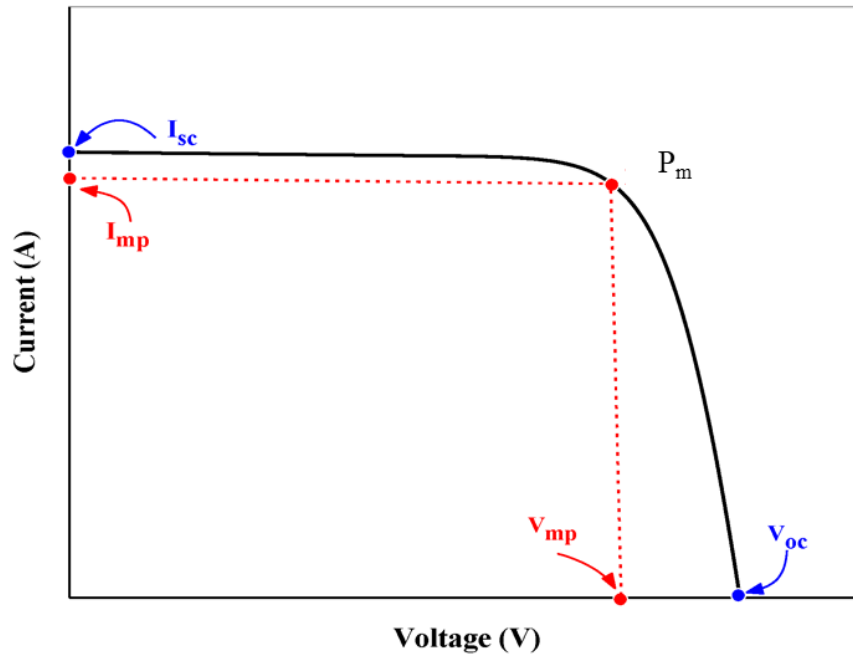


Figure I.14. I-V characteristics of a solar cell

a. Open-Circuit Voltage V_{oc}

The value V_{oc} corresponds to the open-circuit voltage; that is to say, $I=0$. It depends on the characteristics of the electronic junction and the materials. For a given cell, it varies very little with luminous intensity. It is obtained by directly connecting a voltmeter across the cell.

b. Short-Circuit Current I_{sc}

The I_{sc} value corresponds to the intensity of the short-circuit current; that is $V=0$. It is directly proportional to the received radiant energy, the ambient temperature, the speed of the ambient air flow, and the surface area of the cell. Its value is obtained by connecting an ammeter across the cell.

c. Characteristic Power of a Cell P

Under fixed ambient operating conditions; illumination, temperature, speed of circulating ambient air, etc., the electrical power $P(W)$ available at the terminals of a photovoltaic cell is equal to the product of the supplied direct current I by a continuous voltage V .

$$P = V \times I \quad (\text{I.8})$$

P : power measured at the terminals of the photovoltaic cell in Watts;

V : voltage measured at the terminals of the photovoltaic cell in Volts;

I : current intensity measured at the terminals of the photovoltaic cell in Amperes.

d. Maximum Power P_{\max}

The maximum power P_{\max} of a cell corresponds to the point at which the product of the voltage and current intensity is at its maximum. In the case of an ideal cell, the maximum power would correspond to the open-circuit voltage V_{OC} multiplied by the short-circuit current I_{SC} .

$$P_{\max_ideal} = V_{OC} \times I_{SC} \quad (\text{I.9})$$

P_{\max_ideal} : power measured at the terminals of the photovoltaic cell in Watts;

V_{OC} : open-circuit voltage measured at the terminals of the photovoltaic cell in Volts;

I_{SC} : short-circuit current measured at the terminals of the photovoltaic cell in Amperes.

e. Maximum Power Point

The maximum electrical power one solar cell can deliver at its standard test condition. If we draw the I-V characteristics of a solar cell maximum power will occur at the bend point of the characteristic curve. It is shown in the I-V characteristics of solar cell by P_m .

$$P_m = V_{mp} \times I_{mp} \quad (\text{I.10})$$

f. Fill Factor

The ratio between product of current and voltage at maximum power point to the product of short circuit current and open circuit voltage of the solar cell.

$$FF = \frac{P_m}{V_{oc} \times I_{sc}} \quad (\text{I.11})$$

g. Efficiency

It is defined as the ratio of maximum electrical power output to the radiation power input to the cell, and it is expressed in percentage. It is considered that the radiation power on the earth is about 100 mW cm^{-2} for AM1.5 spectrum.

$$\eta = \frac{V_{oc} I_{sc} FF}{P_{in}} \quad (\text{I.12})$$

The efficiency of solar panels depends on the geographic location, cloud coverage, day of the year, etc.

I.12 Conclusion

In this chapter, we have presented the essential basics for understanding the subject. We have reviewed some concepts about semiconductors, solar radiation, and its application in the photovoltaic field. Subsequently, we have explained the operation of photovoltaic cells, and we have addressed thin-film photovoltaic cells and those made of silicon. Then, their main characteristics, as well as the parameters limiting their efficiency and cost.

References

- [1] J.P. Parneix, Physique des Composants à Semi-Conducteurs Physique des Semi Conducteurs, 2005.
- [2] European commission, "Renewable energy – directive, targets, and rules," [Online], [Accessed April 20, 2024], Available at: https://energy.ec.europa.eu/topics/renewable-energy/renewable-energy-directive-targets-and-rules_en.
- [3] M.V. Anne Labouret, Installations photovoltaïques, 5th ed., Dunod, 2012.
- [4] B. Brousse, Réalisation et caractérisation de cellules photovoltaïques organiques obtenues par dépôt physique, Limoges, 2004.
- [5] D. Lincot, Lumière du ciel, énergie de la Terre. La conversion photovoltaïque au service des Hommes, Raison Présente. (2015) 27–37.
- [6] M. BENAICHA, Contribution à l'étude des propriétés physiques et électriques des composés semi-conducteurs III-V. Application à l'effet photovoltaïque., Université de Batna 2-Mustafa Ben Boulaid, 2018.
- [7] H. Amar, Propriétés électriques de cellule solaire à base de Sélénure de Cuivre Indium Gallium $\text{CuIn}_{(1-x)}\text{Ga}_x\text{Se}_2$ (CIGS), Université Mohamed Khider – Biskra Faculté, 2014.
- [8] A. Labouret, M. Viloz, A. Viloz, Installations photovoltaïques-6e éd.: Conception et dimensionnement d'installations raccordées au réseau, Dunod, 2022.
- [9] B. Boualem, Simulation et Optimisation des Cellules Solaires Monolithiques à Double Hétérojonction, à Base de CIGS, Utilisant le Logiciel Atlas-Silvaco., (2020).
- [10] C. Alonso, Contribution à l'optimisation, la gestion et le traitement de l'énergie, Université Paul Sabatier-Toulouse III, 2003.
- [11] P.H. Nguyen, C. Michel, J. Bottin, Etude de la conversion photovoltaïque: effets des résistances parasites des photopiles, Rev. Phys. Appliquée. 18 (1983) 775–779.
- [12] M. HAMLIA, Synthèse et caractérisation par voie électrochimique de couches minces quaternaires de type, UNIVERSITE FERHAT ABBAS – SETIF1, 2016.
- [13] M.A. Green, E.D. Dunlop, J. Hohl-Ebinger, M. Yoshita, N. Kopidakis, X. Hao, Solar cell efficiency tables (version 63), Prog. Photovoltaics Res. Appl. 30 (2022) 3–12. <https://doi.org/10.1002/pip.3506>.
- [14] L. Tsakalacos, Nanotechnology for photovoltaics, CRC press, 2010.
- [15] J. Pastuszak, P. Węgierek, Photovoltaic Cell Generations and Current Research Directions for Their Development, Materials (Basel). 15 (2022). <https://doi.org/10.3390/ma15165542>.
- [16] NREL, NREL, Best Research-Cell Efficiency Chart | Photovoltaic Research | NREL, (2023) <https://www.nrel.gov/pv/cell-efficiency.html>.
- [17] I.M. Dharmadasa, A.E. Alam, How to Achieve Efficiencies beyond 22.1% for CdTe-Based Thin-Film Solar Cells, Energies. 15 (2022). <https://doi.org/10.3390/en15249510>.
- [18] NREL, Best Research-Cell Efficiency Chart | Photovoltaic Research | NREL, (2023).

**Chapter II Properties of
thin-film solar cell materials
based on CdTe**

II.1 Introduction

Numerous Global research labs are intensively studying the properties of chalcopyrite semiconductor materials. The exceptionally high absorption coefficient, direct bandgap, and distinctive electronic, electrical, and optical character traits of these materials, particularly CdTe in the chalcopyrite family, are intriguing. These prominent qualities justify their crucial inclusion in optoelectronic and photovoltaic developments, notably in solar cells.

The fabrication methodology of CdTe thin film solar cells necessitates a tiered deposition of several materials in thin layers on a substrate. A proper understanding of the layers and component materials of the CdTe solar cell is necessary for the improvement of the cell's photovoltaic performance. Therefore, the layers, materials, and their properties of the CdTe cell are presented in detail in this chapter.

II.2 CdTe-based thin film solar cells

Table II.1 presents a summary of select optical, physical, and electrical characteristics of the cadmium telluride (CdTe) layer; these characteristics should be considered approximate due to significant variability stemming from the deposition technique, substrate temperature, and substrate material.

Despite cadmium's high toxicity and tellurium's relative rarity, Cadmium Telluride (CdTe) emerges as the preferable material for the development of cost-effective photovoltaic devices. Cadmium and tellurium, belonging to group 12 and group 16 of the periodic table respectively, exhibit high optical absorption and chemical stability [3]. Therefore, these elements are most suited for the fabrication of thin film solar cells.

The prototypical crystal structure of CdTe is the cubic zincblende (sphalerite) configuration is depicted in **Figure II.1** [4]. Nonetheless, in its thin-film form, CdTe may exhibit two additional phases: either cubic or hexagonal structures [5]. The crystallographic form of CdTe markedly impacts its optical and electrical behaviors: a single-crystal formation is associated with a smaller band gap and an extended carrier lifetime relative to its polycrystalline thin-film counterpart [6]. Furthermore, identical macrostructures can display divergent properties if the thin film is deposited at different substrate temperatures [7].

Additionally, the selection of substrate material whether molybdenum, glass, or stainless steel or the application of post-deposition treatments, such as CdCl₂ deposition followed by air annealing, can influence the band-gap and lattice parameters [8].

Table II.1 Material properties of CdTe [1,2]

Property	CdTe
Absorption coefficient at 600 nm (cm ⁻¹)	6×10^4
Electron affinity (eV)	4.28–4.5
Band gap E _g (300 K) Polycrystalline (eV)	1.45
Band gap E _g (300 K) Single crystal (eV)	1.5
Melting point (K)	1365
Lattice parameter	6.481 Angstrom
Hole mobility (cm ² V ⁻¹ s ⁻¹)	50–80
Electron mobility (cm ² V ⁻¹ s ⁻¹)	1000–1200
Effective density of states (cm ⁻³)	$N_C = 7.9 \cdot 10^{17}$, $N_V = 1.3 \cdot 10^{19}$
Molecular mass (g mol ⁻¹)	240.01
Density (g cm ⁻³)	5.85
Refractive index	3.106 (550 nm)–2.996 (850 nm)

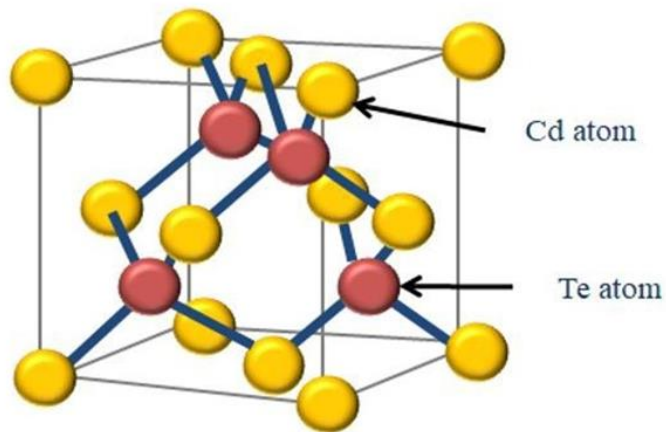


Figure II.1 Crystal structure (zinc blend cubic) of CdTe

CdTe is widely acknowledged as an exceptional material for the absorber layer in solar cells due to its direct bandgap of 1.45 eV, which is optimal for photovoltaic energy conversion and matches the peak of the solar irradiation spectrum. Its substantial optical absorption coefficient ensures that incident photons with energies exceeding the material's bandgap are completely absorbed within just one micron of the surface. Solar cells incorporating CdTe have demonstrated a potential photocurrent of 30.5 mA/cm² under illumination of 100 mW/cm² of sunlight, suggesting a theoretical efficiency ceiling approaching 27% [9]. Historically, peak cell performance was attained using heterojunctions with cadmium sulfide (CdS) as the n-type counterpart. Alternative efforts employing p-type CdTe single crystals in conjunction with indium oxide (In₂O₃), zinc oxide (ZnO), or a thin n-type CdTe layer yielded maximum efficiencies of up to 13.8% [10–12]. The breakthrough for CdTe did not arise from the use of single crystals; instead, leveraging one of its strongest attributes the capability for thin-film solar cell creation was key. Thin-film CdTe/CdS heterojunctions initially achieved 6% efficiency, a landmark dating back to 1972 [13]. The efficiency later surpassed the 10% threshold in the 1980s following post-deposition heat treatment of CdTe/CdS layers in a chlorine atmosphere [13]. By refining the front and back contacts, efficiencies nearly reaching 17% were accomplished in the subsequent decade [14,15]. However, a period of stagnation ensued, hindered by challenges such as the inability to extrinsically dope polycrystalline CdTe thin films and a shift in research focus towards the industrial scale-up of production techniques.

Efficiency rates began to climb once more around 2010, swiftly approaching 20%. This growth is mainly attributable to meticulous optimization of anti-reflective coatings, transparent electrical contacts, and window layers, along with strategic glass substrate selection. These improvements raised the photocurrent from 26.1 mA/cm² in 17.6% efficient cells [15] to 28.59 mA/cm² in 19.6% efficient cells, alongside a modest photovoltage increase [16]. Despite the lack of extensive literature details regarding these advancements, it is apparent that the photocurrent gains resulted not only from refined light harvesting but also from the shrewd adjustment of the CdTe bandgap to extend absorption into longer wavelengths. CdTe_(1-x)(S, Se)_x alloys, particularly with $x \leq 0.05$, exhibit a reduced bandgap compared to pure CdTe, allowing for a 15 nm increase in the cutoff wavelength. This translated into a photocurrent increment of 1 mA/cm². The introduction of the CdTe_(1-x)(S,

Se)_x mixed material also lessens lattice mismatch at the junction, thus promoting better charge transport. In 2015, a thin-film solar cell composed of CdTe_(1-x)(S, Se)_x set a world record efficiency of $(22.1 \pm 0.5)\%$, achieving an open-circuit voltage (V_{oc}) of 0.8872 volts, a short-circuit current (I_{sc}) of 31.69 mA/cm², and a fill factor of 78.5% over a 0.4798 cm² area under the global AM 1.5 spectrum at 25 °C [16,17].

Moreover, the production process of these solar cells is especially suited to large-scale, automated, in-line fabrication, which includes electrical series integration of cells during manufacturing through robotic laser scribing. Employing electrodeposition for the CdTe film application, an 11% efficiency module was produced in 2002 [18]. By the 2010–2011 period, there were ten manufacturers globally capable of producing tens of megawatts per year of CdTe modules, relying on close-spaced sublimation (CSS) or close-spaced vapor transport (CSVT) for the CdTe layer deposition, with reported average module efficiencies between 10% and 12% [19]. By the end of 2012, a 14.4% efficiency was reported, improving to 16.1% by early 2013. March 2014 saw the creation of a 17.5% efficient module, followed by a world record $(18.6 \pm 0.5)\%$ efficiency in 2015. This module presented photovoltaic parameters including a V_{oc} of 110.6 V, an I_{sc} of 1.533 A, and a fill factor of 74.2% across an illuminated area of 7038 cm² under the global AM 1.5 spectrum at a cell temperature of 25 °C [17]. Today, commercial modules with an 18.2% efficiency are accessible on the market. As of the last report, First Solar, boasting an annual production capacity of 2.4 gigawatts peak (GWp), accounts for a market share of 2.3%.

II.3 Different components of a CdTe-based thin film solar cells

In a solar cell utilizing a CdTe structure, the device is fabricated using extremely thin, sequentially deposited layers designed to create a superior heterojunction. Fabrication techniques such as CSS or CSVT lead to the intrinsic formation of p-type CdTe thin films, necessitating the selection of an n-type material to complete the p-n junction. This heterojunction is structured in such a way that it allows the incident solar radiation to penetrate the n-type layer and engage photogeneration within the CdTe layer. The most efficient arrangement uncovered thus far employs a CdS/CdTe combination, with CdS serving as the light-permeable 'window' and CdTe as the light-absorbing 'absorber' medium.

Limiting the CdS layer's thickness to no more than 100 nm is critical for maintaining high levels of transparency. The design ensures that the electrical field is mainly established within the absorber layer, thus maximizing separation and direction of the photogenerated charge carriers toward the external contacts. Supplementary layers finalize the solar cell, facilitating the movement of the generated photocurrent. High-performance CdS/CdTe solar cells are constructed in a superstrate configuration, wherein illumination traverses the substrate first, necessitating a front contact that is both transparent and efficient in electrical conduction. Conversely, the rear contact must form an ohmic connection with the p-type CdTe to optimize photocurrent collection. The main layers of a thin-film-based solar cell are shown in **Figure II.2**:

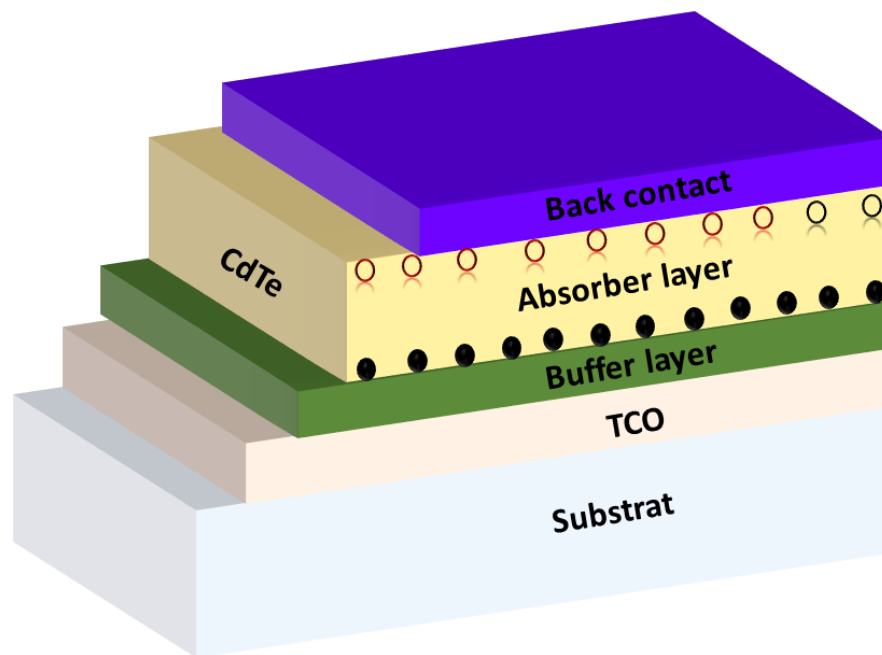


Figure II.2: The CdTe/CdS solar cell

In the alternative substrate configuration, the production process initiates with the rear contact, builds up through the deposition of the CdTe and CdS layers, and concludes with the application of the transparent front contact. This approach is compelling as it permits the use of opaque substrates like metals or polymers, leading to the potential development of flexible solar modules that are lighter, cost-effective, and compatible with roll-to-roll production processes favorable for integration into vehicles and buildings (VIPV and BIPV). A distinct

advantage of this configuration is the separate optimization of CdTe doping and the CdTe/CdS junction formation processes.

The functional performance of CdTe-based solar cells is significantly influenced by the interplay between the component layers, which is contingent upon the sequence of layer deposition an aspect pivotal to the cell's efficacy. Substrate configuration in CdTe/CdS solar cells is relatively nascent, warranting extensive research into layer interactions, material diffusion, interfacial dynamics, back-contact quality, and doping processes.

Concerning the manufacturing process, the primary objectives include:

- depositing the cadmium and tellurium layers cost-effectively;
- activating the structure in a chlorine-rich environment at elevated temperatures;
- pairing the window and absorber layers to establish an efficient heterojunction.

Additional routine steps in thin-film solar cell production encompass the selection of electrical contacts, which must ideally exhibit high conductivity and transparency to solar radiation, particularly for the front contact. In the context of superstrate configurations, the choice of substrate material is critical, requiring it to be maximally transparent to ensure the solar cell's operational longevity. We will now proceed to analyze each of the manufacturing steps, as well as the principal characteristics requisite for the individual materials.

II.3.1 The substrate

In the creation of highly efficient solar cells and modules under a superstrate configuration, transparent rigid glass serves as the substrate, a critical feature since solar radiation must pass through with minimal absorption losses. Soda-lime glass (SLG) is the prevalent commercial glass utilized for this purpose. Composed predominantly of silica (SiO_2) at proportions of 75% to 76%, it offers considerable resistance to thermal stress, though the high melting point and viscosity of silica present challenges in processing. To address this, substances like sodium oxide (Na_2O), commonly referred to as "soda" are integrated at about 14% to reduce the glass transition temperature. However, soda's presence increases the glass's solubility in water. To improve chemical stability, calcium oxide (CaO), known as "lime" at 9%, along with magnesium oxide (MgO) and alumina (Al_2O_3), are incorporated to enhance the glass's durability.

Cost efficiency is achieved by substituting pure chemicals with inexpensive minerals like trona, sand, and feldspar. However, this substitution can introduce impurities, such as iron oxide (Fe_2O_3) and manganese dioxide (MnO_2), which diminish transparency within the visible solar spectrum. Consequently, iron-free glass variants are employed in CdTe cell production, which affords an 8% improvement in transparency for wavelengths below 300 nm [3].

Flexible substrates, such as DuPont's polyimide, have been explored owing to their compatibility with high-rate roll-to-roll processes, allowing for the fabrication of extensive, lightweight photovoltaic devices at a reduced cost. While the optical transparency of polyimide aligns with standard SLG at longer wavelengths (Figure II.3), it falls short below 530 nm in terms of suitability for photovoltaic applications even when utilizing thin foils resulting in a minimum photocurrent deficit of 3 mA/cm². This limitation, coupled with the material's thermal constraints, restricts the efficiency of solar cells crafted from this polymer to not exceed 14% [20].

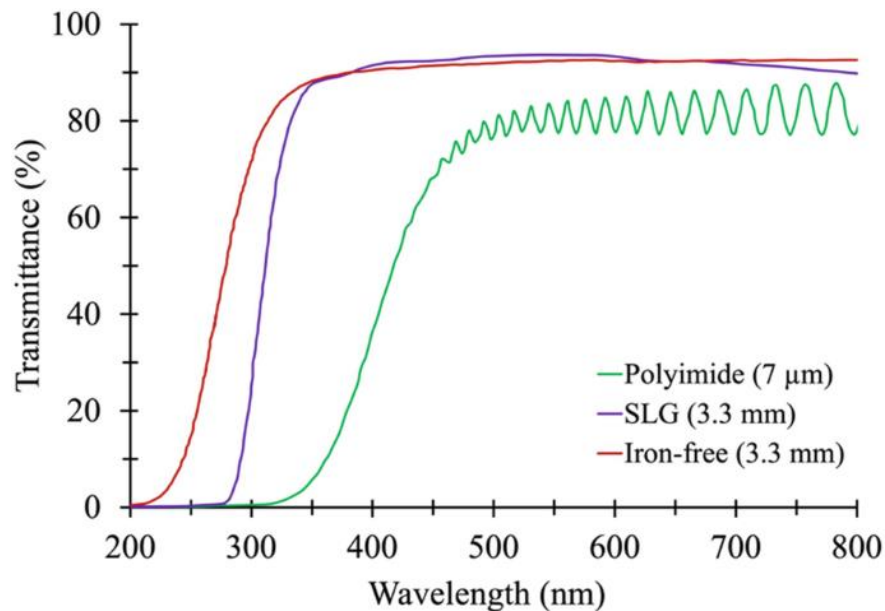


Figure II.3: Transmittance spectra of commonly used substrates such as soda-lime glass (SLG) and polyimide in CdTe-based solar cells [16].

II.2.2 The front contacts

For the optimal operation of thin-film solar cells, the front contact requires a semiconductor that exhibits high conductivity while simultaneously allowing light to traverse the cell. The dual necessity for transparency and robust conductivity is addressed through the deployment of transparent conductive oxides (TCOs). TCOs meeting this dual requisite typically manifest near 90% visible light transparency (**Figure II.4**) and exhibit electrical conductivities reaching $10^4 \Omega^{-1}\text{cm}^{-1}$ with wide band gaps exceeding 3 eV [16]. The prevalent materials utilized for this purpose include indium tin oxide (ITO), aluminum-doped zinc oxide (ZAO), and fluorine-doped tin oxide (FTO).

TCOs in a standard configuration must also possess an electron affinity under 4.5 eV to preclude the formation of Schottky contacts with the CdS buffer layer. While oxides are intrinsically insulating, their n-type conductivity is augmented by doping with donor impurities, transforming them into degenerate semiconductors with free carrier concentrations in the range of 10^{18} to 10^{20}cm^{-3} . In the realm of CdTe solar cells, the most prevalent TCOs are $\text{SnO}_2:\text{F}$ (FTO), $\text{ZnO}:\text{Al}$ (AZO), and $\text{In}_2\text{O}_3:\text{Sn}$ (ITO).

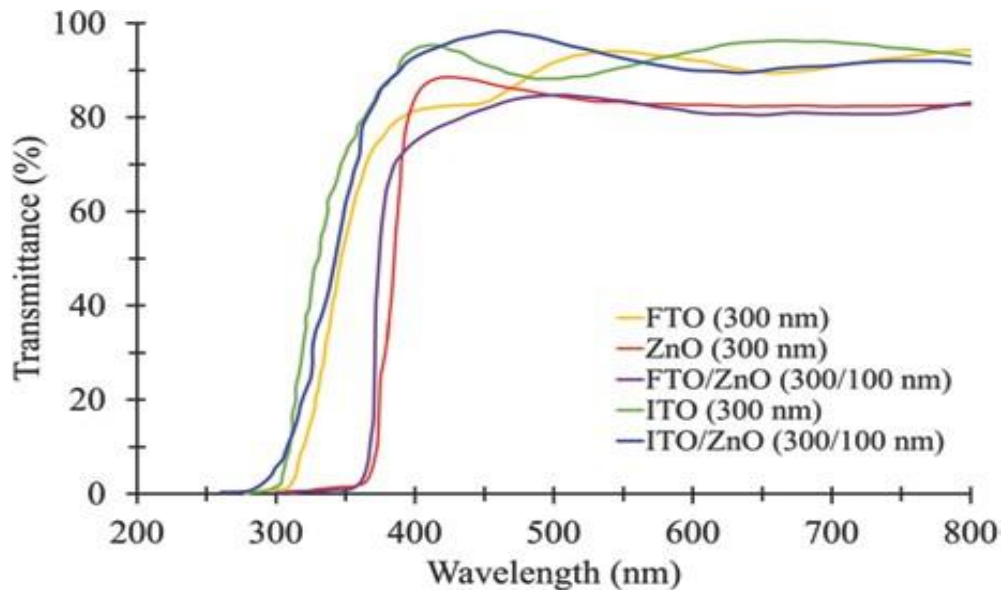


Figure II.4: Illustrates the transmittance spectra of SLG, coated solely with FTO or ITO, and SLG coated with FTO or ITO coupled with ZnO serving as a HRT layer [16].

Historically, more sophisticated TCOs like Cd_2SnO_4 (CTO) have been employed to enhance conductivity and transparency, thereby achieving superior efficiency [21]. However, for large-scale manufacturing, materials that can be readily deposited over extensive areas are favored, with FTO being the common choice due to its long-term stability.

Nevertheless, intrinsic oxides, known as high-resistivity transparent (HRT) layers, are often utilized between the TCO and CdS to prevent shunt paths through pinholes in the thin CdS layer and to fine-tune band alignment. HRT layers facilitate the reduction of CdS layer thickness which is crucial for harvesting energy in wavelengths below 500 nm by diminishing parasitic absorption. This thinning process also contributes to an increase in the open-circuit voltage, with the electrical resistivity of HRT layers ranging from 10^2 to $10^5 \text{ } \Omega\cdot\text{cm}$, thus mitigating shunting issues that could arise from micropinholes [9].

TCOs, being the initial layers deposited onto the substrate, can influence the structure and properties of the solar cell. Diffusion of impurities from TCOs into the device junction or the absorber can occur, and the crystal structure of the TCOs can affect the grain structure of CdS and CdTe, with consequent impacts on their electrical characteristics [22,23]. Consequently, TCOs must also exhibit chemical and physical stability [24].

II. 3.3 Buffer Layer

The most commonly paired n-type semiconductor with p-type CdTe is CdS, which shows n-type conductivity due to stoichiometric defects like sulfur vacancies during film formation. Cadmium sulfide CdS is a semiconductor made up of the combination of atoms from column II (Cd) with those from column VI (S) of the periodic table of chemical elements. CdS has two types of structures: the cubic zinc blende structure of sphalerite (**Figure II.5 a**) with a tetrahedral arrangement of atoms, and the hexagonal wurtzite structure (**Figure II.5 b**). The blende type structure is a face-centered cubic (FCC) structure whose primitive cell contains 4 cations (Cd^{+2}) and four anions (S^{-2}). Each species of a constituent is surrounded at equal distance by four atoms of the other constituent. This defines a regular tetrahedron with atoms occupying the vertices.

The structure of CdS has a lattice parameter $a = 5.8 \text{ } \text{\AA}$, and for the Wurtzite phase, the lattice parameters are $a = 4.1 \text{ } \text{\AA}$ and $c = 6.7 \text{ } \text{\AA}$ [25,26]. CdS, with a band gap of 2.42 eV,

permits light up to 512 nm wavelength while blocking near-ultraviolet light to which the substrate made of soda-lime glass (SLG) and TCO layers are transparent [27]. Self-doping processes in CdS achieve resistivities around 10^6 to $10^7 \Omega \cdot \text{cm}$, similar to those obtained with CdTe films.

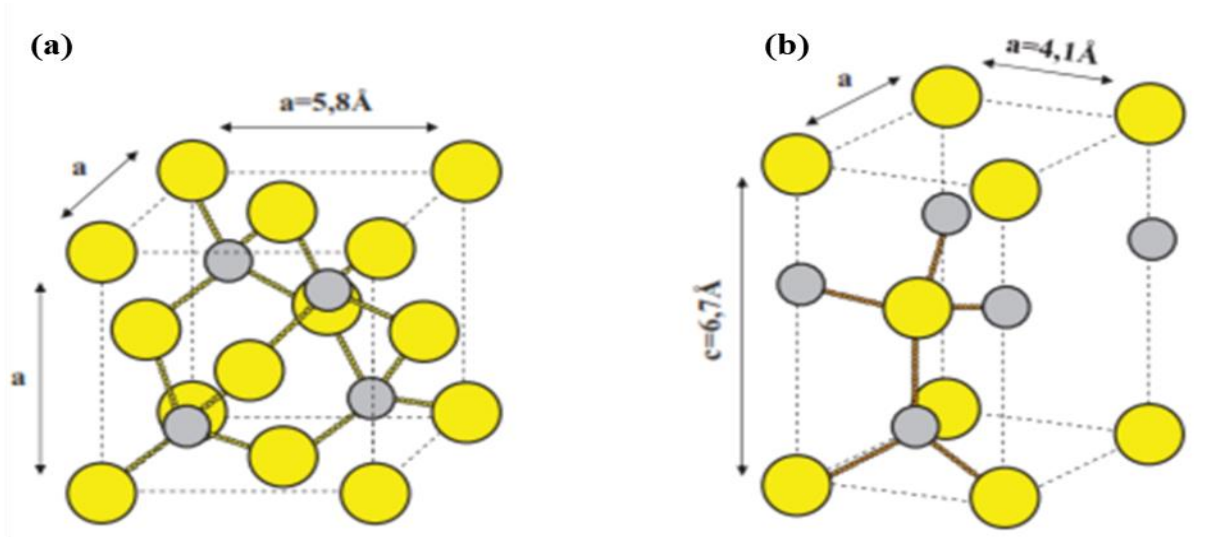


Figure II.5: The two types of CdS lattice structure (a) cubic zinc blende structure of sphalerite (b) hexagonal wurtzite structure .

For an efficient p/n junction in solar cells, the electric field should primarily exist in the p-type region (CdTe), a condition met as electron mobility in CdS is much higher than hole mobility in CdTe, provided the carrier density in p-type CdTe is significantly lower than n-type CdS. Under dark conditions, this condition doesn't hold; however, illumination activates photoconductivity in CdS, which helps extend the electric field into CdTe.

Considering transparency for sunlight wavelengths shorter than the bandgap cut-off, since the absorption coefficient (α) is unmodifiable, thin films become a solution to achieve a lower optical density ($\alpha \cdot d$), allowing light passage despite a high α (with thickness $t \leq 100 \text{ nm}$ and $t < d$, where t is the film thickness and d is average absorption length).

Alternative window materials with a greater bandgap have been explored to better harness the visible solar spectrum. The ZnCdS alloy, with a bandgap ranging from CdS's 2.42 eV to ZnS's 3.6 eV, seemed promising. However, this didn't yield the anticipated improvements in photovoltaic parameters like open-circuit voltage (V_{oc}) and short-circuit

current (I_{sc}) for ZnCdS/CdTe cells [28]. The likeliest explanation for this is the increase in interface defects since the Zn–Cd–S–Te system does not minimize structural defects as effectively as the Cd–S–Te system, which are key in reducing photogenerated carrier recombination.

In deposition processes, CdS is either laid down at sub-200 °C, a low-temperature (L-T) range, or above, which falls into the high-temperature (H-T) range. Chemical bath deposition (CBD) yields high-density, compact, and pinhole-free CdS films but is unsustainable on an industrial scale due to its slow pace and waste production necessitating costly recycling [29,30]. Sputtering, an L-T method, is therefore preferred for large-scale manufacturing, although it simulates H-T effects. RF sputtering does not produce CdS films of sufficient quality for CdTe solar cells unless reactive gases containing fluorine or oxygen are introduced. Such reactive RF sputtering achieves high-quality CdS films conducive to forming robust CdS/CdTe heterojunctions (**Figure II.6**).

Using H-T techniques like close-spaced sublimation (CSS), higher quality CdS films are obtained. The addition of oxygen during CSS in an otherwise pure argon environment alters the growth equilibrium, slowing down the deposition [31]. This results in densely packed films without pinholes due to the oxide formation at the grain boundaries. Yet, an oxide layer on the film's surface is a byproduct, necessitating a high-temperature (400 °C) hydrogen post-annealing process to achieve high-efficiency solar cells.

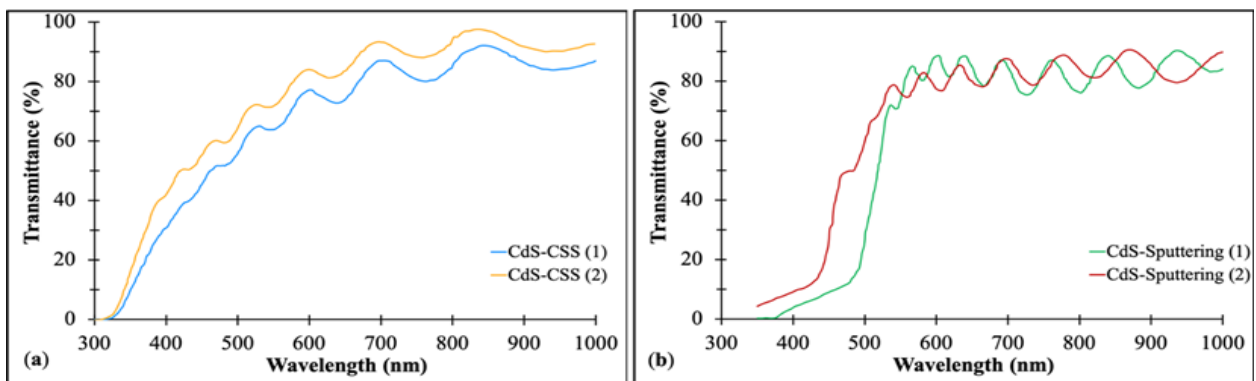


Figure II.6: Transmittance spectra of sputtered CdS film : (a) prepared by CSS in Ar + O₂ atmosphere: (1) as-deposited, (2) after annealing for 30 min at 420 °C in 400 mbar of Ar containing 20% of H₂; (b) 80 nm thick sputtered CdS film: (1) deposited in pure Ar and (2) deposited in Ar + CHF₃ [16].

Furthermore, due to the recognized toxicity of cadmium (Cd), the scientific community has been exploring alternative buffer layer compositions that maintain comparable efficiencies. In the pursuit of non-toxic alternatives, various research groups have experimented with multiple buffer layers and deposition techniques to achieve high efficiency in alternative thin film photovoltaic technologies like CIGS or CZTS solar cells. Among the prevalent cadmium-free buffer layers utilized are zinc sulfide (ZnS), zinc sulfide with oxygen and hydroxyl additives (ZnS(O,OH)), zinc oxysulfide (Zn(O,S)), and zinc magnesium oxide (ZnMgO) [32–34].

II.3.4 The Absorber Layer

Several investigations have been conducted on different structures, including homojunction, heterojunction, p-i-n, and Schottky barrier, for the production of CdTe-based solar cells [35,36]. It has been established that heterojunction is the most efficient structure, likely due to the intermixing layer formed during CdTe deposition or post-deposition heat treatments. This layer removes structural native defects, resulting in a window/absorber interface closely resembling a homojunction, demonstrating high efficiency and confirming the absence of recombination centers near the junction.

Both low-temperature (L-T) and high-temperature (H-T) deposition technologies are utilized for CdTe thin film production. The highest efficiency devices are typically achieved through H-T processes such as close-spaced sublimation (CSS) and close-spaced vapor transport (CSVV), which are industrially implemented in commercially available 18% efficiency CdTe-based modules. However, these processes result in large, columnar, slightly defective grains, and pinhole formation. The intrinsic doping of CSS-deposited CdTe films produces dark p-type conductivity in the range of $(10^{-4}/10^{-5}) \Omega^{-1} \cdot \text{cm}^{-1}$ [16]. Due to the film's series resistance, further thickness reduction of the CdTe layer is crucial to mitigate these electrical limitations.

To improve film quality and reduce defect formation, oxygen is added to the inert gas in the CSS or CSVV process, resulting in the formation of a less defective CdTe layer and promoting a denser growth of the CdTe film. In the case of sputtering deposition, it yields a CdTe layer with an n-type conductivity of about $10^{-3} \Omega^{-1} \cdot \text{cm}^{-1}$. Adding a sputtered thin film on

top of a CSS-deposited one has been observed to alleviate pinholes, enhance minority carrier lifetime, and prevent shunt paths in the junction region.

Additionally, CdTe-based solar cells have been optimized using CdTe_(1-x)Se_x alloys to achieve higher efficiency [37]. These improvements encompass the adjustment of the stoichiometric composition 'x' to produce graded energy gap profiles, which enhance solar light collection [38]. Furthermore, the replacement of the CdS layer with MgZnO and the addition of Se in CdTe_(1-x)Se_x alloys have contributed to higher efficiency solar cells, reaching a record efficiency of over 22% [17].

Multiple deposition techniques such as RF magnetron sputtering have been explored to realize high-density films with good adhesion to the substrate, leading to the production of 14% efficient solar cells in the early 2000s. This comprehensive research and innovation continue to improve the efficiency and developmental possibilities of CdTe-based solar cells.

II.3.5 The Back Contact

The back contact constitutes the portion of the solar cell opposite the sunlight-exposed side, serving the function of connecting the cell to the external circuit. In contrast to other technologies like CuInGaSe₂ or Cu₂ZnSnSe₄, where a metal like molybdenum is adequate to establish the contact. In CdTe solar cells, establishing an effective back contact presents challenges due to CdTe's high electron affinity, which necessitates a contact metal with a work function above 5.7 eV, not available among current metals. This often results in a Schottky barrier when employing available metals. To mitigate this, a strategy of heavily doping the p-type surface of CdTe and then applying a conductive buffer layer has been used to create a quasi-ohmic contact [39]. Previous practices involved applying a Cu/metal bi-layer, particularly Cu/Au, to increase carrier concentration, although this led to instability due to copper diffusion. Conditions to reduce diffusion include etching the CdTe to create a Te-rich layer and forming a more stable Cu_xTe compound, where x is less than 1.4, rather than the unstable Cu₂Te [40,41].

Alternate copper configurations, like Cu/graphite and Cu/Mo combinations, have been explored, and treating the CdTe with Cu above a diffusion barrier followed by a Mo layer has been particularly effective at lowering series resistance [42]. ZnTe:Cu back contact systems

are currently among the most reliable, with ZnTe layering helping to reduce carrier recombination [43–45]. However, there is a critical balance between efficiency gains and the risk of degradation associated with copper application, with 4-5% copper being optimal [46]. Attempts to eliminate copper altogether have been met with varied success, but such Cu-free back contacts typically yield lower efficiencies than those containing copper [47]. Newer methods have introduced copper via CuCl solutions, providing even distribution of copper, improving device stability, and presumably enhancing the solubility of Cu_{Cd} acceptors due to the chlorine [48]. In sum, while copper is essential for better-performing back contacts in CdTe solar cells, its application must be carefully controlled to optimize performance and longevity.

II.4 Conclusion

In this study, we have delineated the trajectory and developmental heritage of the cadmium telluride (CdTe) solar cell alongside a comprehensive exposition of its multiple merits that underpinned our selection. Subsequently, an in-depth manifestation of each constituent layer and material involved in the CdTe solar cell employed within our research has been elucidated, with a thorough discussion of their respective properties. The benefits and characteristics emphasized in this segment of the text underscore the superiority of the CdTe solar cell as a highly favorable contender, poised to serve as a viable and cost-effective substitute for the conventional, bulkier, and costlier crystalline silicon (c-Si) cells that currently predominate in the photovoltaic sector.

References

- [1] J. Poortmans, V. Arkhipov, *Thin film solar cells: fabrication, characterization and applications*, John Wiley & Sons, 2006.
- [2] A. Luque, S. Hegedus, *Photovoltaic Science and Engineering*, (2003).
- [3] A. Bosio, G. Rosa, N. Romeo, Past, present and future of the thin film CdTe/CdS solar cells, *Sol. Energy*. (2018) 31–43. <https://doi.org/10.1016/j.solener.2018.01.018>.
- [4] D. Sharma, R. Mehra, B. Raj, Design and Analysis of Various Solar Cell Technologies for Improvements in Efficiencies, *Indian J. Eng. Mater. Sci.* 29 (2022) 557–567. <https://doi.org/10.56042/ijems.v29i5.51066>.
- [5] T.H. Myers, S.W. Edwards, J.F. Schetzina, Optical properties of polycrystalline CdTe films, *J. Appl. Phys.* 52 (1981) 4231–4237.
- [6] A. Abd El-Mongy, A. Belal, H. El Shaikh, A. El Amin, A comparison of the physical properties of CdTe single crystal and thin film, *J. Phys. D. Appl. Phys.* 30 (1997) 161.
- [7] R. Sathyamoorthy, S.K. Narayandass, D. Mangalaraj, Effect of substrate temperature on the structure and optical properties of CdTe thin film, *Sol. Energy Mater. Sol. Cells*. 76 (2003) 339–346.
- [8] S. Lalitha, R. Sathyamoorthy, S. Senthilarasu, A. Subbarayan, Influence of CdCl₂ treatment on structural and optical properties of vacuum evaporated CdTe thin films, *Sol. Energy Mater. Sol. Cells*. 90 (2006) 694–703.
- [9] U.P. Singh, N.B. Chaure, *Recent Advances in Thin Film Photovoltaics*, 2022.
- [10] T. Nakazawa, K. Takamizawa, K. Ito, High efficiency indium oxide/cadmium telluride solar cells, *Appl. Phys. Lett.* 50 (1987) 279–280.
- [11] J.A. Aranovich, D. Golmayo, A.L. Fahrenbruch, R.H. Bube, Photovoltaic properties of ZnO/CdTe heterojunctions prepared by spray pyrolysis, *J. Appl. Phys.* 51 (1980) 4260–4268.
- [12] J. Mimila-Arroyo, Y. Marfaing, G. Cohen-Solal, R. Triboulet, Electric and photovoltaic properties of CdTe pn homojunctions, *Sol. Energy Mater.* 1 (1979) 171–180.
- [13] D. Bonnet, H. Rabenhorst, New results on the development of a thin-film p-CdTe-n-CdS heterojunction solar cell, in: *Photovolt. Spec. Conf. 9 Th*, Silver Spring, Md, 1972: pp. 129–132.
- [14] J. Britt, C. Ferekides, Thin-film CdS/CdTe solar cell with 15.8% efficiency, *Appl. Phys. Lett.* 62 (1993) 2851–2852.
- [15] X. Wu, J.C. Keane, R.G. Dhere, C. DeHart, D.S. Albin, A. Duda, T.A. Gessert, S. Asher, D.H. Levi, P. Sheldon, 16.5%-efficient CdS/CdTe polycrystalline thin-film solar cell, in: *Proc. 17th Eur. Photovolt. Sol. Energy Conf.*, James & James Ltd.: London, 2001.
- [16] A. Bosio, S. Pasini, N. Romeo, The history of photovoltaics with emphasis on CdTe solar cells and modules, *Coatings*. 10 (2020). <https://doi.org/10.3390/coatings10040344>.
- [17] M.A. Green, E.D. Dunlop, D.H. Levi, J. Hohl-Ebinger, M. Yoshita, A.W.Y. Ho-Baillie, Solar cell efficiency tables (version 54), *Prog. Photovoltaics Res. Appl.* 27 (2019) 565–575. <https://doi.org/10.1002/pip.3171>.
- [18] D. Cunningham, M. Rubcich, D. Skinner, Cadmium telluride PV module manufacturing at BP Solar, *Prog. Photovoltaics Res. Appl.* 10 (2002) 159–168.

- [19] A. Bosio, D. Menossi, S. Mazzamuto, N. Romeo, Manufacturing of CdTe thin film photovoltaic modules, *Thin Solid Films*. 519 (2011) 7522–7525.
- [20] A. Salavei, E. Artegiani, F. Piccinelli, S. Di Mare, D. Menossi, A. Bosio, N. Romeo, A. Romeo, Flexible CdTe solar cells on polyimide and flexible glass substrates, in: *Proc. 31st Eur. Photovolt. Sol. Energy Conf. Berlin/Heidelberg, Ger.*, 2015: pp. 14–18.
- [21] X. Wu, R.G. Dhere, D.S. Albin, T.A. Gessert, C. Dehart, J.C. Keane, A. Duda, T.J. Coutts, S. Asher, D.H. Levi, High-efficiency CTO/ZTO/CdS/CdTe polycrystalline thin-film solar cells, National Renewable Energy Lab., Golden, CO.(US), 2001.
- [22] E. Artegiani, D. Menossi, A. Salavei, S. Di Mare, A. Romeo, Analysis of the influence on the performance degradation of CdTe solar cells by the front contact, *Thin Solid Films*. 633 (2017) 101–105.
- [23] S.N. Alamri, A.W. Brinkman, The effect of the transparent conductive oxide on the performance of thin film CdS/CdTe solar cells, *J. Phys. D. Appl. Phys.* 33 (2000) L1.
- [24] N. Romeo, A. Bosio, V. Canevari, M. Terheggen, L.V. Roca, Comparison of different conducting oxides as substrates for CdS/CdTe thin film solar cells, *Thin Solid Films*. 431 (2003) 364–368.
- [25] R. Scheer, H.-W. Schock, *Chalcogenide photovoltaics: physics, technologies, and thin film devices*, John Wiley & Sons, 2011.
- [26] M. Elbar, Etude par simulation numérique d'une cellule solaire en CIGS à multi-jonction par le logiciel Tcad Silvaco, (2018).
- [27] G. Korotcenkov, *Handbook of II-VI Semiconductor-Based Sensors and Radiation Detectors*, 2023. <https://doi.org/10.1007/978-3-031-19531-0>.
- [28] G. Kartopu, A.J. Clayton, W.S.M. Brooks, S.D. Hodgson, V. Barrioz, A. Maertens, D.A. Lamb, S.J.C. Irvine, Effect of window layer composition in Cd_{1-x}Zn_xS/CdTe solar cells, *Prog. Photovoltaics Res. Appl.* 22 (2014) 18–23.
- [29] R. Ortega-Borges, D. Lincot, Mechanism of chemical bath deposition of cadmium sulfide thin films in the ammonia-thiourea system: in situ kinetic study and modelization, *J. Electrochem. Soc.* 140 (1993) 3464.
- [30] J.M. Dona, J. Herrero, Chemical bath deposition of CdS thin films: an approach to the chemical mechanism through study of the film microstructure, *J. Electrochem. Soc.* 144 (1997) 4081.
- [31] N. Romeo, A. Bosio, V. Canevari, The role of CdS preparation method in the performance of CdTe/CdS thin film solar cell, in: *3rd World Conf. On Photovoltaic Energy Conversion*, 2003. *Proc., IEEE*, 2003: pp. 469–470.
- [32] M. Powalla, G. Voorwinden, D. Hariskos, P. Jackson, R. Kniese, Highly efficient CIS solar cells and modules made by the co-evaporation process, *Thin Solid Films*. 517 (2009) 2111–2114.
- [33] D. Hariskos, R. Menner, P. Jackson, S. Paetel, W. Witte, W. Wischmann, M. Powalla, L. Bürkert, T. Kolb, M. Oertel, New reaction kinetics for a high-rate chemical bath deposition of the Zn (S, O) buffer layer for Cu (In, Ga) Se₂-based solar cells, *Prog. Photovoltaics Res. Appl.* 20 (2012) 534–542.
- [34] M. Nakamura, K. Yamaguchi, Y. Kimoto, Y. Yasaki, T. Kato, H. Sugimoto, Cd-free Cu (In, Ga)(Se, S) 2 thin-film solar cell with record efficiency of 23.35%, *IEEE J. Photovoltaics*. 9 (2019) 1863–1867.
- [35] T.C. Anthony, A.L. Fahrenbruch, M.G. Peters, R.H. Bube, Electrical properties of CdTe films and junctions, *J. Appl. Phys.* 57 (1985) 400–410.

- [36] T.L. Chu, S.S. Chu, S.T. Ang, Electrical properties of CdS/CdTe heterojunctions, *J. Appl. Phys.* 64 (1988) 1233–1237.
- [37] M.D. Mia, C.H. Swartz, S. Paul, S. Sohal, C.R. Grice, Y. Yan, M. Holtz, J. V Li, Electrical and optical characterization of CdTe solar cells with CdS and CdSe buffers—A comparative study, *J. Vac. Sci. Technol. B.* 36 (2018).
- [38] S.-H. Wei, S.B. Zhang, A. Zunger, First-principles calculation of band offsets, optical bowings, and defects in CdS, CdSe, CdTe, and their alloys, *J. Appl. Phys.* 87 (2000) 1304–1311.
- [39] C.S. Ferekides, V. Viswanathan, D.L. Morel, RF sputtered back contacts for CdTe/CdS thin film solar cells, in: *Conf. Rec. Twenty Sixth IEEE Photovolt. Spec. Conf., IEEE, 1997*: pp. 423–426.
- [40] X. Wu, J. Zhou, A. Duda, Y. Yan, G. Teeter, S. Asher, W.K. Metzger, S. Demtsu, S.-H. Wei, R. Noufi, Phase control of Cu_xTe film and its effects on CdS/CdTe solar cell, *Thin Solid Films.* 515 (2007) 5798–5803.
- [41] A. V Nawarange, A.D. Compaan, Optimization of back contacts for CdTe solar cells using sputtered Cu_xTe , in: *2011 37th IEEE Photovolt. Spec. Conf., IEEE, 2011*: pp. 1317–1321.
- [42] N. Suyama, T. Arita, Y. Nishiyama, N. Ueno, S. Kitamura, M. Murozono, CdS/CdTe solar cells by the screen-printing-sintering technique, in: *IEEE Conf. Photovolt. Spec., IEEE, 1990*: pp. 498–503.
- [43] T.A. Gessert, A.R. Mason, P. Sheldon, A.B. Swartzlander, D. Nilas, T.J. Coutts, Development of Cu-doped ZnTe as a back-contact interface layer for thin-film CdS/CdTe solar cells, *J. Vac. Sci. Technol. A Vacuum, Surfaces, Film.* 14 (1996) 806–812.
- [44] J. V Li, J.N. Duenow, D. Kuciauskas, A. Kanevce, R.G. Dhere, M.R. Young, D.H. Levi, Electrical characterization of Cu composition effects in CdS/CdTe thin-film solar cells with a ZnTe: Cu back contact, in: *2012 IEEE 38th Photovolt. Spec. Conf. Part 2, IEEE, 2012*: pp. 1–5.
- [45] N. Amin, K. Sopian, M. Konagai, Numerical modeling of CdS/CdTe and CdS/CdTe/ZnTe solar cells as a function of CdTe thickness, *Sol. Energy Mater. Sol. Cells.* 91 (2007) 1202–1208.
- [46] J. Tang, D. Mao, T.R. Ohno, V. Kaydanov, J.U. Trefny, Properties of ZnTe: Cu thin films and CdS/CdTe/ZnTe solar cells, in: *Conf. Rec. Twenty Sixth IEEE Photovolt. Spec. Conf., IEEE, 1997*: pp. 439–442.
- [47] A.E. Abken, O.J. Bartelt, Sputtered Mo/Sb₂Te₃ and Ni/Sb₂Te₃ layers as back contacts for CdTe/CdS solar cells, *Thin Solid Films.* 403 (2002) 216–222.
- [48] E. Artegiani, D. Menossi, H. Shiel, V. Dhanak, J.D. Major, A. Gasparotto, K. Sun, A. Romeo, Analysis of a novel $CuCl_2$ back contact process for improved stability in CdTe solar cells, *Prog. Photovoltaics Res. Appl.* 27 (2019) 706–715.

**Chapter III Description of
the Silvaco-Atlas simulation
software**

III.1 Introduction

Modeling and physical simulation have become a very important tool for understanding the functioning of devices and physical mechanisms because the optimizations through simulation processes are more readily available, less expensive, and faster than those of experimental processes and can provide information that is difficult or impossible to measure experimentally. Simulation helps users to gain a better understanding of the behavior and properties of devices by increasing the speed of processes and reducing the risks of the experience and the uncertainties of the tests. The TCAD simulator (Technology Computer Aided Design) is a complete set of independent tools for the physical and technological simulation of electronic devices. It allows the integration of technological design aspects with electrical simulation, with the aim of saving time and development costs, and to envision and optimize solutions to improve the performance of devices. Several simulators are available on the market, examples include; PC1D, AMPS1D, ISE, SYNOPSIS, SCAPS, SILVACO... etc [1-5].

Silvaco-Atlas is a powerful simulator program in two dimensions (2D) and three dimensions (3D). It serves as a global support for analyzing and optimizing the performance of semiconductor devices. It provides a wide variety of mathematical and physical models and an appropriate mesh structure, and it also uses sophisticated numerical techniques [3].

In this chapter, we present a relatively detailed description of Silvaco. This software includes a wide range of comprehensive studies in the development and characterization of solar cells. We will use the Silvaco-Atlas part to generate the results of the electrical characteristics of the studied solar cell.

III.2 Silvaco Overview

Silvaco (SILicon VALley COrporation) is an American international company, with its headquarters in Santa Clara, California. It stands as a leading provider of integrated professional simulation software suites, furnishing a broad array of programs for the modeling of various electronic domains, including both analog and digital circuitries. The company's offerings span from basic modeling to comprehensive integrated circuit design schematics and extraction toolsets [4].

Founded in 1984 by Dr. Ivan Pestic, the TCAD-Silvaco software represents a 2D/3D simulation platform utilizing the finite element method . It is capable of simulating not only the electrical, optical, and thermal characteristics of devices but also the technological processes involved in the creation of electronic structures, such as deposition, etching, and doping through implantation or diffusion [4].

These simulations facilitate the optimization of numerous manufacturing parameters and enable the prediction of semiconductor devices' performance, particularly solar cells. The tools available within Silvaco are categorized into core and interactive tools.

TCAD Silvaco introduces advanced physical models, leveraging efficient numerical methods and algorithms, alongside innovative meshing techniques, thus delivering simulation outcomes that closely mirror real-world results. A notable benefit of this simulator lies in its capability to render physically intricate phenomena comprehensible.

III.3 Presentation of Silvaco-Atlas Software

SILVACO International is a company specialized in modeling and simulation software for semiconductor materials. Its integrated TCAD (Technology Computer Aided Design) tool provides modeling and simulation capabilities for simple circuits as well as for detailed integrated circuit manufacturing. Atlas is a simulator for two-dimensional and three-dimensional physical-based devices. It predicts the electrical behavior of specified semiconductor structures and provides insight into the internal physical mechanisms associated with the device operation. Atlas can be used independently or as a foundational tool in the Virtual Wafer Fab simulation environment of Silvaco. In the sequence of predicting the impact of process variables on circuit performance, the device simulation fits between process simulation and model extraction [5].

ATLAS uses external description tools such as *ATHENA* or its own file commands (inputs) to be entered directly into *DevEdit* and *DeckBuild*, which facilitates its use. *ATHENA* is software for the simulation of technological manufacturing processes, while *ATLAS* is software for the simulation of the electrical behavior of components. *DevEdit* is an environment specific to structure (dimension, doping, ...) and meshing. *DeckBuild* is an environment (text input) where the simulation program is defined through text commands, and

the structure and mesh can also be defined in *DeckBuild*. *Tonyplot* is an environment where one can view the results of simulations (component structure, distributions of various quantities, electrical characteristics I-V...).

Most Atlas simulations use two input files. The first input file is a text command file containing the commands to be executed by Atlas (command file). The second input file is a structure file (structure file) that defines the structure to be simulated. Atlas produces three types of output files. The first type of output file is the run output or execution file (execution output), which gives us the progress as well as error and warning messages during the simulation. The second type of output file is the log file or journal (log files) which stores all the voltage and current terminals during the device analysis. The third type of output file is the solution file (solution files) that stores the 2D and 3D data related to the solution variable values in the device at a given current-voltage point. **Figure III.1** shows the types of incoming and outgoing information from Atlas.

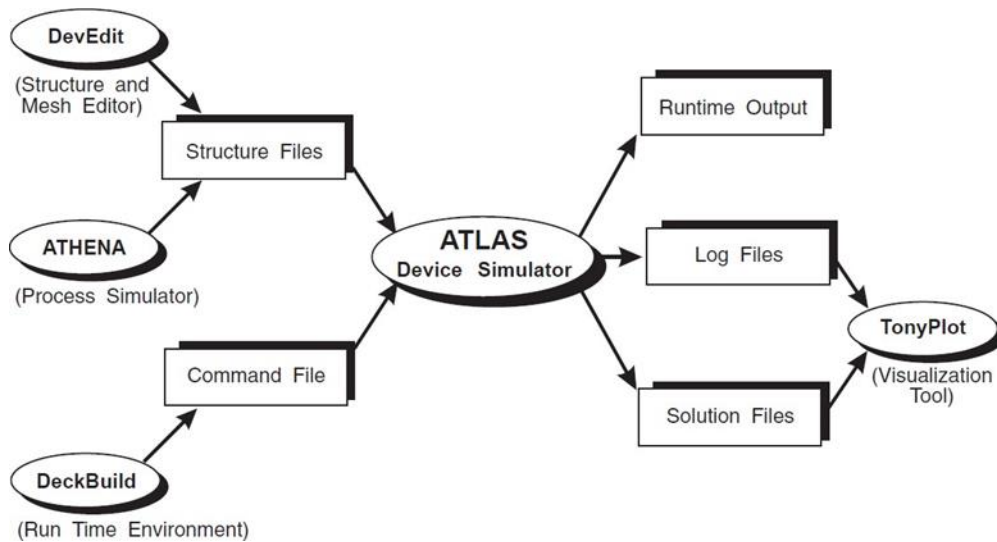


Figure III.1: Types of input and output information of Atlas [4].

III.4 The main groups and categories of commands and instructions of Silvaco-Atlas

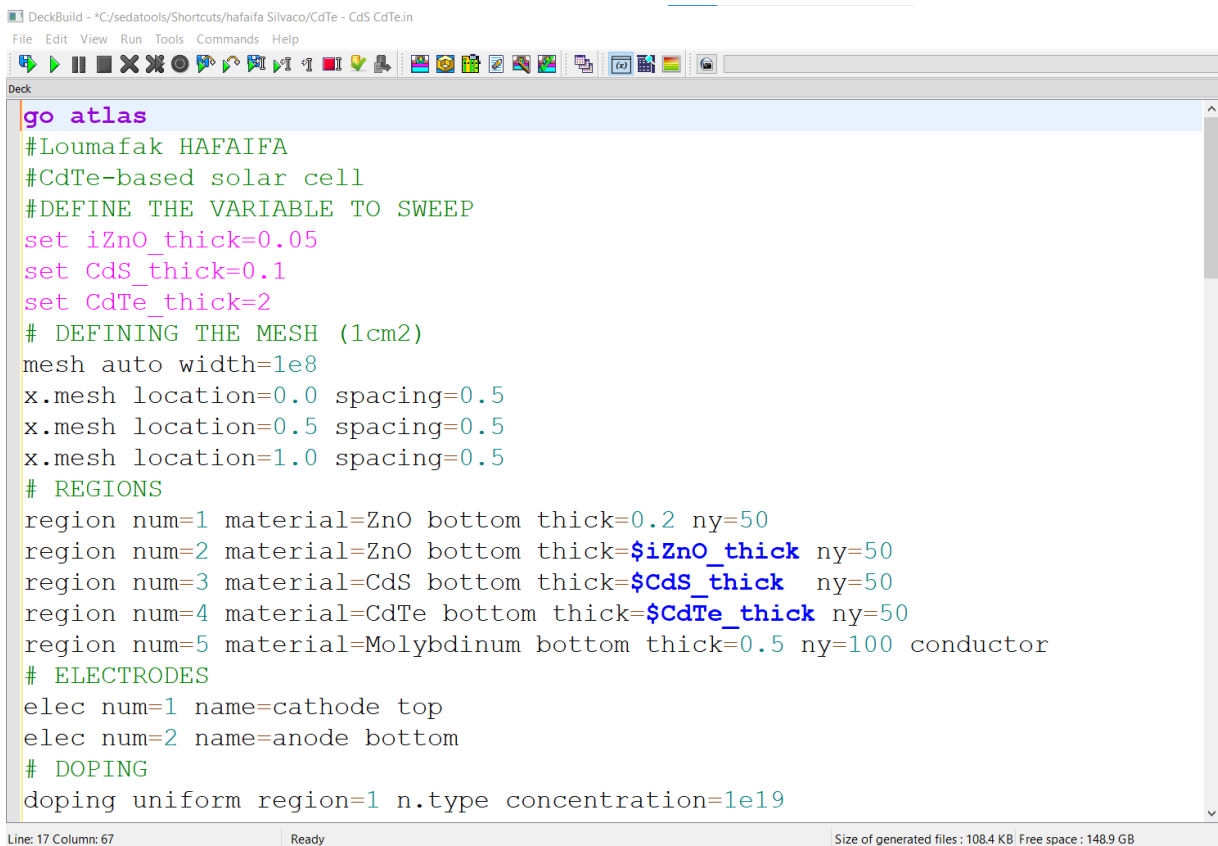
The programming logic of *ATLAS* is subject to special commands and command sequences specific to Silvaco-Atlas. To create a device in *ATLAS*, several instructions are used to finely adjust each desired input parameter. The user must use the environment called *DeckBuild*, which requires a very specific set of instructions to accurately design the device to be modeled. There are five groups of instructions that must appear in the correct order. **Figure III.2** summarizes the groups or categories of commands of Atlas programming logic with the main instructions in each group. The order of instructions in these groups, such as mesh determination, structure determination, and solution groups, is also important. The format and order are important when designing a device. Otherwise, an error message appears, which can lead to incorrect operation or program termination. If the parameters or material models are determined in the wrong order, this can also lead to incorrect operation or program termination, or they may not be usable in calculations.

<i>Group</i>	—————	<i>Statements</i>
1. Structure Specification	—————	MESH REGION ELECTRODE DOPING
2. Material Models Specification	—————	MATERIAL MODELS CONTACT INTERFACE
3. Numerical Method Selection	—————	METHOD
4. Solution Specification	—————	LOG SOLVE LOAD SAVE
5. Results Analysis	—————	EXTRACT TONYPLOT

Figure III.2: The groups or categories of command logic of Silvaco-Atlas programming [4].

III.5 Structure Determination

Under the structure determination are several instructions that allow the user to define the environment in which the simulations will be executed. The structure is determined by defining the mesh, regions, electrodes, and the type and density of doping through text commands that are specific to the Silvaco-Atlas software and must be properly ordered according to the software's commands. Silvaco-Atlas receives the input commands contained within the DeckBuild simulation environment. **Figures III.3** and **III.4** show the DeckBuild simulation environment window displaying some constructive commands of our simulated CdTe solar cell by the Silvaco-Atlas software before and after starting the command executions.



```

go atlas
#Loumafak HAFIFA
#CdTe-based solar cell
#DEFINE THE VARIABLE TO SWEEP
set iZnO_thick=0.05
set CdS_thick=0.1
set CdTe_thick=2
# DEFINING THE MESH (1cm2)
mesh auto width=1e8
x.mesh location=0.0 spacing=0.5
x.mesh location=0.5 spacing=0.5
x.mesh location=1.0 spacing=0.5
# REGIONS
region num=1 material=ZnO bottom thick=0.2 ny=50
region num=2 material=ZnO bottom thick=$iZnO_thick ny=50
region num=3 material=CdS bottom thick=$CdS_thick ny=50
region num=4 material=CdTe bottom thick=$CdTe_thick ny=50
region num=5 material=Molybdenum bottom thick=0.5 ny=100 conductor
# ELECTRODES
elec num=1 name=cathode top
elec num=2 name=anode bottom
# DOPING
doping uniform region=1 n.type concentration=1e19

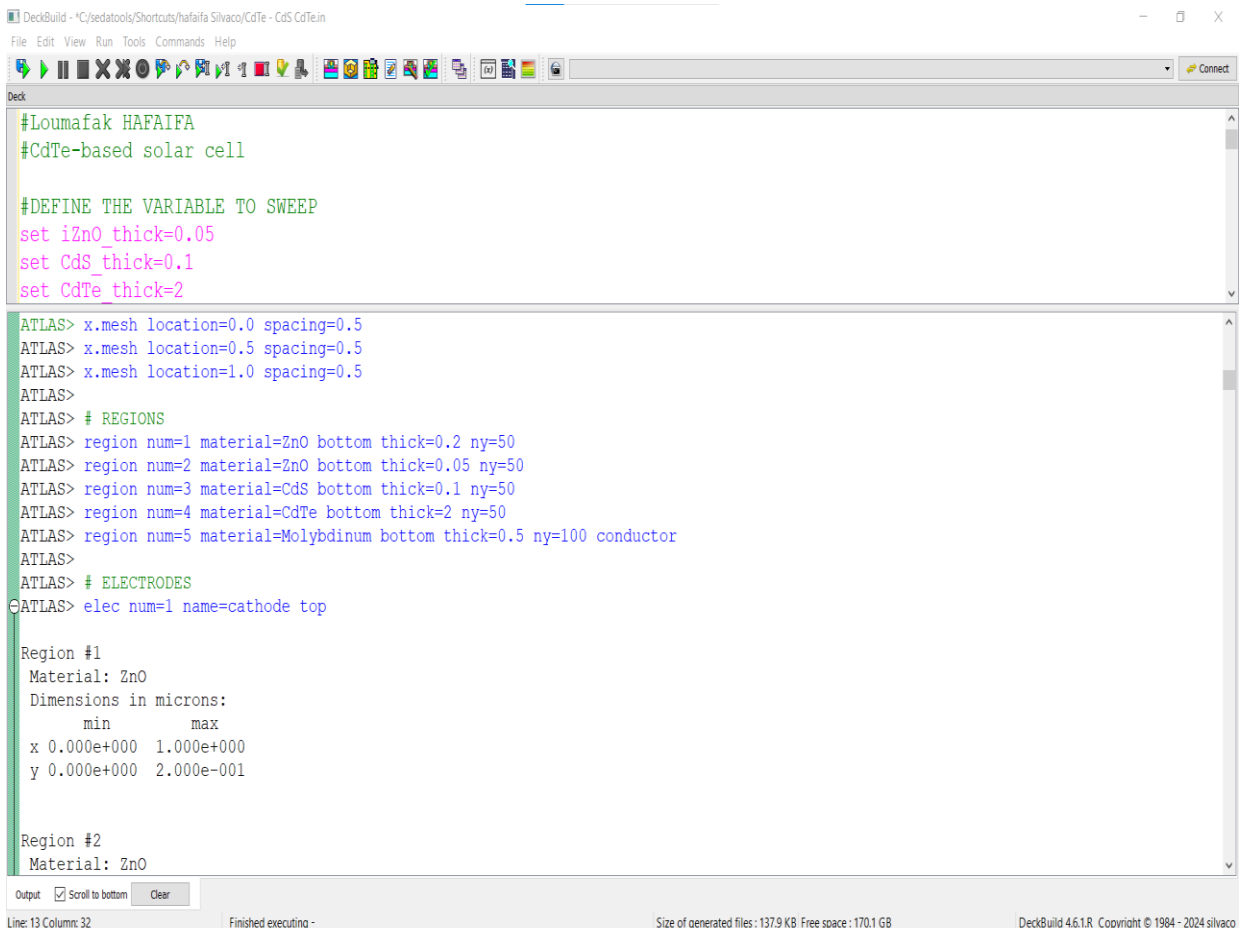
```

Line: 17 Column: 67 Ready Size of generated files : 108.4 KB Free space : 148.9 GB

Figure III.3: The DeckBuild simulation window of Silvaco-Atlas software displaying some constructive commands of our simulated CdTe solar cell before the start of command executions.

As shown in **Figure III.3**, the DeckBuild simulation environment window is divided into two sub-windows. The upper sub-window of the DeckBuild simulation environment is intended for displaying the Silvaco-Atlas software commands in text form. The lower sub-window of DeckBuild is intended for displaying program command executions, information, and results extracted from the execution of commands. Atlas is called to execute these latter by the following command: "go atlas". The format of the Silvaco-Atlas commands is as follows:

<STATEMENT>< PARAMETER> = <VALUE>



```

DeckBuild - *C:/sedatools/Shortcuts/hafaifa Silvaco/CdTe - CdS CdTe.in
File Edit View Run Tools Commands Help
Deck
#Loumafak HAFIFA
#CdTe-based solar cell

#DEFINE THE VARIABLE TO SWEEP
set iZn0_thick=0.05
set CdS_thick=0.1
set CdTe_thick=2

ATLAS> x.mesh location=0.0 spacing=0.5
ATLAS> x.mesh location=0.5 spacing=0.5
ATLAS> x.mesh location=1.0 spacing=0.5
ATLAS>
ATLAS> # REGIONS
ATLAS> region num=1 material=ZnO bottom thick=0.2 ny=50
ATLAS> region num=2 material=ZnO bottom thick=0.05 ny=50
ATLAS> region num=3 material=CdS bottom thick=0.1 ny=50
ATLAS> region num=4 material=CdTe bottom thick=2 ny=50
ATLAS> region num=5 material=Molybdenum bottom thick=0.5 ny=100 conductor
ATLAS>
ATLAS> # ELECTRODES
ATLAS> elec num=1 name=cathode top

Region #1
Material: ZnO
Dimensions in microns:
      min      max
x 0.000e+000 1.000e+000
y 0.000e+000 2.000e-001

Region #2
Material: ZnO
  
```

Output Scroll to bottom

Line: 13 Column: 32 Finished executing - Size of generated files: 137.9 KB. Free space: 170.1 GB DeckBuild 4.6.1.R Copyright © 1984 - 2024 silvaco

Figure III.4: The DeckBuild simulation window of Silvaco-Atlas software displaying some constructive commands of our simulated CdTe solar cell after the execution of the commands has started.

III.5.1 Mesh Determination

The mesh is a series of horizontal and vertical lines. In our study, the mesh used is two-dimensional. Therefore, only the x and y parameters are defined. The general format for mesh definition is [6]:

$$x.mesh\ location=<value>\ spacing=<value>$$

$$y.mesh\ location=<value>\ spacing=<value>$$

The mesh plays an important role in obtaining good simulation results. The choice of mesh must be made to balance between execution speed and the accuracy of results. A coarse mesh produces a rapid simulation but with less precise results, while a fine mesh slows down the simulation but yields more accurate results. Therefore, a fine mesh is more advantageous from the perspective of obtaining good simulated results. **Figure III.5** shows the mesh of our CdTe solar cell structure as displayed by the Tonyplot window of Silvaco-Atlas. Due to the very precise values used in our mesh, these horizontal and vertical lines cannot be distinguished.

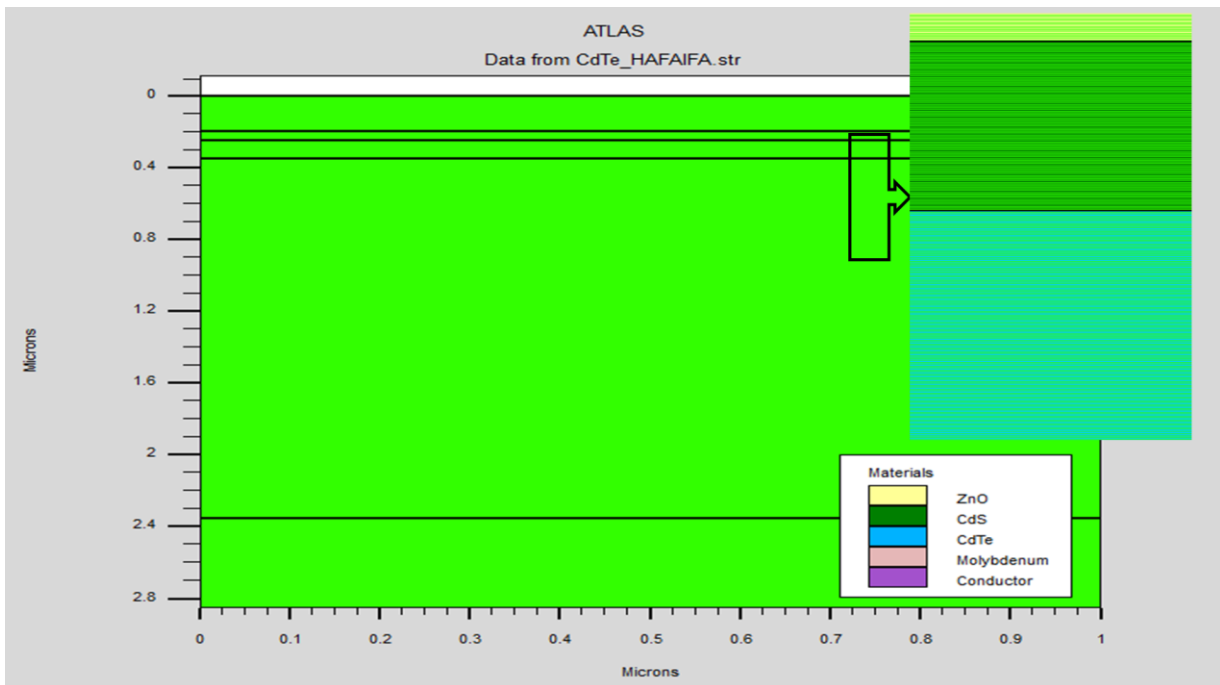


Figure III.5: The mesh of our CdTe solar cell structure displayed by the Tonyplot window of the Silvaco-Atlas software.

III.5.2 Determination of regions (layers) and names of materials

The regions (layers) are determined by the *REGION* instruction. It defines each layer, its position, and the name of its component materials. The general format of the commands that determine the regions (the component layers of the cell) and the name of the materials for each region is as follows [5]:

REGION number=<integer> <material type> <position>.

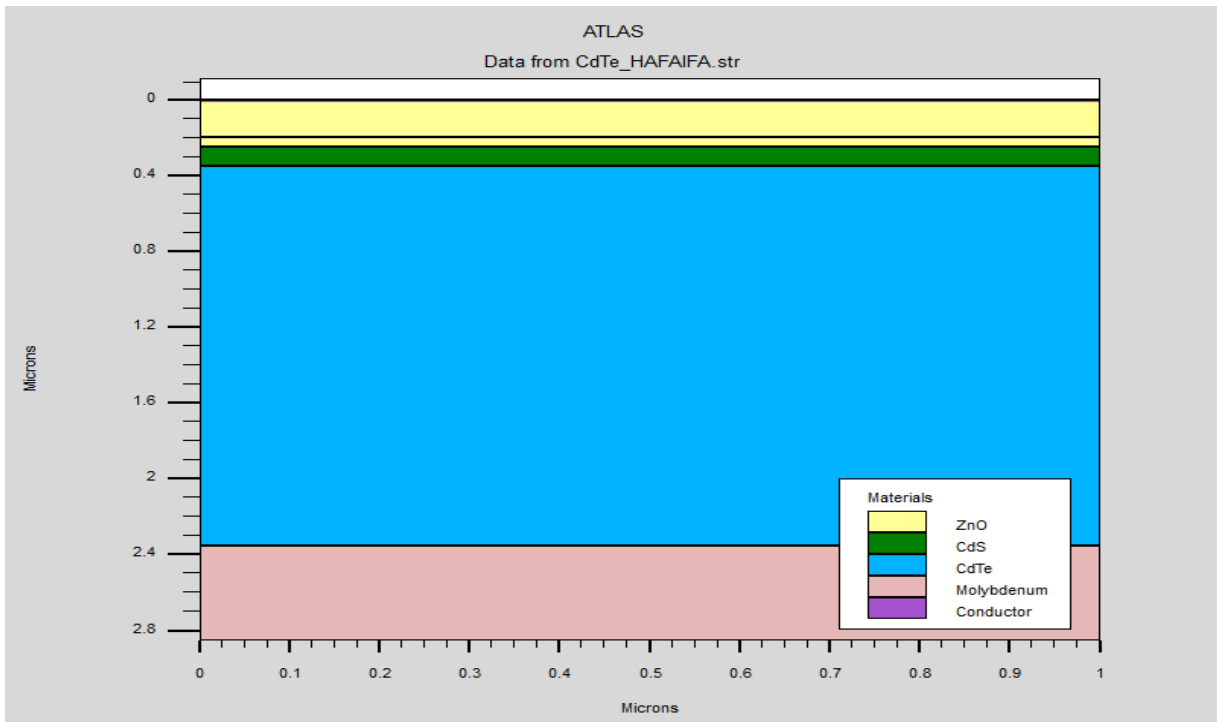


Figure III.6: The regions and materials for each region of our CdTe solar cell displayed by Silvaco-Atlas software.

III.5.3 Determination of electrodes

In the context of detailing the configuration for electrode placement within the previously established mesh, it is essential to articulate the precise locations and denominations of the electrodes. This determination can be applied to any designated area within the mesh. For the purposes of this dissertation, the incorporation of both a cathode and an anode within the CdTe solar cell was executed. The nomenclature for denoting the electrodes adheres to the following format:

ELECTRODE NAME = <electrode name> <position>.

The declarations of *BOTTOM* and *TOP* are utilized to indicate the positioning of the electrode at either the device's lower or upper extremity, respectively. In instances where these designations are not applicable, it is mandatory to delineate the boundary positions using *X.MIN*, *X.MAX* for the *x*-axis, and *Y.MIN*, *Y.MAX* for the *y*-axis.

Figure III.3 shows the position of the anode and the cathode by values assigned to *y* of our CdTe-based solar cell structure.

III.5.4 Determination of doping

The other aspect of the determination of the structure that needs to be defined is the doping. It is determined by the *DOPING* instruction. This determination includes the uniform distribution, position, type, and concentration of doping. The general format of the commands that determine the doping is as follows:

DOPING <distribution type> <dopant type> <position parameters>.

The commands that determine the doping of each layer of our CdTe solar cell are illustrated in Figure III.3.

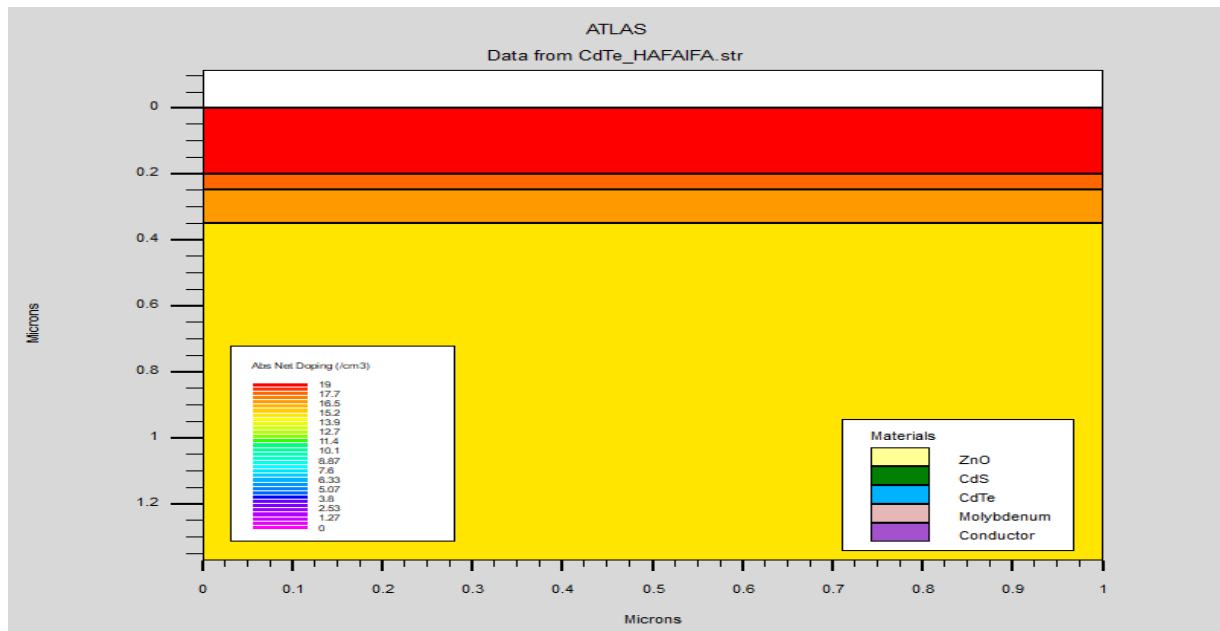


Figure III.7: The doping density distribution for each region of our CIGS solar cell structure displayed by Silvaco-Atlas.

Figure III.7 shows the doping density distribution for each region of CdTe solar cell structure displayed by the Tonyplot window of the Silvaco-Atlas software.

III.6 Determination of materials and models

III.6.1 Determination of materials

The *MATERIAL* instruction is used to determine a set of different electrical and optical parameters of each material component. In semiconductors, these electrical properties include the bandgap, electron affinity, permittivity, mobilities, state densities. Optical properties are the refractive index, absorption, extinction... The general format of the commands that determine the materials and their properties is as follows:

MATERIAL material=<material name> <material definition and parameters>

III.6.2 Determination of models

Physical Physical models in semiconductors have been modeled in the form of mathematical expressions linking electrostatic potential and carrier density. The physical models are classified into five categories [7,8]:

- charge carrier mobility
- generation-recombination mechanisms
- transport statistics
- impact ionization
- tunnel effect

The syntax for the Model command is as follows:

MODELS <model flag> <general parameter> <model dependent parameters>

The choice of model depends on the materials selected for the simulation. The example below activates several models. *MODELS CONMOB FLDMOB SRH*

CONMOB is the model for doping concentration-dependent mobility. *FLDMOB* is the model for electric field-dependent mobility. *SRH* is the *Shockley-Read-Hall* recombination model.

III.6.3 Determination of Defects (traps) and interfaces

The *TRAP* instruction is used to define the properties of defects of each material such as type, defect density... The *INTERFACE* instruction is used to define the surface recombination velocity at interfaces between semiconductors or insulators.

III.6.4 Determination of the solar spectrum

The *BEAM* instruction is used to define the type and various solar spectra used. The origin of *BEAM* (light beam) is defined by *X.ORIGIN*, *Y.ORIGIN*, and *ANGLE* parameters which specify the direction of propagation of the beam relative to the X-axis and the wavelengths *WAVELENGTH*. The general format of the commands that determine the models is as follows: *BEAM* <Solar spectrum parameters> <*X.ORIGIN*> <*Y.ORIGIN*> <*ANGLE*> <*WAVELENGTH*>

III.7 Determination of the numerical calculation method

There are several numerical methods to calculate solutions to semiconductor device problems. The numerical method that was used to solve a system of strongly coupled differential equations is the *NEWTON* method. The methods used are determined by the *METHOD* instruction.

III.7.1 Determination of the solution

The determination of solutions is carried out by the following instructions: *LOG*, *SOLVE*, *LOAD*, and *SAVE*. The *LOG* instruction is used to record all endpoint characteristics in a data file. After a *LOG* command is recorded. The *SOLVE* instruction follows the Log instruction. It looks for a solution for one or more voltage polarization points. The *LOAD* instruction is introduced, from an existing file, for each voltage polarization point, the previous solutions as an initial proposal. The *SAVE* instruction allows the recording of all obtained information [8].

III.7.2 Analysis of results

The *EXTRACT* instruction is used to extract specific parameter values from the recorded log file or the solution file. The *TONYPLOT* instruction allows the Silvaco-Atlas

software to automatically save a structure file, plot it, and view it in the TonyPlot window. In our case, the *EXTRACT* instruction allows us to obtain photovoltaic performance parameters such as short-circuit current density J_{SC} , open-circuit voltage V_{OC} , form factor FF, and conversion efficiency η (J_{SC} , V_{OC} , FF, and η) of our CdTe solar cell, and the TonyPlot window can display the current-voltage curve of the solar cell. **Figure III.8** shows the current-voltage curve of our basic CdTe solar cell displayed by the TonyPlot window of the Silvaco-Atlas software.

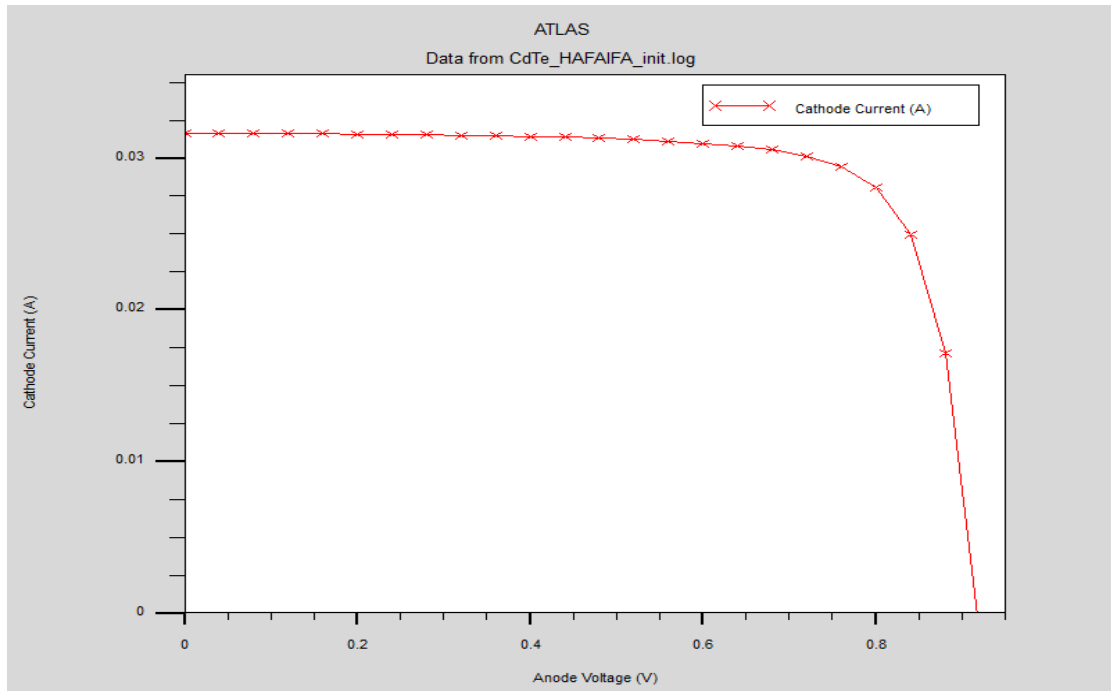


Figure III.8: The current-voltage curve of our basic CdTe solar cell displayed by the TonyPlot window of the Silvaco-Atlas software.

III.8 Conclusion

We have presented the TCAD-Silvaco simulation software used in our CdTe solar cell simulation work. Then, we presented its operation mode, its main commands and instructions for programming the Silvaco-Atlas software that determine the main characteristics of our CdTe solar cell, such as meshing, structure, regions (layers), materials, doping, electrodes... They have all been illustrated by images, examples, and results from our simulation of the CdTe solar cell. Thus, the different models and numerical methods used by the Silvaco-Atlas software have been presented.

References

- [1] S.O. Oyedele, B. Aka, Numerical Simulation of Varied Buffer Layer of Solar Cells Based on Cigs, *Model. Numer. Simul. Mater. Sci.* 07 (2017) 33–45. <https://doi.org/10.4236/mnsms.2017.73003>.
- [2] A. Haddout, A. Raidou, M. Fahoume, A review on the numerical modeling of CdS/CZTS-based solar cells, *Appl. Phys. A Mater. Sci. Process.* 125 (2019) 0. <https://doi.org/10.1007/s00339-019-2413-3>.
- [3] T. Joseph Mebelson, K. Elampari, A study of electrical and optical characteristics of CZTSe solar cell using Silvaco Atlas, *Mater. Today Proc.* 46 (2021) 2540–2543. <https://doi.org/10.1016/j.matpr.2021.01.758>.
- [4] Atlas User's Manual, SILVACO Inc, Santa Clara, CA 95054, California, USA, 2018.
- [5] K. Bessem, Etude par Tcad-SILVACO d'une structure MOS pour la réalisation de capteurs ISFET: parametres technologiques et electriques, Mémoire Magister. Electron. Univ. Mentouri–Constantine. (2010).
- [6] S. Daniel, Modeling radiation effect on a triple junction solar cell using silvaco atlas, Monterey· Naval Postgraduate School (2012).
- [7] B. BOUALEM, Simulation et optimisation des cellules solaires monolithiques a double heterojonctions, a base de cigs utilisant le logiciel atlas-silvaco, Doctoral dissertation. Univ Djillali Liabes of Sidi Bel Abbes (2020).
- [8] M. Elbar, Etude par simulation numérique d'une cellule solaire en CIGS à multi-jonction par le logiciel Tcad Silvaco, Doctoral dissertation. Univ Mohamed Khider – Biskra (2018).

Chapter IV Results and discussion

IV.1 Introduction

In the face of a deepening global energy crisis driven by international conflicts, epidemics, natural disasters, and significant climate change events, such as COVID-19, the Russia-Ukraine war, the Turkey-Syria earthquake, and Israeli invasion and annihilation war of the Gaza Strip (2023–present) there is an intensified demand for environmentally friendly energy solutions. The pursuit of sustainable development amidst these crises has highlighted solar energy particularly thin-film solar cells, like Cadmium Telluride (CdTe) solar cells as a viable alternative to depleting fossil fuels. CdTe solar cells are recognized for their efficiency and cost-effectiveness, attributable to their optimal optical and electronic properties, and have emerged as a leading technology, holding the highest market share among thin-film solar technologies. Recent advancements have significantly enhanced their efficiency, with achievements that include conversion efficiencies of up to 22.1% [1].

Despite their success, the toxicity of cadmium (Cd) and Cadmium Sulfide (CdS), which are used as buffer layers in these cells, has prompted research into less harmful alternatives. Zinc chalcogenides (ZnO, ZnS, and ZnSe) are being explored as promising substitutes because of their suitable band gaps and n-type semiconductor properties, which could potentially form better p–n junctions with the CdTe absorber layer. These materials are not only less reactive with chlorine an element used in enhancing the performance of CdTe cells but also mitigate long-term degradation issues associated with CdTe/CdS interfaces.

Furthermore, computational simulation studies, particularly those using Silvaco-Atlas software, are critical in optimizing solar cell designs to minimize material losses, improve efficiency, and reduce costs.

Our comprehensive study seeks to provide insights into improving the quality and performance of CdTe-based thin-film solar cells by examining the impact of alternative buffer layers. Investigating variables such as the thickness of the absorber and buffer layers, as well as doping density, we aim to identify optimal parameters for high-quality, non-toxic buffer materials that can enhance the optoelectronic properties of these solar cells. This offers a path forward in the development of cleaner and more efficient energy sources amidst global energy and environmental challenges.

IV.2 Conceptual and Numerical Model

Silvaco-Atlas software, being a powerful simulation tool, empowers researchers to not only analyze but also enhance the performance of semiconductor devices, including solar cells, which often exhibit complex physical structures. Its capabilities extend to the accurate prediction of thermal, electrical, and optical characteristics in both established and novel semiconductor devices [2].

We use Silvaco-Atlas to obtain crucial photovoltaic cell (PSC) parameters such as power conversion efficiency (PCE), fill factor (FF), short-circuit current density (JSC), and open-circuit voltage (V_{OC}) through simulation. These parameters are essential for evaluating and optimizing the performance of solar cells.

The Poisson equation (**Equation IV.1**), the carriers continuity equations (**Equations IV.2,3**), and the drift-diffusion equations (**Equations IV.4,5**) serve as the mathematical foundation for these simulations, enabling us to model and analyze the behavior of charge carriers within the solar cell device. By leveraging Silvaco-Atlas, we can gain valuable insights into the operation of CdTe solar cells and optimize their designs to improve efficiency and performance.

$$\Delta V = -\frac{q}{\epsilon}(p - n + N_D - N_A + N_t) \quad (\text{IV.1})$$

Where Δ is the Laplacian operator. The Poisson equation shows a relationship between each of the electrostatic potential (V), the doping density (N_D and N_A are donor and acceptor), the electron charge (q), the permittivity (ϵ), hole and electron densities (p and n) and the defect density (N_t)

The hole and electron continuity equations are expressed as follows:

$$-\frac{1}{q} \frac{dJ_n}{dx} = G_{op}(x) - R_n \quad (\text{IV.2})$$

$$\frac{1}{q} \frac{dJ_p}{dx} = G_{op}(x) - R_p \quad (\text{IV.3})$$

Where, J_n , J_p are the current densities of electrons and holes and R_n , R_p are recombination velocities for direct band.

The drift-diffusion equations are expressed as follows:

$$J_n = -\frac{\mu_n n}{q} \frac{\partial E_{Fn}}{\partial x} \quad (\text{IV.4})$$

$$J_p = -\frac{\mu_p p}{q} \frac{\partial E_{Fp}}{\partial x} \quad (\text{IV.5})$$

Where μ_n and μ_p are the electron and hole mobility, E_{Fn} and E_{Fp} are the n-type and p-type carrier fermi level.

The principal performance indicators for the solar cell are derived from the analysis of its current–voltage (I - V) characteristics. The aggregate current (I) constitutes the summation of the dark current and the light-induced current (photocurrent, I_{ph}). This relationship is mathematically represented by the renowned Shockley equation [3,4]:

$$I = I_{ph} - I_0 \left(\exp\left(\frac{qV}{akT}\right) - 1 \right) \quad (\text{IV.6})$$

Where I is the net current flowing through the solar cell, I_0 is the saturation reverse current, q is the electron charge, V is the applied voltage, a is the ideality factor, k is the Boltzmann constant, and T is the absolute temperature.

- The I_{sc} (short-circuit current) when $V=0$:

$$I_{sc} = I_{ph} \quad (\text{IV.7})$$

- The V_{oc} (open circuit voltage):

$$V_{oc} = \frac{akT}{q} \ln\left(\frac{I_{ph}}{I_0}\right) \quad (\text{IV.8})$$

- The FF (fill factor):

$$FF = \frac{P_{max}}{V_{oc} I_{sc}} \quad (\text{IV.9})$$

- The η (Efficiency):

$$\eta = \frac{P_{max}}{P_{in}} = \frac{V_{oc} I_{sc} FF}{P_{in}} \quad (\text{IV.10})$$

P_{max} is the maximum power, and P_{in} is the incident optical power.

IV.3 Design and Material Parameters of CdTe Thin Film Solar Cells

In the current study, we present a CdTe-based thin-film solar cell constructed on a glass substrate. This cell is composed of a multilayer structure that commences with a window layer comprised of n-type transparent conductive oxide (ZnO) and intrinsic layer (i-ZnO), the latter serving to equalize the surface distribution of current density and mitigate potential shunt or leakage currents at the junction [5]. Following this is a n-doped buffer layer, for which cadmium-free zinc chalcogenide-based alternatives are suggested to replace the conventional CdS layer. The core of the cell is formed by a p-type CdTe absorber layer, and the structure is completed with a Mo-coated back glass substrate, as depicted in **Figure IV.1**. The illustration also details the varying thicknesses and doping levels of each layer. Illumination conditions are specified as a 1 kW/m² power density under an AM1.5G solar spectrum at ambient temperature.

For simulation purposes in Silvaco-Atlas software, we have meticulously determined the requisite primary parameters of each layer based on a comprehensive review of literature, empirical studies, and precedent scholarly efforts, collated in **Table IV.1** [3,6,9,11,13,15–18]. Moreover, the optoelectronic properties of Molybdenum have been acquired from the SOPRA database within the Silvaco-Atlas library [19].

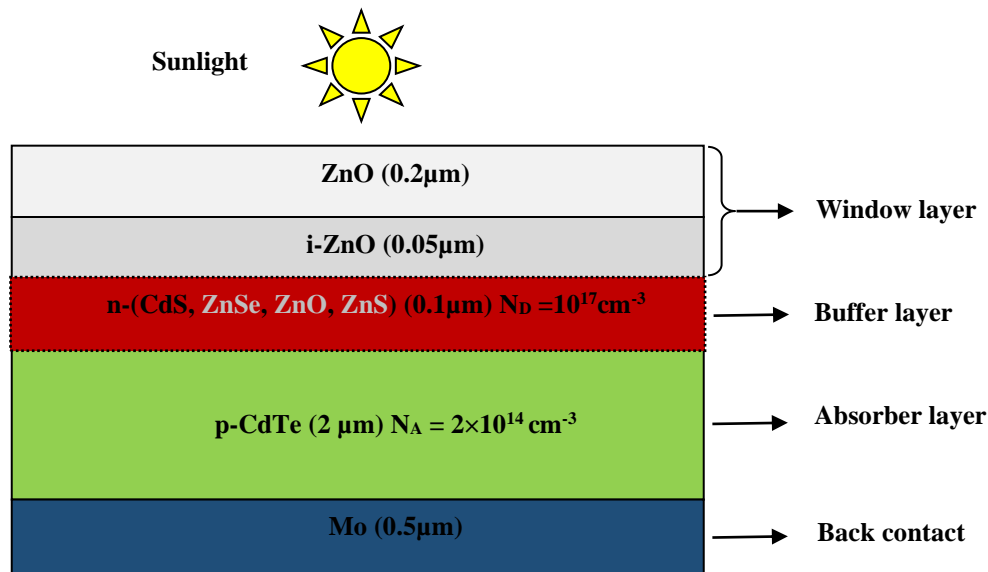


Figure IV.1: Schematic representation of the proposed CdTe/CdS thin film solar cell structure.

Table IV.1 Material properties and parameters employed in the numerical simulation of CdTe thin-film solar cells.

Parameters	i-ZnO [6]	n-CdS [6–8]	n-ZnS [7]	n-ZnSe [6,9,10]	n-ZnO [7,8]	p-CdTe [8,11–14]
ϵ_r (F cm ⁻¹): Relative permittivity	9	10	8.32	10	9	19.6
E_g (eV): Band gap energy	3.3	2.4	3.68	2.9	3.3	1.5
χ_e (eV): Electron affinity	4.5	4.5	4.5	4.2	4.5	4.28
N_v (cm ⁻³): VB effective density of states	1.8×10^{19}	1.8×10^{19}	1.5×10^{19}	1.8×10^{19}	1.8×10^{19}	1.8×10^{19}
N_c (cm ⁻³): CB effective density of states	2.2×10^{18}	2.2×10^{18}	2.2×10^{18}	2.2×10^{18}	2.2×10^{18}	8×10^{17}
μ_n (cm ² /Vs): Electron mobility	100	100	250	100	100	100
μ_p (cm ² /Vs): Hole mobility	25	25	40	25	25	25

IV.4 Discussion and Analysis of Results

IV.4.1 Numerical Simulation of the CdTe Solar Cell

In the present study, numerical simulations were conducted on a standard CdTe/CdS solar cell using parameter values enumerated in **Table IV.1**. The simulation outputted a current-voltage (J-V) curve, which is depicted in **Figure IV.2**. From this curve, we extracted key photovoltaic performance metrics, namely the short-circuit current (I_{sc}), open-circuit voltage (V_{oc}), fill factor (FF), and conversion efficiency (η), which are summarized in **Table IV.2**. These performance indicators are crucial for evaluating the effectiveness of the solar cell design.

To ascertain the reliability of our simulation model, we compared the derived performance parameters with both experimental data and other simulation outcomes for an equivalent structure incorporating a CdS buffer layer, as shown in **Table IV.2**. The congruence of our results with empirical findings and prior simulations corroborates the validity of our model and the parameters chosen for the simulation process.

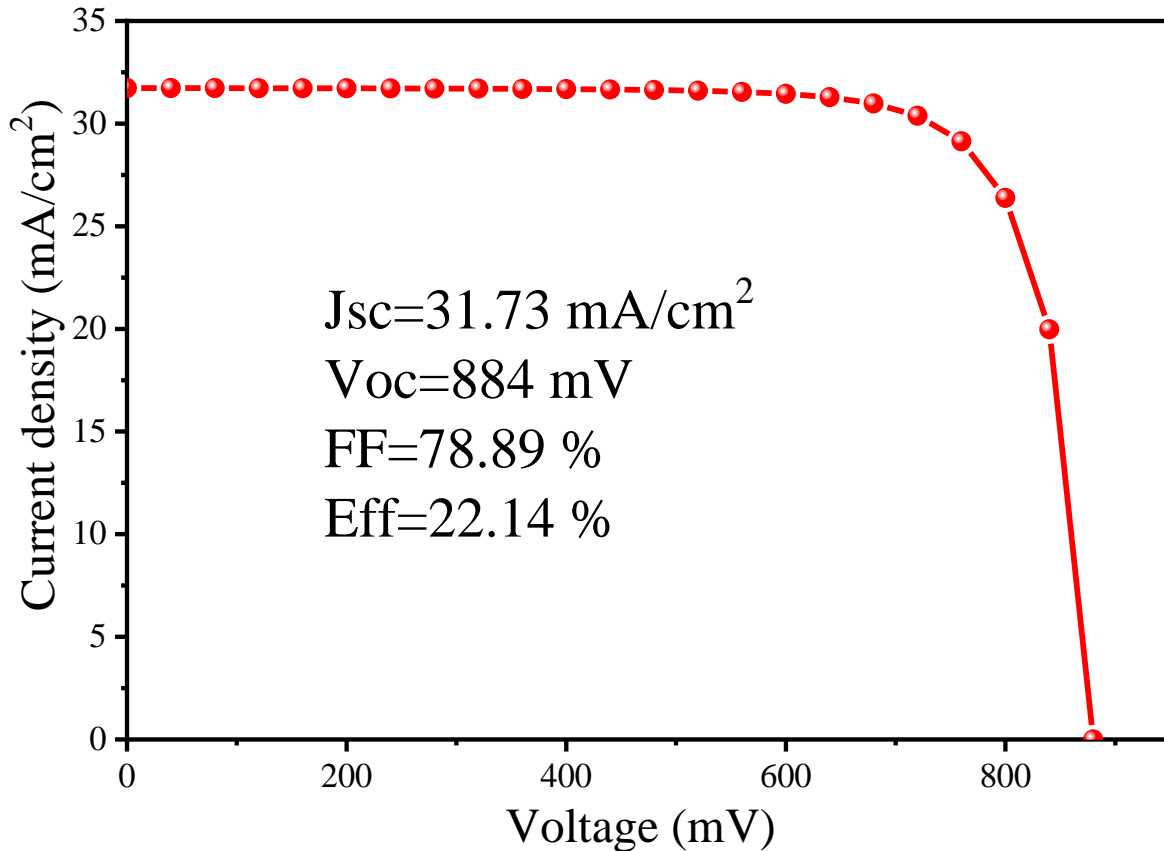


Figure IV.2: Current density-voltage (J-V) characteristics of the CdTe solar cell.

Table IV.2 Comparative of CdTe/CdS solar cells photovoltaic performance parameters between different results.

	J_{sc} (mA/cm ²)	V_{oc} (mV)	FF (%)	η (%)
Reference cell	31.73	884	78.89	22.14
Experimental results [1]	31.69	887	78.5	22.1
Simulation results [18]	31.34	872	83.80	22.9

IV.4.2 Influence of Different Buffer Layers

In this section, the effects of employing cadmium-free materials specifically ZnSe,

ZnO, and ZnS as alternative buffer layers in cadmium telluride (CdTe) thin-film solar cells are explored. Current-voltage (J-V) characteristics were ascertained through simulation studies. As depicted in **Figure IV.3**, the integration of these alternative buffers (ZnSe, ZnO, and ZnS) considerably improves the electrical performance of the CdTe solar cells.

Relative to the conventional, toxic cadmium sulfide (CdS) buffer layer, the substitution with these materials leads to an enhancement in power conversion efficiency by 0.9% to 2.34% and a fill factor (FF) increment of up to 3%. The underlying mechanism for this enhancement is postulated to be the increase in the optical band gap of the alternative buffers of 0.5 eV for ZnSe, 0.9 eV for n-type ZnO, and 1.28 eV for ZnS compared to the band gap of CdS. The increase in band gap is correlated with a rise in the short-circuit current density (J_{sc}) from 31.73 mA/cm² with the CdS buffer to 34.46 mA/cm² when ZnS is employed as the buffer layer.

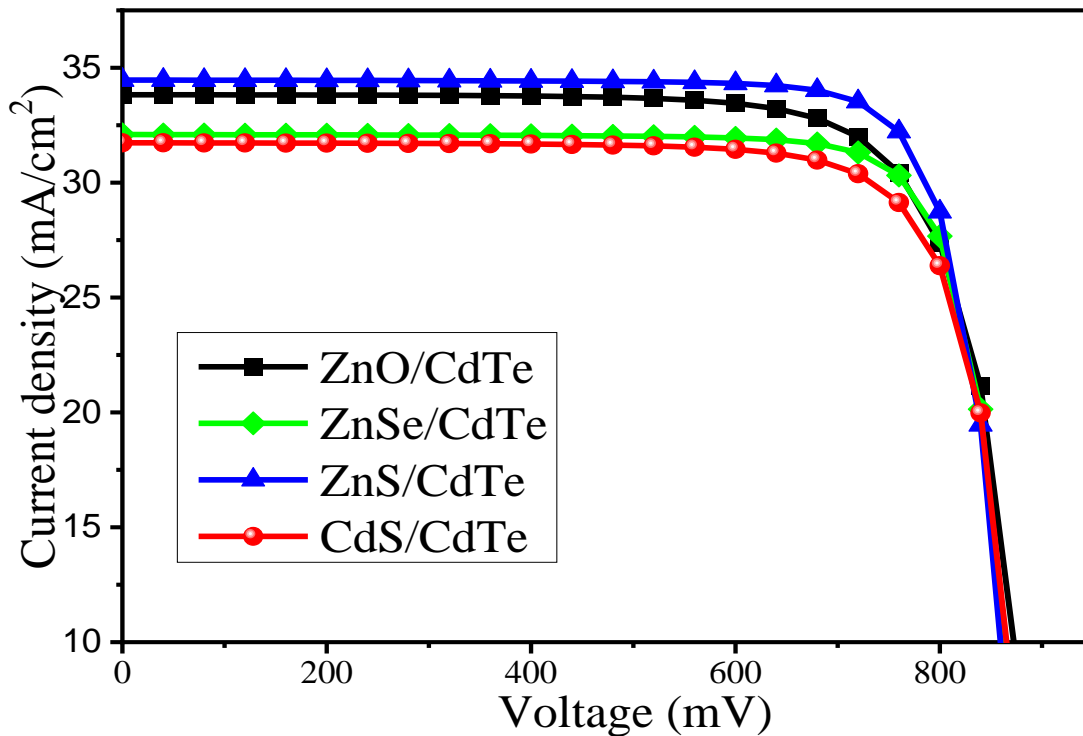


Figure IV.3: J-V characteristics of CdTe solar cells incorporating various buffer layers, including CdS, ZnSe, ZnO, and ZnS.

Table IV.3 Numerically simulated photovoltaic performance parameters of CdTe cells incorporating various buffer layers.

	Jsc (mA/cm ²)	Voc (mV)	FF (%)	η (%)
CdTe/CdS	31.73	884	78.89	22.14
CdTe/ZnSe	32.09	876	81.86	23.04
CdTe/ZnO	33.82	888	76.92	23.13
CdTe/ZnS	34.46	877	81	24.48

IV.4.3 Correlation Between Buffer Layer Characteristics and CdTe Cell Efficiency

Investigations into the pivotal role of buffer layer properties, specifically thickness and doping concentration, reveal significant implications for the efficiency of CdTe solar cells. This analysis adheres to a methodical approach in which the buffer layer thickness and doping levels are selectively varied while ensuring that other physical parameters remain constant, thereby isolating their effects. Within this examination, buffer layers composed of CdS, ZnSe, ZnO, and ZnS are systematically modified from 0.01 to 0.12 μm in thickness, with accompanying data outlined in **Table IV.1** and graphical representations provided in **Figure IV.4**. These representations correlate crucial photovoltaic parameters with buffer layer thickness. The simulations yield conclusive evidence that buffer layer thickness is a determinant of solar cell performance. A thinner buffer layer is preferable, as it reduces optical absorption and resistive losses [21], which are detrimental to the cell's efficacy. This finding is corroborated by similar experimental results previously reported by [22]. As the thickness escalates, a notable drop in short-circuit current density (Jsc) is observed, particularly for ZnS and CdS, whereas ZnO and ZnSe reflect minimal variance. Efficiency (η) trends similarly, with an increase in short-circuit current correlating to enhanced efficiency.

Open-circuit voltage (V_{OC}) attains optimal figures at minimal thicknesses, and despite V_{OC} exhibiting minor modulations for CdS and ZnO as thickness grows, a rapid decline is evident for ZnS and ZnSe at thicknesses beyond 0.04 μm. The fill factor (FF), another critical solar cell metric, reaches its peak performance at a buffer layer thickness of 0.04 μm for ZnS and ZnSe, with no noteworthy changes detected thereafter.

Thus, all buffer layers achieve high efficiency at 0.01 μm thickness (CdS, ZnS, and ZnO) and 0.02 μm (ZnSe). Consequently, a 0.01 μm thickness stands optimal for all buffer layer thicknesses, a finding corroborated by similar results previously reported, reinforcing the potential to engineer a more cost-efficient CdTe solar cell with a thinner buffer layer to maximize absorption.

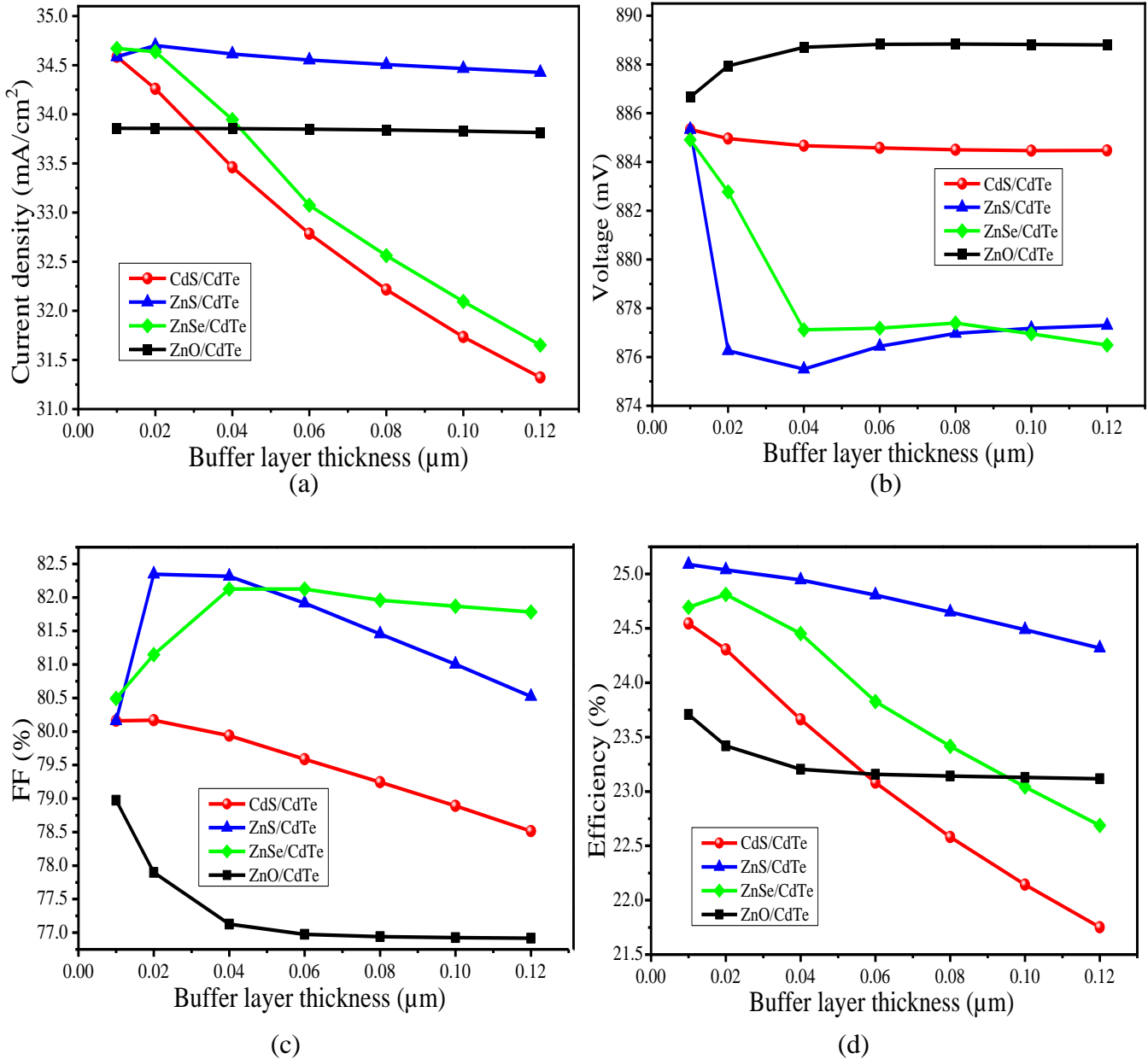


Figure IV.4: Investigation of the influence of buffer layer thickness on CdTe solar cell performance parameters: (a) J_{SC} (b) V_{oc} (c) Fill factor FF (d) Efficiency η .

Parallel to thickness optimization, donor doping density (N_D) is calibrated, varying from 10^{17} to 10^{19} cm^{-3} , while maintaining all other doping densities and parameters steady. **Figure IV.5** delineates the simulated effects of doping density on performance, illustrating that beyond a threshold of 10^{18} cm^{-3} , changes in performance parameters are negligible. This finding designates 10^{18} cm^{-3} as the superior doping concentration for all buffer materials, optimizing cell performance parameters.

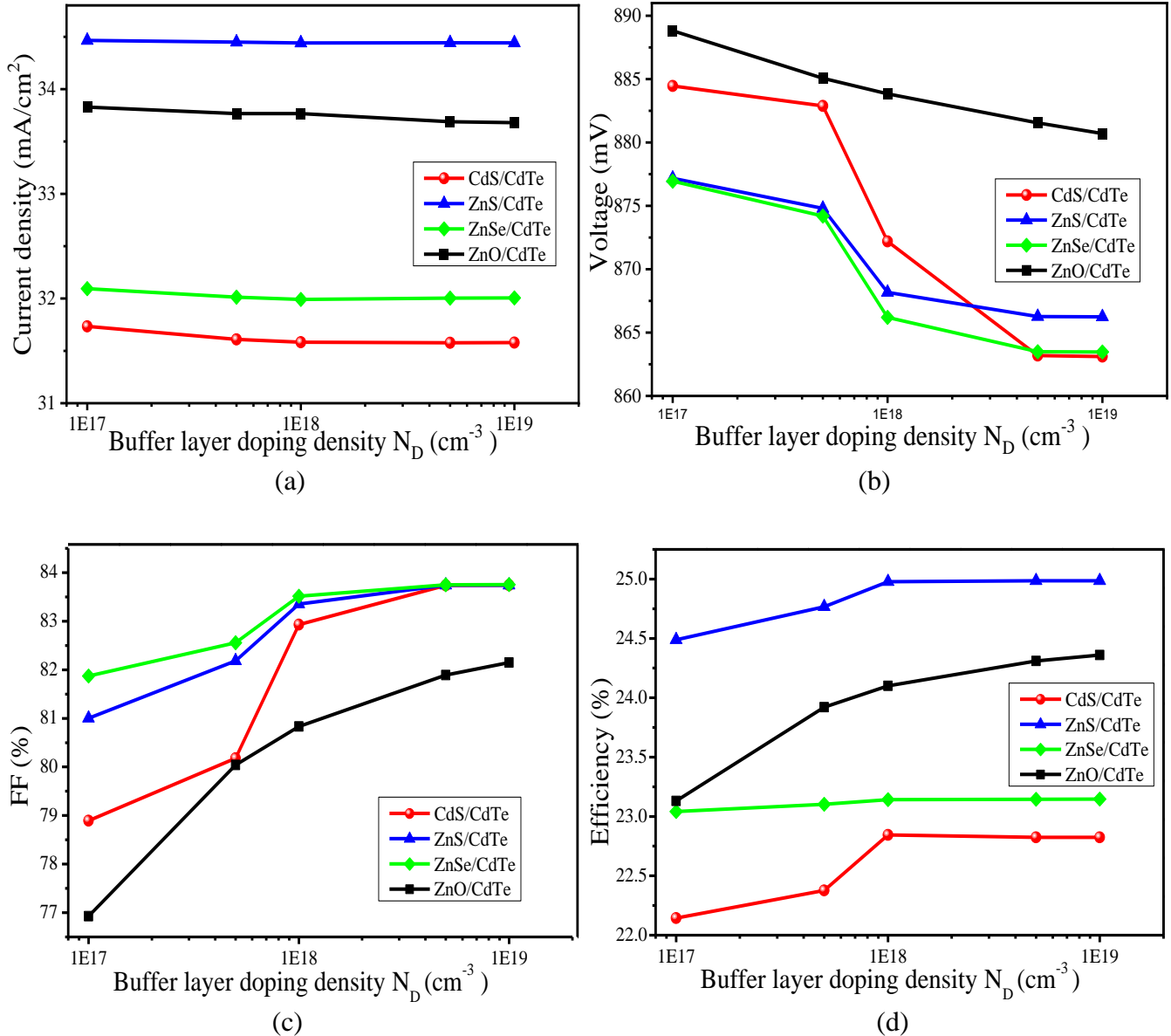


Figure IV.5: Evaluation of CdTe solar cell performance parameters as a function of donor defect density (N_D): (a) J_{sc} (b) V_{oc} (c) Fill factor FF (d) Efficiency η .

IV.4.4 Impact of Absorber Layer Thickness Variation

The thickness of the absorber layer is a critical determinant of the performance metrics in photovoltaic cells. To elucidate its effects on the parameters of solar cells, the thickness of the cadmium telluride (CdTe) absorber layer was varied between 1 μm and 4 μm . **Figure IV.6** illustrates the resultant impact on the open-circuit voltage (V_{OC}), short-circuit current density (J_{SC}), fill factor (FF), and overall conversion efficiency across different buffer layer configurations.

An initial rapid enhancement in performance metrics is noted as the absorber layer thickness increases from 1 μm to 2.5 μm , after which the parameters plateau between 2.5 μm and 4 μm . The escalation in thickness up to 2.5 μm , as depicted in **Figure IV.6 d**, correlates with a heightened photon absorption, with a concomitant rise in the number of photons absorbed, thereby maximizing the solar cell efficiency. This observed behavior aligns with findings from a preceding study [23], which suggests that a thickness of 2.5 μm is adequate to absorb approximately 99% of incident photons. Concurrently, both V_{OC} and J_{SC} demonstrate a marginal increase with the thickness of the absorber layer up to 2.5 μm , contributing to the enhanced efficiency. Thus, an absorber layer thickness of 2.5 μm is designated as the optimal value for CdTe solar cells.

However, augmenting the thickness beyond this optimal point to 4 μm is counterproductive for carrier collection efficiency. The reason for this decrease in performance is attributed to elevated recombination events at the interface, which occur due to the greater thickness, as detailed in reference [24]. Despite the increase in generated carriers resulting from enhanced light absorption, this increase in recombination reduces the effective collection of carriers, thereby diminishing the cell efficiency.

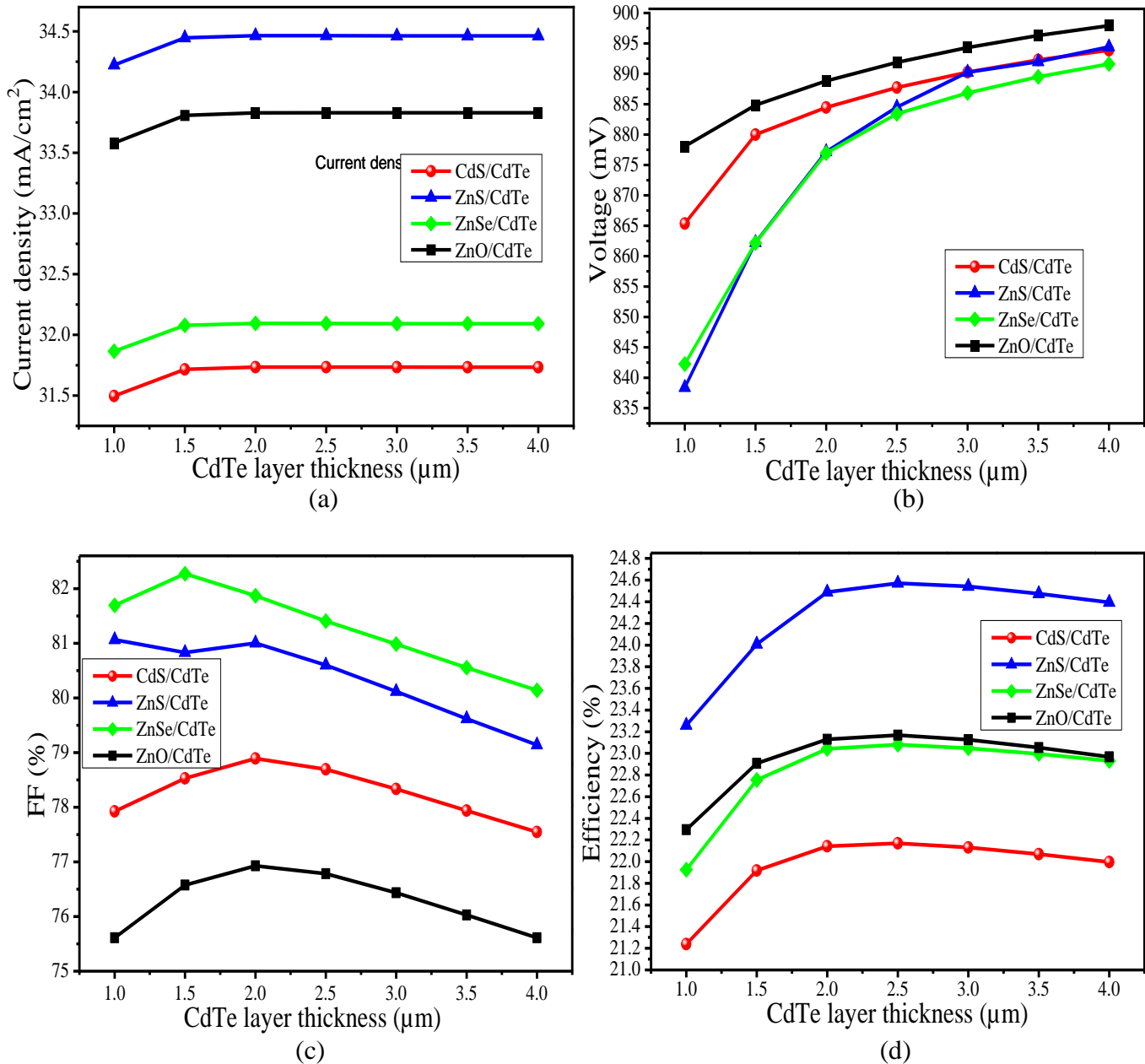


Figure IV.6: Examination of the impact of absorber layer thickness on CdTe solar cell performance parameters: (a) J_{SC} (b) V_{oc} (c) Fill factor FF (d) Efficiency η .

IV.4.5 Comparative Performance Analysis of Optimized CdTe Cell with Various Buffer Layers

The study presents an optimized configuration of a cadmium telluride (CdTe) solar cell, which was simulated incorporating the ideal parameters for layer thickness and doping

concentration identified as $0.01 \mu\text{m}$ and 10^{18} cm^{-3} , respectively, for all buffer layers. Additionally, the CdTe absorber layer was optimized at a thickness of $2.5 \mu\text{m}$.

Figure IV.7 displays the current-voltage (I-V) characteristics of the optimized CdTe solar cells with different buffer layers. The use of ZnSe, ZnO, and ZnS as buffer layers yielded superior efficiency compared to the conventional CdS/CdTe configuration, as well as efficiencies reported in previous designs of CdTe-based solar cells, as cited in references [14,25–30]. The performance outcomes of the novel optimized CdTe solar cell design are systematically compared with those from prior research in **Table IV.4**. The observed high conversion efficiency substantiates the efficacy of these structures, surpassing the performance of other cell structures, cited in the references.

The efficiency of the proposed solar cell, characterized by its short-circuit current and conversion efficiency, surpasses that of the reference cell and various other previously simulated CdTe-based solar cell designs. This optimized configuration of the solar cell not only exhibits the highest level of efficiency among those studied but also has the potential to be more economically viable compared to other CdTe-based solar cell designs, suggesting a competitive advantage in both performance and cost-effectiveness.

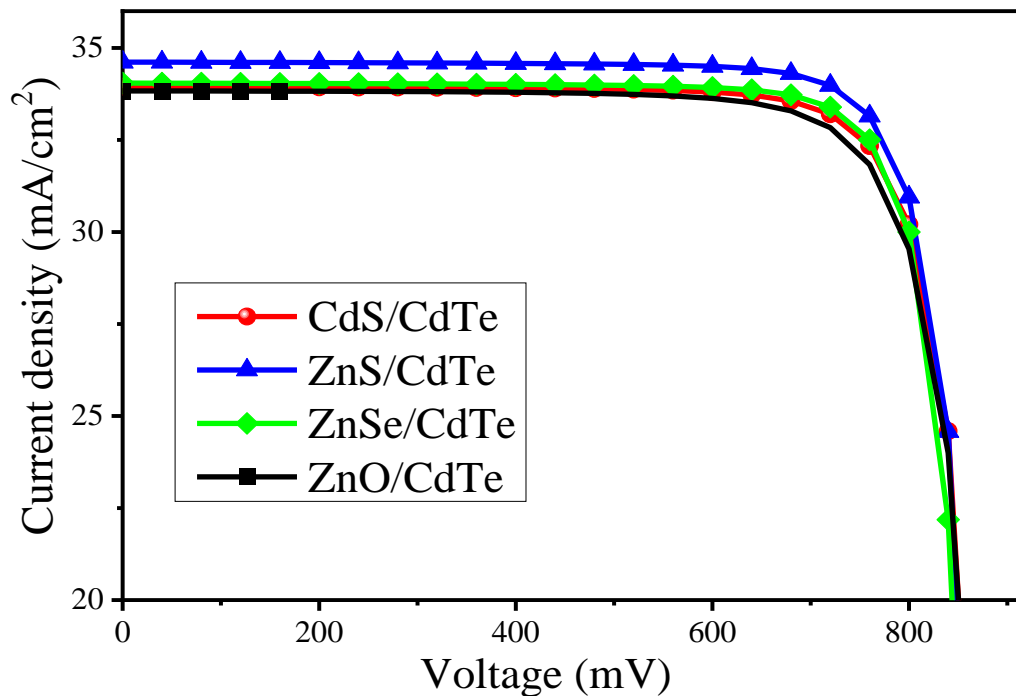


Figure IV.7: Current-voltage characteristics of the optimized CdTe solar cells.

Table IV.4 Comparison between suggested structure and previous works.

		Jsc (mA/cm ²)	Voc (mV)	FF (%)	η (%)
Our Simulation	ZnS/CdTe	34.65	881	82.54	25.23
	ZnSe/CdTe	34.46	883	82.27	25.04
	CdS/CdTe	34.37	885	81.54	24.82
	ZnO/CdTe	33.84	887	80.58	24.20
[30]	CdS/CdTe	31.99	894	84.72	24.22
[33]	ZnTe/ZnS/CdTe	29.32	1010	72.06	21.38
[34]	CdS/CdTe	27.59	1030	85.83	24.35
[17]	ZnS/CdTe/BSF	24.812	1024	86.92	22.10
[17]	ZnS/CdTe	22.985	901	85.58	17.73
[11]	CdS/CdTe	29.09	950	83.47	23.00
[18]	CdZnS/CdTe	16.20	1098	86.89	15.46
[9]	CdS/CdTe/BSF	24.26	1060	87.5	22.51

IV.4.6 Effect of Operating Temperature on the Performance of Optimized CdTe Cell

The impact of operating temperature on the performance of solar cells is a critical factor that warrants comprehensive investigation. Solar panels, which are commonly installed in outdoor environments, frequently operate at temperatures surpassing 300 K due to the absorption and conversion of sunlight into heat [31]. Recent studies have revealed that elevated temperatures induce heightened levels of strain and stress within the structural components of solar cells [32]. Consequently, this thermal stress leads to an increase in interfacial defects, disorder, and suboptimal interconnectivity between the various layers of the solar cell [33]. These thermally-induced imperfections have a detrimental effect on the power output, energy efficiency, overall performance, and operational lifetime of the solar cell. Therefore, understanding and mitigating the influence of high operating temperatures is crucial for optimizing the functionality and longevity of solar cells in real-world applications.

The influence of operating temperature on the performance characteristics of optimized cadmium telluride (CdTe) solar cells was systematically investigated over a temperature spectrum ranging from 260 K to 340 K, in increments of 20 K. The corresponding simulation outcomes are depicted in **Figure IV.8**.

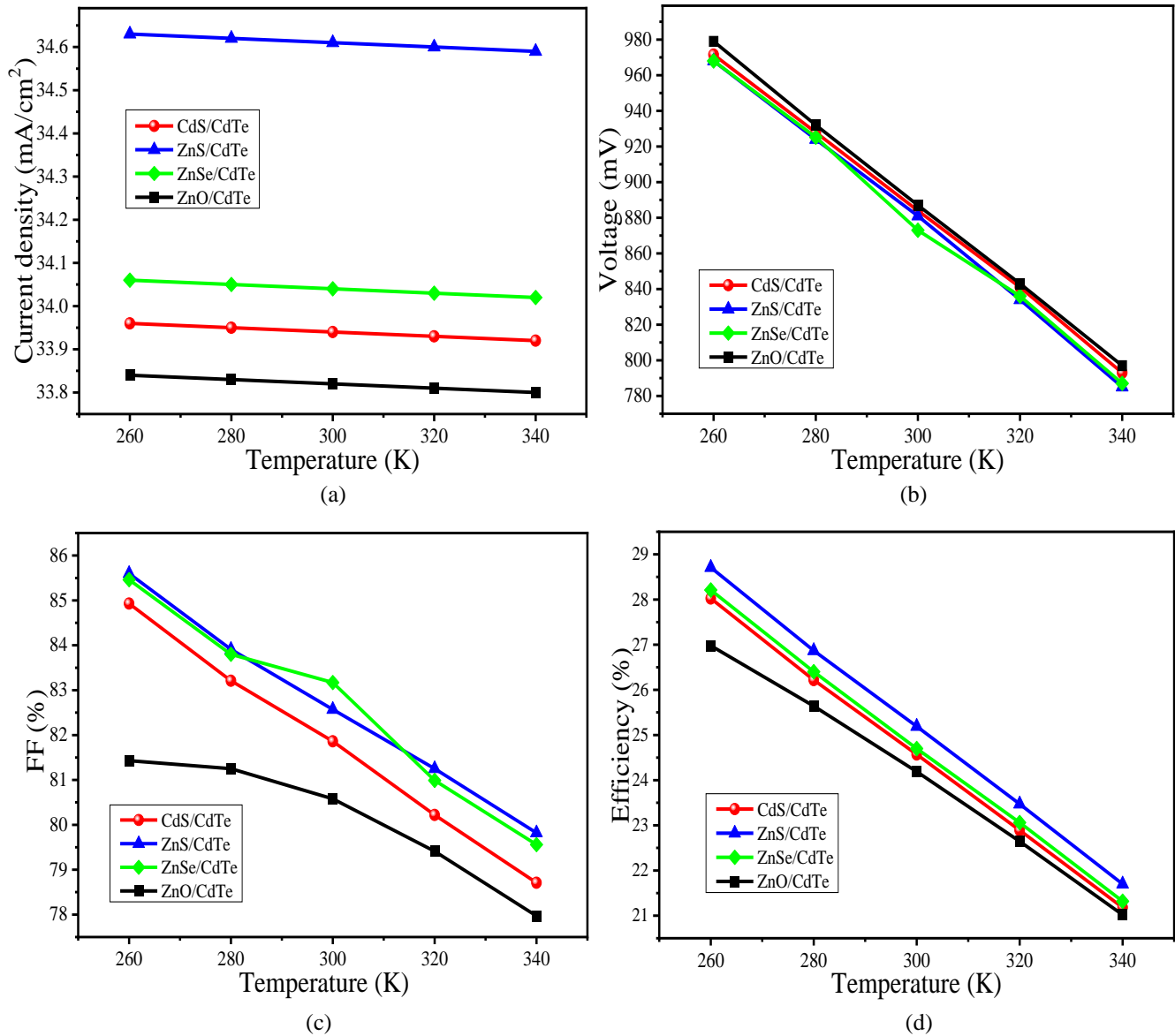


Figure IV. 8: Assessment of the effect of operating temperature on CdTe solar cell performance parameters: (a) J_{sc} (b) V_{oc} (c) Fill factor FF (d) Efficiency η .

The empirical data indicates a discernible degradation in the performance of the solar cell with an ascending operating temperature across the examined spectrum for different buffer layers. A rise in temperature can induce alterations in the conductivity of materials, thereby diminishing the performance of the CdTe thin-film solar cell system. This thermal effect is attributed to the increased kinetic energy of electrons, which promotes their recombination prior to reaching the depletion zone for collection.

It is evident that all performance metrics deteriorate with an increase in temperature. The most significantly impacted parameter is the open-circuit voltage (V_{oc}), which exhibits a precipitous decline as temperature increases, attributable to the negative correlation of the saturation current with temperature as described by **Equation (IV.11)**. The variation in V_{oc} is governed by the stipulated equation [35].

$$V_{oc} = \frac{E_g}{q} - \frac{akT}{q} \ln\left(\frac{I_{0-}}{I_{ph}}\right) \quad (\text{IV.11})$$

Thermal excitation diminishes the band gap, leading to elevated electron energies and an amplified saturation current, owing to the exponential surge in charge carrier density with temperature. Concurrently, the short-circuit current density (J_{sc}) experiences a marginal reduction, predominantly due to augmented recombination rates at elevated temperatures.

The peak efficiency is recorded at the lower threshold of 260 K, where the efficiency of our proposed cells surges by approximately 5% over that at ambient temperature. However, upon elevating the temperature of the CdTe cells from 260 K to 340 K, a significant drop in efficiency is observed: from 30.47% to 21.73% for CdTe/ZnS, from 30.14% to 21.42% for CdTe/CdS, from 30.25% to 21.52% for CdTe/ZnSe, and from 28.20% to 21.02% for CdTe/ZnO. Analogous trends in performance parameters have been corroborated by other studies [34–36].

The operational temperature exerts a substantial impact on the efficacy of solar cells; lowering the operating temperature can significantly enhance cell efficiency. To this end, various cooling methodologies for photovoltaic (PV) cells have been developed, including water cooling and forced evaporative cooling [37,38]. The adoption of active cooling mechanisms, such as forced air circulation, may effectively mitigate thermal effects on panels [39], thereby sustaining high efficiencies in PV systems. This innovative strategy could markedly advance the practical deployment of solar PV technologies.

IV.5 Conclusion

In the present study, we have systematically analyzed the optoelectronic characteristics of cadmium telluride (CdTe) thin-film solar cells incorporating alternative buffer layers through simulations conducted with Silvaco Atlas software. Our comparative assessment reveals that CdTe solar cells employing zinc sulfide (ZnS), zinc selenide (ZnSe), and zinc oxide (ZnO) as cadmium-free buffer layers exhibit promising potential as replacements for the traditional cadmium sulfide (CdS)/CdTe solar cells. The photovoltaic performance, notably the efficiency and the short-circuit current density (J_{sc}), is notably enhanced in cells incorporating ZnS and ZnSe as buffer layers through optimization of critical parameters, leading to an increase in generated photocurrent.

Optimization procedures established an ideal absorber layer thickness of 2.5 μm , while the doping concentration and thickness for all buffer layers were determined to be $1 \times 10^{18} \text{ cm}^{-3}$ and 0.01 μm , respectively. These optimized configurations yielded significant improvements in cell efficiency. Among the buffer layers evaluated, those with ZnS and ZnSe achieved the highest recorded efficiencies of 25.23% and 25.04%, respectively. Additionally, our simulation results indicate that the performance of CdTe solar cells is inversely related to the rise in operational temperature across all buffer layer types.

The findings from the simulations of the proposed CdTe thin-film solar cell configurations underscore their environmental sustainability, cost-effectiveness, and high efficiency. This study provides a valuable framework for researchers in the design and development of advanced CdTe-based solar cells and may offer practical insights for experimentalists to fabricate such cells in future endeavors.

References

- [1] M.A. Green, E.D. Dunlop, J. Hohl-Ebinger, M. Yoshita, N. Kopidakis, K. Bothe, D. Hinken, M. Rauer, X. Hao, Solar cell efficiency tables (Version 60), *Prog. Photovoltaics Res. Appl.* 30 (2022) 687–701. <https://doi.org/10.1002/pip.3595>.
- [2] Atlas User's Manual, SILVACO Inc, Santa Clara, CA 95054, California, USA, 2018.
- [3] B. Sara, Z. Baya, B. Zineb, Investigation of Cu(In, Ga)Se₂ solar cell performance with non-cadmium buffer layer using TCAD-SILVACO, *Mater. Sci. Pol.* 36 (2018) 514–519. <https://doi.org/10.2478/msp-2018-0054>.
- [4] S. Lee, S. Kim, Y. Kim, J. Park, J. Yi, Computational design of high efficiency a-Si:H/CIGS monolithic tandem solar cell, *Optik (Stuttg.)* 173 (2018) 132–138. <https://doi.org/10.1016/j.ijleo.2018.08.004>.
- [5] A. Sylla, S. Touré, J.P. Vilcot, Numerical modeling and simulation of CIGS-based solar cells with ZnS buffer layer, *ARPN J. Eng. Appl. Sci.* 13 (2018) 64–74. <https://doi.org/10.4236/OJMSI.2017.54016>.
- [6] D. Daksh, S. Mishra, B. Singh Sengar, Simulation of antimony chalcogenide thin film solar cell with high-efficiency, *Mater. Today Proc.* 76 (2022) 336–340. <https://doi.org/10.1016/j.matpr.2022.11.374>.
- [7] S. Tobbeche, S. Kalache, M. Elbar, M.N. Kateb, M.R. Serdouk, Improvement of the CIGS solar cell performance: structure based on a ZnS buffer layer, *Opt. Quantum Electron.* 51 (2019). <https://doi.org/10.1007/S11082-019-2000-Z>.
- [8] B. Metin, N. Kavasoglu, A.S. Kavasoglu, *Physica B : Condensed Matter AFORS-HET simulation for investigating the performance of ZnO / n-CdS / p-CdTe / Ag solar cell depending on CdTe acceptor concentration and temperature*, *Phys. B Condens. Matter.* 649 (2023) 414504. <https://doi.org/10.1016/j.physb.2022.414504>.
- [9] J. Qu, L. Zhang, H. Wang, X. Song, Y. Zhang, H. Yan, Simulation of double buffer layer on CIGS solar cell with SCAPS software, *Opt. Quantum Electron.* 51 (2019). <https://doi.org/10.1007/S11082-019-2100-9>.
- [10] B. Sara, Z. Baya, B. Zineb, Investigation of Cu(In, Ga)Se₂ solar cell performance with non-cadmium buffer layer using TCAD-SILVACO, *Mater. Sci. Pol.* 36 (2018) 514–519. <https://doi.org/10.2478/MSP-2018-0054>.
- [11] S. Ahmmed, A. Aktar, M.F. Rahman, J. Hossain, A.B.M. Ismail, A numerical simulation of high efficiency CdS/CdTe based solar cell using NiO HTL and ZnO TCO, *Optik (Stuttg.)* 223 (2020). <https://doi.org/10.1016/j.ijleo.2020.165625>.
- [12] D. Ratnasinghe, H. Mahabaduge, A. Mlc, Optimization of the absorber layer thicknesses and the surface defect densities of CdTe/Si tandem device Muthuthanthrige Lilani Attygalle Optimization of the absorber layer thicknesses and the surface defect densities of CdTe/Si tandem device, 2021. <https://www.researchgate.net/publication/353071086>.
- [13] A. Kuddus, M.F. Rahman, J. Hossain, A.B.M. Ismail, Enhancement of the performance of CdS/CdTe heterojunction solar cell using TiO₂/ZnO bi-layer ARC and V₂O₅BSF layers: A simulation approach, *EPJ Appl. Phys.* 92 (2020). <https://doi.org/10.1051/EPJAP/2020200213>.
- [14] N.M.D. Putra, Sugianto, P. Marwoto, R. Murtafiatin, D.P. Permadis, The SCAPS-1D modeling of ZnO/CdS/CdTe thin film: Analysis of thickness and stoichiometric

- fraction of absorber layer on solar cell performance, *J. Phys. Conf. Ser.* 1918 (2021). <https://doi.org/10.1088/1742-6596/1918/2/022029>.
- [15] S. Tobbeche, S. Kalache, M. Elbar, M.N. Kateb, M.R. Serdouk, Improvement of the CIGS solar cell performance: structure based on a ZnS buffer layer, *Opt. Quantum Electron.* 51 (2019). <https://doi.org/10.1007/s11082-019-2000-z>.
- [16] B. Metin, N. Kavasoglu, A.S. Kavasoglu, AFORS-HET simulation for investigating the performance of ZnO/n-CdS/p-CdTe /Ag solar cell depending on CdTe acceptor concentration and temperature, *Phys. B Condens. Matter.* 649 (2023). <https://doi.org/10.1016/J.PHYSB.2022.414504>.
- [17] N.A. Khan, K.S. Rahman, F. Haque, N. Dhar, M.A. Islam, M. Akhtaruzzaman, K. Sopian, N. Amin, Design optimization of CdTe thin film solar cells from numerical analysis, 8th Int. Conf. Electr. Comput. Eng. Adv. Technol. a Better Tomorrow, ICECE 2014. (2015) 508–511. <https://doi.org/10.1109/ICECE.2014.7026862>.
- [18] C. Series, The SCAPS-1D modeling of ZnO / CdS / CdTe thin film : analysis of thickness and stoichiometric fraction of absorber layer on solar cell performance The SCAPS-1D modeling of ZnO / CdS / CdTe thin film : analysis of thickness and stoichiometric fraction of , (2021). <https://doi.org/10.1088/1742-6596/1918/2/022029>.
- [19] M.W. Bouabdelli, F. Rogti, M. Maache, A. Rabehi, Performance enhancement of CIGS thin-film solar cell, *Optik (Stuttg).* 216 (2020). <https://doi.org/10.1016/j.ijleo.2020.164948>.
- [20] N. Barreau, J.C. Bernède, S. Marsillac, C. Amory, W.N. Shafarman, New Cd-free buffer layer deposited by PVD: In₂S₃ containing Na compounds, *Thin Solid Films.* 431–432 (2003) 326–329. [https://doi.org/10.1016/S0040-6090\(03\)00216-5](https://doi.org/10.1016/S0040-6090(03)00216-5).
- [21] X.B. Xu, X.Y. Wang, W.P. Gu, S. Quan, Z. Zhang, Study on influences of CdZnS buffer layer on CdTe solar cells, *Superlattices Microstruct.* 109 (2017) 463–469. <https://doi.org/10.1016/j.spmi.2017.05.033>.
- [22] A. Cantas, F. Turkoglu, E. Meriç, F.G. Akça, M. Ozdemir, E. Tarhan, L. Ozyuzer, G. Aygun, Importance of CdS buffer layer thickness on Cu₂ZnSnS₄-based solar cell efficiency, *J. Phys. D. Appl. Phys.* 51 (2018) 275501.
- [23] D. Parashar, V.S.G. Krishna, S.N. Moger, R. Keshav, M.G. Mahesha, Thickness Optimization of ZnO/CdS/CdTe Solar Cell by Numerical Simulation, *Trans. Electr. Electron. Mater.* 21 (2020) 587–593. <https://doi.org/10.1007/S42341-020-00209-9>.
- [24] R. Rafieirad, B.A. Ganji, Efficiency Improvement of Perovskite Solar Cells by Utilizing CuInS Thin Layer: Modeling and Numerical Study, *IEEE Trans. Electron Devices.* 68 (2021) 4997–5002. <https://doi.org/10.1109/TED.2021.3102536>.
- [25] D.M. Dey, M. Dey, M.A. Matin, N. Amin, High efficient and stable ultra-thin cdte solar cell with a potential copper telluride BSF, *Proc. 9th Int. Conf. Electr. Comput. Eng. ICECE 2016.* (2017) 590–593. <https://doi.org/10.1109/ICECE.2016.7853989>.
- [26] I.E. Tinedert, F. Pezzimenti, M.L. Megherbi, A. Saadoun, Design and simulation of a high efficiency CdS/CdTe solar cell, *Optik (Stuttg).* 208 (2020) 164112. <https://doi.org/10.1016/j.ijleo.2019.164112>.
- [27] J.N. Sameera, M.A. Islam, S. Islam, T. Hossain, M.K. Sobayel, M. Akhtaruzzaman, N. Amin, M.J. Rashid, Cubic Silicon Carbide (3C–SiC) as a buffer layer for high efficiency and highly stable CdTe solar cell, *Opt. Mater. (Amst).* 123 (2022). <https://doi.org/10.1016/J.OPTMAT.2021.111911>.
- [28] A.H. Munshi, J.M. Kephart, A. Abbas, T.M. Shimpi, K.L. Barth, J.M. Walls, W.S. Sampath, Polycrystalline CdTe photovoltaics with efficiency over 18% through

- improved absorber passivation and current collection, *Sol. Energy Mater. Sol. Cells*. 176 (2018) 9–18. <https://doi.org/10.1016/j.solmat.2017.11.031>.
- [29] S.R. Al Ahmed, J. Ferdous, M.S. Mian, Development of a novel CdTe/ZnS/ZnTe heterojunction thin-film solar cells: a numerical approach, *IOP SciNotes*. 1 (2020) 024802. <https://doi.org/10.1088/2633-1357/ABA1F7>.
- [30] I.E. Tinedert, A. Saadoune, I. Bouchama, M.A. Saeed, Numerical modelling and optimization of CdS/CdTe solar cell with incorporation of Cu₂O HT-EBL layer, *Opt. Mater. (Amst)*. 106 (2020). <https://doi.org/10.1016/j.optmat.2020.109970>.
- [31] M.A. Green, E.D. Dunlop, J. Hohl-Ebinger, M. Yoshita, N. Kopidakis, A.W.Y. Ho-Baillie, Solar cell efficiency tables (Version 55), *Prog. Photovoltaics Res. Appl.* 28 (2020) 3–15. <https://doi.org/10.1002/pip.3228>.
- [32] A.M. Bagher, M.M.A. Vahid, M. Mohsen, Types of solar cells and application, *Am. J. Opt. Photonics*. 3 (2015) 94–113.
- [33] T. Ouslimane, L. Et-taya, L. Elmaimouni, A. Benami, Impact of absorber layer thickness, defect density, and operating temperature on the performance of MAPbI₃ solar cells based on ZnO electron transporting material, *Heliyon*. 7 (2021) e06379. <https://doi.org/10.1016/j.heliyon.2021.e06379>.
- [34] M. Boubakeur, A. Aissat, M. Ben Arbia, H. Maaref, J.P. Vilcot, Enhancement of the efficiency of ultra-thin CIGS/Si structure for solar cell applications, *Superlattices Microstruct.* 138 (2020). <https://doi.org/10.1016/j.spmi.2019.106377>.
- [35] M. Abderrezek, M. Fathi, F. Djahli, Comparative study of temperature effect on thin film solar cells, *J. Nano- Electron. Phys.* 10 (2018). [https://doi.org/10.21272/JNEP.10\(2\).02027](https://doi.org/10.21272/JNEP.10(2).02027).
- [36] M. Fathi, M. Abderrezek, F. Djahli, M. Ayad, Study of Thin Film Solar Cells in High Temperature Condition, *Energy Procedia*. 74 (2015) 1410–1417. <https://doi.org/10.1016/j.egypro.2015.07.788>.
- [37] K.A. Moharram, M.S. Abd-Elhady, H.A. Kandil, H. El-Sherif, Enhancing the performance of photovoltaic panels by water cooling, *Ain Shams Eng. J.* 4 (2013) 869–877. <https://doi.org/10.1016/j.asej.2013.03.005>.
- [38] A.H. Alami, Effects of evaporative cooling on efficiency of photovoltaic modules, *Energy Convers. Manag.* 77 (2014) 668–679. <https://doi.org/10.1016/j.enconman.2013.10.019>.
- [39] A. Hussien, A. Eltayesh, H.M. El-Batsh, Experimental and numerical investigation for PV cooling by forced convection, *Alexandria Eng. J.* 64 (2023) 427–440. <https://doi.org/10.1016/j.aej.2022.09.006>.

General Conclusion

This present work focuses on the study, through numerical simulation, of a inorganic CdTe-based thin-film solar cell with the aim of designing an optimal structure offering the best possible electrical efficiency. The numerical simulation was carried out using the two-dimensional simulator Atlas-Silvaco.

A literature review was conducted to allow us to better understand the subject of our study. At first, we recalled some basic concepts on the theory of solar cells. We explored the state of the art in photovoltaic cell technology and the various constraints that cause losses that can influence the performance of a photovoltaic cell. We then devoted a more or less detailed study to CdTe-based thin-film solar cells. This part includes a technological analysis and a recent presentation on solar cells, through a synthesis of different techniques, technologies, and records concerning the performance and efficiency of this type of solar cells.

A part of this work was devoted to a relatively detailed presentation of the Atlas-Silvaco simulation software. Finally, our study will end with a final part that will present and process our results from the numerical simulation of the studied structure.

The CdTe thin-film solar cell was chosen in our study because of its advantages and components. In the simulation part, numerical simulations were performed to investigate the performance of CdTe thin film solar cells utilizing various Cd-free zinc chalcogenide-based buffer layers (ZnO, ZnSe, ZnS) as alternatives to the conventionally used CdS. The baseline CdS/CdTe solar cell structure was first validated against previous experimental and theoretical results, yielding a conversion efficiency of 22.14%.

Replacing the CdS buffer layer with ZnO, ZnSe, and ZnS resulted in improved efficiencies of 23.04%, 23.13%, and 24.48%, respectively, at an optimized buffer layer thickness of approximately 0.1 μm . Further optimization of the absorber and buffer layer thicknesses and doping densities enabled achieving best efficiencies of 25.23% and 25.04% for the ZnS and ZnSe buffer layers, demonstrating their potential as high-performance Cd-free alternatives.

The superior performance of the Zn-based buffer layers can be attributed to their larger bandgaps compared to CdS, allowing more photons to reach the CdTe absorber layer and reducing optical absorption losses, especially in the short wavelength range (400-500 nm).

Moreover, these materials are less susceptible to detrimental interactions with chlorine during cell fabrication that can lead to the formation of insulating CdCl_2 precipitates and degrade the buffer/absorber interface. The reduced interface diffusion with Zn-based buffers may also mitigate potential long-term stability issues in CdTe solar cells.

In conclusion, the results of this simulation study provide strong evidence for the viability of Cd-free zinc chalcogenide buffer layers, particularly ZnS and ZnSe, as high-efficiency and environmentally friendly alternatives to CdS in CdTe thin film solar cells. The achieved efficiencies over 25% with optimized ZnS and ZnSe buffers represent a significant advancement over the baseline CdTe/CdS structure. These findings motivate further experimental work to validate the simulation results and accelerate the development of Cd-free CdTe photovoltaic devices.

Continued research efforts in this direction, along with techno-economic and lifecycle assessments, are essential to bring this promising thin film technology closer to large-scale commercial realization and contribute to the sustainable generation of clean solar electricity. Successful deployment of high-efficiency and eco-friendly CdTe solar cells can play a vital role in addressing the escalating global energy demands and environmental challenges in the face of multiple world crises.

Annex 1:

Scientific production

- **Loumafak Hafafa**, Mostefa Maache , Zehor Allam, Achouak Zebeir, *Simulation and performance analysis of CdTe thin film solar cell using different Cd-free zinc chalcogenide-based buffer layers*. Results in Optics 14 (2024): [100596](https://doi.org/10.1016/j.rio.2023.100596).
<https://doi.org/10.1016/j.rio.2023.100596>
- **Loumafak Hafafa**, Mostefa Maache and Mohamed Wahid Bouabdelli, *Improving the Performance of CZTS/CZTSSe Tandem Thin Film Solar Cell*. Journal of Nano- and Electronic Physics 16 (2) (2024): [https://doi.org/10.21272/jnep.16\(2\).02018](https://doi.org/10.21272/jnep.16(2).02018)
- **Loumafak Hafafa**, Mostefa Maache and Mohamed Wahid Bouabdelli, *Improved performance of CdTe thin-film solar cell through key parameters*, Journal of Theoretical and Applied Physics, 18 (2024) 1–10: <https://dx.doi.org/10.57647/j.jtap.2024.1803.35>

Annex 2:

International communications

- **Loumafak Hafafa**, Mostefa Maache and Mohamed Wahid Bouabdelli, *Effects of the different buffer layers on the performance of CZTSe solar cell*, 1st international conference on chemical matters and environment preservation IC-CMEP'22 March 09-10, 2022, Ouargla-Algeria.
- **Loumafak Hafafa**, Mostefa Maache , Zehor Allam, Achouak Zebeir, *Investigation of CZTSSe thin film solar cell performance with non-cadmium buffer layer*, 1st International Conference on Recent and Innovative Results in Engineering and Technology, August 16-18, 2023, Konya, Turkey.
- Yacine Djalab, Rabah Moussa, Mostafa Maache, Yazid Benbouzid, Abderrazak Djenidi and **Loumafak Hafafa**, *Theoretical prediction of physical and chemical properties of the ZnO_{1-x}Se_x ternary alloy*, 1st international conference on chemical matters and environment preservation IC-CMEP'22 March 09-10, 2022, Ouargla-Algeria.

- Selma Rabhi, Perrin-Pellegrino, M.C. Benoudia, K. Hoummada, **Loumafak Hafaifa**, *Thickness Effect on the Solid-State Reaction of a Ni/GaAs System for microelectronic devices*, 1st International Conference on Recent and Innovative Results in Engineering and Technology, August 16-18, 2023, Konya, Turkey.
- **Loumafak Hafaifa**, Mostefa Maache and Mohamed Wahid Bouabdelli, *Effect of the Substrate on the Structural Properties of Cu₂ZnSnS₄ Thin Films Synthesized by Electrodeposition*, 1st International Conference on Computational & Applied Physics, March 8, 2022, Blida-Algeria.
- **Loumafak Hafaifa**, Mostefa Maache and Mohamed Wahid Bouabdelli, *Investigation of CIGS solar cell performance with different buffer layers*, 1st International Conference on Engineering and Applied Natural Sciences on 10-13 May in 2022 at Konya/Turkey

National communications

- **Loumafak Hafaifa**, Mostefa Maache, Selma Rabhi, *Impact of double buffer layer on the performance of CIGS thin film solar cell*, The first National Conference on Matter Sciences NCSM2023 December 20, 2023, Djelfa, Algeria.
- **Loumafak Hafaifa**, Mostefa Maache and Mohamed Wahid Bouabdelli, *Optimization of the CdS buffer layer for high efficiency CZTSe solar cells*, 1st National Conference Online in Materials Physics, May 15th 2022, Eltarf-Algeria
- **Loumafak Hafaifa**, Mostefa Maache and Mohamed Wahid Bouabdelli, *Effect of gallium contents on the CIGS cell performance*, 1st National Conference on Materials Sciences and Engineering (MSE'22) 28-29 June 2022, Khenchela, Algeria.
- Achouak Zebeir, Zehor Allam, Mostefa Maache, **Loumafak Hafaifa**, *optimization des cellules solaires CuInSe₂ a couche mince: simulation SCAPAS-ID et influence de l'épaisseur absorbante*, The first National Conference on Matter Sciences NCSM2023 December 20, 2023, Djelfa, Algeria.
- Zineb Ibtissem Gouchida, Mostefa Maache, Yazid Benbouzid Achouak Zebeir, **Loumafak Hafaifa**, *Etude par simulation SCAPAS-ID d'une cellule solaire en couches minces à base de*

CZTSSe l'effet de l'épaisseur de la couche absorbante, 1st National Conference on Science & Technology 1st NCST22, 27th-28th June 2022, Mascara, Algeria.

- Zehor Allam, Razika Adjouz, Achouak zebeir, **Loumafak Hafaifa**, *Optimizing the Performance of Cd_{0.2} Zn_{0.8}S/CdTe Solar Cells: A Numerical Investigation*, 2nd National Conference on Renewable Energy, Photovoltaic Materials and Devices (NC-PEPVMD'24), 17-18 January 2024, Bechar, Algeria.